arXiv:0910.0806v1 [astro-ph.CO] 5 Oct 2009

NATURE OF CLUSTERING OF LARGE SCALE STRUCTURES

THESIS SUBMITTED TO THE UNIVERSITY OF DELHI

FOR THE DEGREE OF

DOCTOR OF PHILOSOPHY



By

JASWANT KUMAR YADAV

DEPARTMENT OF PHYSICS AND ASTROPHYSICS

UNIVERSITY OF DELHI

DELHI – 110 007

INDIA

December, 2008

DECLARATION

It is certified that the work presented in this thesis **"Nature of clustering of large scale structures"** has been carried out at the Department of Physics & Astrophysics of the University of Delhi under the supervision of Dr. T. R. Seshadri.

The work reported in this thesis is original and it has not been submitted earlier for any degree to any university.

Jaswant Kumar Yadav
(Candidate)

To my parents....

Acknowledgements

I would like to thank my supervisor Dr. Terizhandhur Rajagopalan Seshadri for suggesting this topic of research for my thesis. His able and continuous guidance over the years has been invaluable. During the whole period of my thesis he has given me a lot of freedom, which has contributed immensely to my growth as a researcher. He has always been there like a brother, discussing research as well as any personal difficulty if I had. Thanks Sesh, you have been an excellent motivator, very friendly and above all a wonderful supervisor.

I am also deeply grateful to my collaborators and friends in this field. I have benefitted immensely from my collaborations with Somnath Bharadwaj and J.S. Bagla, whose insights into physics and computers have taught me a lot. I thank them for enriching my vision of science. It has been interesting and stimulating to work with Biswajit Pandey. I have also had many interesting discussions on scientific and philosophical matters with Sanil and Keshwarjit.

I sincerely thank Kulshreshtha sir and all the other teachers for their continuous encouragement and guidance since my M. Sc. days. Over the last five years I have received a great deal of help about administrative matters from Mrs. Dawar. Thanks are also due to staff at the documentation center, Library and at finance section. I thank CSIR, Govt. of India, for providing me research fellowship during a part of my thesis. Computational work for a part of this thesis was carried out at the cluster computing facility in the Harish-Chandra Research Institute (http://cluster.hri.res.in).

On the personal front - I am grateful to all the friends and non-friends at Room number 184 and IRC in the department. It is not practical to name everyone but I

would like to thank everyone by thanking the "student's director" Mr. Ranjit Kumar at 184 and Miss Shalini at IRC. I have had a great time with all of them sharing different softwares and other scientific information. There are also many people outside Delhi University who have been a lot of help to me. I collectively thank all the friends at HRI, CTS-IITKGP and at IUCAA for all the help and support.

Ma and Pita Ji, I dedicate this thesis to you. You both are my ever lasting source of inspiration and energy. My respected brother Ashok, my Bhabhi Ji and my cute, little nephew Golu are too near to be thanked ! But for your confidence and the faith you put in me, it would have been impossible for me to survive these long years of academic pursuit ! It is difficult to say it in person, but let me take this opportunity to say that this is the tribute I found most suitable for all your love, support and understanding ! I wish and pray, I can offer you much more in days to come. I also thank my cousin Satbir Singh for all the encouragement.

I must acknowledge my wife and best friend, Suman, without whose love, support, understanding and encouragement, I would not have finished this thesis. Thank you, Suman, for being what you are.

Date: Jaswant Kumar Yadav

Place: Delhi University, Delhi

List of publications

This thesis is based on following publications.

1. *"Testing homogeneity on large scales in Sloan Digital Sky Survey Data Release One"*,
 Jaswant Yadav, S. Bharadwaj, B. Pandey & T. R. Seshadri
 MNRAS, 2005, 364, 601

2. *"Fractal Dimensions of a Weakly Clustered Distribution and the Scale of Homogeneity"*
 J. S. Bagla, **Jaswant Yadav** & T.R. Seshadri
 MNRAS, 2008, 390, 829

Presentations in International Conferences

1. *"Fractal Dimension as a probe of Homogeneity"*
 Jaswant Yadav, J.S. Bagla & T. R. Seshadri
 To appear in proceedings of conference on "Frontiers in Numerical Gravitational Astrophysics" held at *ERICE, ITALY* from *June 27 -July 5, 2008*

2. *"Effects of finite number and clustering on fractal Dimension"*
 Jaswant Yadav
 International Conference on Gravitation and Cosmology, Inter University Centre for Astronomy and Astrophysics, Pune, India, December 2007

3. *"Fractal Dimension of a weakly clustered Distribution"*

 Jaswant Yadav

 International Workshop on the probes of large scale structures, Inter University Centre for Astronomy and Astrophysics, Pune, India, July 2008

Abstract

In the standard cosmological model the Universe is assumed to have begun approximately 13 billion years ago when it began expanding from an inconceivably hot and dense state. Since then, the Universe has continued the process of expansion and cooling, eventually reaching the cold sparse state that we observe today. Galaxy surveys carried out in the 20^{th} century have revealed that the distribution of galaxies in the Universe is far from random at least on the scales of the survey. This distribution is highly structured over a range of scales. Surveys being currently undertaken and being planned for the future will provide a wealth of information about these structures. The ultimate goal of this exercise is not only to describe galaxy clustering but also to explain how this clustering arose as a consequence of evolutionary processes acting on the initial conditions that we see in the Cosmic Microwave Background Anisotropy data.

In order to achieve this goal, we would like to describe cosmic structures quantitatively. We need to build a mathematically quantifiable description of structures or distribution of points. Identifying the region where the scaling laws apply to these distributions and the nature of these scaling laws is an important part of understanding as to which physical mechanisms have been responsible for the organizations of the clusters, superclusters of galaxies and voids between them. Finding the region where these scaling laws are broken is equally important since it indicates the transition to different underlying physics of structure formation.

The present thesis focuses on characterizing the distribution of points and galaxies using **multifractal analysis**. In this attempt the main emphasis is on calculating the Minkowski-Bouligand fractal dimension (D_q) of the distribution of points over different

scales and hence finding the scale of homogeneity of the distribution. Effect, of finite size of the sample and clustering in the distribution, on the D_q has been studied in detail. The assumption that the large scale distribution of matter in the Universe is homogeneous has been verified with multifractal analysis of the data from Sloan Digital Sky Survey.

The thesis starts with a broad introduction to standard model of cosmology with special emphasis on the formation and distribution of structures in the Universe. A review of different analytical formalisms and important observations has been presented. A set of notations of different physical and statistical quantities of interest has been provided.

A detailed review of literature, regarding various statistical techniques for the characterizing the distribution of matter over large scales, has been presented. The standard analysis of two point correlation function has been discussed. The need to look for a statistical technique which does not presuppose the homogeneity of the distribution on the scale of the sample region has been motivated. In this direction fractal dimension as an alternative to N point correlation functions has been discussed. Various definitions of fractal dimension which are useful to quantify distribution of points in various density environments have been presented. A correct prescription to describe the galaxy distribution in the Universe has been presented in the form of Minkowski Bouligand dimension.

A detailed derivation of Minkowski Bouligand dimension for both homogeneous as well as weakly clustered distribution has been presented. The benchmark dimension to quantify the finite size homogeneous distribution of points has been obtained. An analytical expression for the contribution of weak clustering to the deviation of fractal dimension from the euclidian dimension has been derived. Baryon acoustic oscillations prior to matter radiation decoupling give rise to a bump in the correlation function at a scale of $\sim 100\,h^{-1}$Mpc. The effect of this bump in correlation function on the behavior of fractal dimension of clustered distribution has also been discussed. The multifractal technique has been applied to the unbiased (e.g. the L_* type of galaxies) as well as

biased (e.g. Large Redshift Galaxies) tracers of underlying matter distribution in the concordant model of cosmology.

In the end the application of multifractal analysis to the distribution of galaxies in the Sloan Digital Sky survey has been presented. This exercise has been undertaken to obtain the scale of homogeneity of the Universe. The galaxy distribution from the SDSS has been projected on the equatorial plane and a 2-dimensional multi-fractal analysis has been carried out by counting the number of galaxies inside circles of different radii r in the range $5\,h^{-1}$Mpc to $150\,h^{-1}$Mpc. The comparison of the galaxy distribution with different realizations of point distributions from an N-Body simulation has been presented. It has been concluded that the galaxy distribution in the volume limited subsamples of sloan digital sky survey is homogeneous on large scales well within the survey region.

Contents

Acknowledgements **iv**

List of publications **vi**

Abstract **viii**

1 Introduction **1**

1.1 **Motivation of our investigation** 3

1.2 **Hot Big Bang** 5

1.2.1 Cosmic Expansion 7

1.2.2 Cosmic Constituents 7

1.2.3 The ΛCDM Model 11

1.3 **The Gravitation Instability** 12

1.4 **The Linear Regime** 14

1.4.1 Cosmic Velocity Flow Perturbations 15

1.4.2 Growth of Cosmic Structure 16

1.5 **Gaussian Random Fields** 17

1.5.1 The shape of the power spectrum 19

1.6 **The nonlinear Regime** 20

1.6.1 Hierarchical Clustering 21

1.6.2 Anisotropic collapse 23

1.6.3 The Cosmic Web 25

1.7 **Ideas about Galaxy Distribution** . . . 26
1.7.1 The cosmological Principle . . . 28
1.8 **Surveys of Cosmic Structures** . . . 28
1.8.1 Cfa and SSRS survey . . . 29
1.8.2 The Las Campanas Redshift Survey . . . 30
1.8.3 2dF galaxy redshift survey . . . 30
1.8.4 Sloan Digital Sky Survey . . . 30
1.9 **Goals and outline of this thesis** . . . 31

2 Statistical tools to analyze Distribution of Galaxy 34
2.1 **Introduction** . . . 34
2.2 **The Standard Correlation Function Analysis** . . . 36
2.2.1 Estimators of Two point Correlation Function . . . 40
2.2.2 Difficulties of the Standard Analysis . . . 42
2.2.3 Higher Order Correlation Function . . . 44
2.3 **Other Statistical Measures** . . . 45
2.3.1 Moments of Counts in Cells and Void Probability . . . 45
2.3.2 Nearest Neighbor Distances . . . 46
2.3.3 Need of fractal Hypothesis . . . 46
2.4 **On the "Definition" of Fractals** . . . 47
2.4.1 Application of fractals . . . 48
2.4.2 The Hausdorff Dimension . . . 49
2.4.3 Fractal Dimension of orthogonal projections and intersections . . . 51
2.5 **Other Fractal Dimensions** . . . 52
2.5.1 Similarity Dimension . . . 52
2.5.2 Box Counting Dimension . . . 55
2.6 **Probability and Probability Measure** . . . 57
2.6.1 Information Dimension . . . 58
2.6.2 Correlation Dimension . . . 59

2.6.3 The Generalized Dimension 60
2.7 **Lacunarity** 62

3 Fractal Dimensions of a Homogeneous and Weakly Clustered Distribution 64
3.1 **Introduction** 65
3.2 **Fractal Dimensions** 69
3.3 **Fractal Dimension for a Homogeneous Distribution** 73
3.4 **Fractal dimension of a Weakly Clustered Distribution** 75

A 78
A.1 **Derivation of D_q for Homogeneous Distribution** 78
A.2 **Derivation of D_q for a Weakly Clustered Distribution** 80

4 Fractal Dimension as a measure of Homogeneity 85
4.1 Introduction 86
4.2 **Multifractal Multinomial Distribution** 87
4.3 **Discussion** 92
4.4 **Conclusions** 98

5 Testing homogeneity on large scales in the Sloan Digital Sky Survey 100
5.1 **Introduction** 101
5.2 **Galaxy Sample : The Sloan digital Sky Survey** 105
5.2.1 Redshift-Distance Formula 108
5.2.2 SDSS-DR1 110
5.2.3 N-Body Data 111
5.3 **Method of Analysis** 112
5.4 **Results and Discussions** 116

B 122
B.1 **Survey Coordinate System** 122

B.2 **SQL Query to get data from SDSS Data Server** 122

6 Summary and future prospectus **124**

List of Tables

1 Most recent derived values of cosmological parameters (WMAP5 +SDSS; Komatsu et al., 2008) 11
1 Generation of various multinomial multifractal Distribution 88

List of Figures

1.1 Large scale structures in SDSS main galaxy redshift sample 2
1.2 Sky projection of Cosmic Microwave Background 9
2.1 Graph of the Hausdorff d-measure $H_d(F)$ against d for a set F 50
2.2 Construction of the von Koch curve 54
4.1 Multifractal Multiplicative cascade distribution of points 89
4.2 Comparison of our model with observed fractal dimension for a random Distribution of points 90
4.3 Comparison of our model with observed fractal dimension for a weakly clustered distribution Distribution of points 91
4.4 Linearly extrapolated two point correlation function for the best fit model for WMAP-3 93
4.5 Estimated deviation of the Minkowski-Bouligand dimension from the physical dimension 95
4.6 Components of ΔD_q for an LRG like population of galaxies for $q = 4$ 97
5.1 SDSS Telescope 106
5.2 Projection of SDSS DR6 Imaging sample 107
5.3 Projection of SDSS DR6 spectroscopic sample 108
5.4 Two dimensional galaxy distribution of SDSS 111
5.5 Two dimensional galaxy distribution of the simulated slices of $\Lambda\mathrm{CDM}$ model 113
5.6 $C_q(r)$ for $q = -4$ 117
5.7 $C_q(r)$ for $q = 4$ 118
5.8 The spectrum of generalized dimension 119

Chapter 1

Introduction

Cosmology is the Scientific study of the cosmos a whole. An essential part of cosmology is to test theoretical models with observations. During the last decades we have witnessed an unprecedented advance in both theory and observations of the Universe. For the first time we have the tools to answer some of the most fundamental questions in cosmology.

The current paradigm of cosmology states that the the Universe originated some 13.7 billion years ago as an extremely energetic event out of which all matter, energy and indeed spacetime emerged into existence. This is known as the Hot Big Bang Theory (Hoyle, 1950). This extremely dense and hot Universe expanded and cooled down. The evolution of the Universe is dictated by gravity which is the weakest force in nature. The Big Bang Theory provides an answer to the evolution of the Universe and its global properties. However, understanding of the theory of structure formation is still incomplete within the framework of Big Bang Cosmology.

The large galaxy surveys indicate that the galaxy and matter distribution on scales even up to a few dozen Megaparsecs is far from homogeneous (see figure 1.1). Starting with systematic redshift surveys like the CfA survey (Huchra & Geller, 1982; de Lapparent, Geller & Huchra, 1986) and the Las Campanas Redshift Survey (Shectman et al., 1996) up to the major 2dFGRS and SDSS mapping campaigns (Colless et al., 2003), we have learnt that galaxies are large associations of different objects from a few up to hundreds of Megaparsec (Oort, 1983).

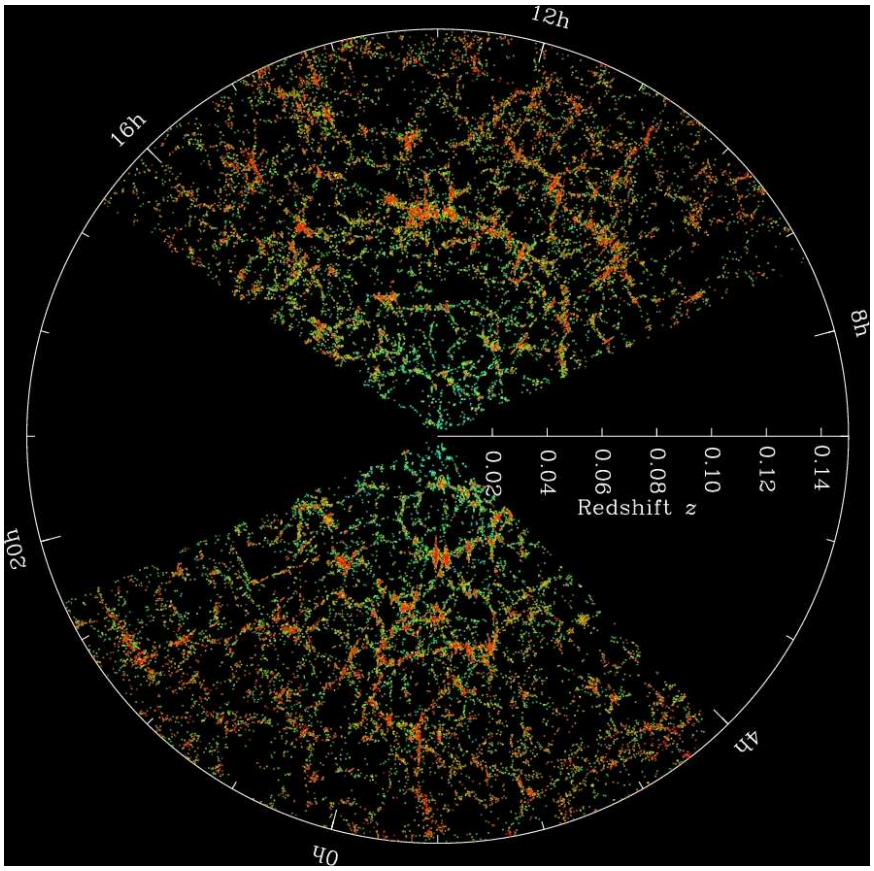


Figure 1.1: Slices through the SDSS $3-$dimensional map of the distribution of galaxies. Earth is at the center, and each point represents a galaxy, typically containing about 100 billion stars. Galaxies are colored according to the ages of their stars, with the redder, more strongly clustered points showing galaxies that are made of older stars. The outer circle is at a distance of two billion light years. The region between the wedges was not mapped by the SDSS because dust in our own Galaxy obscures the view of the distant universe in these directions. Both slices contain all galaxies within -1.25 and 1.25 degrees declination. Figure Courtesy : Michael Blanton and the Sloan Digital Sky Survey team

The most outstanding concentrations of galaxies are the clusters of galaxies (Bahcall, 1989). They are the most massive, and most recently fully collapsed and virilized objects in the Universe. The richest clusters contain many tens (~ 50 to 1000) of galaxies within a relatively small region of only a few Megaparsecs in length scale. A typical example of a rich cluster is the Coma cluster $A1656$. Clusters of galaxies contain dense and compact concentrations of dark matter, representing overdensities $\Delta \approx 1000$. Galaxies and stars only form a minor constituent of clusters, they are trapped and embedded in the deep gravitational wells of dark matter. These are best identified as a bright source of X-ray emission, emerging from the diffuse extremely hot $(107-108K)$ intracluster gas trapped inside them (Böhringer et al., 2001). A richly structured network of elongated filaments bridges the space in between massive clusters. They form highly coherent canals along which matter is accreted on to the clusters located at the nodes of the network. The canonical example of a filament is the Pisces-Perseus supercluster, a system of clusters and filaments extending over more than $100h^{-1}Mpc$. It includes the massive Perseus cluster which is one of the most prominent clusters in the nearby Universe.

Filaments appear to frame tenuous planar agglomerations known as walls. Because of their low surface density walls are usually difficult to identify. Walls and filaments define the boundaries of vast near-empty regions of space, the voids, with dimensions ranging up to $30-50h^{-1}Mpc$ (see e.g. Kirshner et al., 1981, 1987; de Lapparent, Geller & Huchra, 1986; Colless et al., 2003). Voids play a dominant role in the spatial organization of matter on Megaparsec scales. While they occupy most of space, their narrow spacing define a framework of interconnected clusters, filaments and walls that pervades the whole of the visible Universe. This pattern has become known as the Cosmic Web (Bond, Kofman & Pogosyan, 1996; Springel, 2005).

1.1 Motivation of our investigation

A large amount of theoretical work has been directed towards understanding the formation and properties of the elements of the Cosmic Web as a result of the gravitational

growth of initially tiny random density and velocity fluctuations (Peebles, 1980; Springel, 2005). These studies describe the formation and properties of the structural elements of the Cosmic Web based on the primordial density field. Some of them can be used to obtain a general or statistical description of its individual components (Zel'Dovich, 1970; Bardeen et al., 1986; Bond & Myers, 1996a; Shen et al., 2006) while others go one step further and elucidate the complex relation between them (Bond, Kofman & Pogosyan, 1996); see also (van de Weygaert, 2002, 2005). The different morphologies of the Cosmic Web define unique cosmic environments in terms of local density, dynamics and gravitational influence. This is reflected in their internal structure and particular dynamics. The influence of the Cosmic Web is also seen on galactic scales. The same processes that give rise to the Megaparsec scale matter distribution also affect the properties of the galaxies.

A detailed statistical analysis of the Cosmic Web is very much relevant for our understanding of the formation of structure in the Universe. It is also important for defining the diverse cosmic environments in which galaxies form and evolve. There are some techniques for identifying and quantifying the morphological elements in the Cosmic Web, however, many of them have several limitations.

A proper characterization of the Cosmic Web is crucial in order to identify, differentiate, select and isolate the different morphological and dynamical environments. The availability of such a method would open up unprecedented possibilities for a much better, focused and well-defined study of the cosmic web. It will provide a physically better definition of cosmic environment than hitherto available and pave the way for a crisp and considerably improved assessment and understanding of the influence on the formation of galaxies.

In the rest of this chapter we review the basic theoretical background that will be used in this thesis. Section 1.2 describes the Hot big Bang model of the Universe. We describe a theoretical framework for growth of structures from primordial fluctuation in section 1.3. The linear as well as non linear regimes of structure formation are described in section 1.4 to 1.6. The ideas of galaxy distribution and observations are explained in

section 1.7 and 1.8. We conclude this chapter by defining the goals and an outline of this thesis in section 1.9.

For a more complete discussion we refer the reader to the textbooks by Peebles (1980, 1993); Padmanabhan (1993, 2002); Peacock (1999); Narlikar (2002); Coles & Lucchin (2002); Liddle & Lyth (2000); Martínez & Saar (2002) and Gabrielli et al. (2005). For a good and up-to-date overview of the current knowledge on the Big Bang universe see Roos (2008).

1.2 Hot Big Bang

The theoretical framework on which most theories of our Universe are based is the Cosmological Principle. It states that the Universe is homogeneous and isotropic. General theory of relativity, proposed by Albert Einstein, explains and describes gravity. General relativity is a metric theory that describes gravity as the manifestation of the curvature of spacetime. This theory implies that the Universe should either be expanding or contracting. This is true for universes with flat, hyperbolic and spherical curvature. Usually these curvatures are denoted by means of the scaled curvature coefficient k. It has the values $k = 0$ for a flat space, $k = +1$ for a spherical space and $k = -1$ for a negatively curved hyperbolic space. The spacetime metric of these universes can be described by the Robertson-Walker metric,

$$ds^2 = c^2dt^2 - a^2(t)\left(dr^2 + {R_c}^2{S_k}^2\left(r/R_c\right)\left(d\theta^2 + sin^2\theta d\phi^2\right)\right) \tag{1.1}$$

where R_c is the radius of curvature and $S_k(r)$ is the function given by

$$S_k(x) = \begin{cases} \sin(x) & k = +1 \\ x & k = 0 \\ \sinh(x) & k = -1 \end{cases} \tag{1.2}$$

The variable t is the proper *cosmic time*, synchronized on the basis of Weyl's postulate[1]. The dimensionless scale factor $a(t)$ describes the expansion (or contraction) of the Universe and may be normalized with respect to the present-day value, i.e. $a(t_0) = 1$. c is the velocity of light and r, θ, ϕ are the usual spherical coordinates. Friedman (1922) solved Einstein's field equations for general homogeneous and isotropic Universe models and derived the time dependence of the expansion factor. The resulting equations are known as the Friedman-Robertson-Walker-Lemaitre (FRW) equations. They form the basis of almost all of modern cosmology,

$$\frac{\ddot{a}}{a} = -\frac{4\pi G}{3}\left(\rho + \frac{3p}{c^2}\right) + \frac{\Lambda}{3} \tag{1.3}$$

and

$$\left(\frac{\dot{a}}{a}\right)^2 = \frac{8\pi G\rho}{3} - \frac{kc^2}{a^2 {R_0}^2} + \frac{\Lambda}{3} \tag{1.4}$$

In the Friedman-Robertson-Walker-Lemaitre equations G is Newton's gravitational constant, ρ is the energy density of the universe, p is the pressure of the various cosmic components, Λ is the cosmological constant and R_0 is the present-day value of the curvature radius.

The evolution of the energy density (ρ) of the Universe can be inferred from the energy equation obtained by combining the FRW equation 1.3 and 1.4. This is given by

$$\dot{\rho} + 3\left(\rho + \frac{p}{c^2}\right)\frac{\dot{a}}{a} = 0 \tag{1.5}$$

The macroscopic nature of the medium is expressed by the equation of state, $p = p(\rho)$, which for most cosmologically relevant components may be expressed as

$$p = w\rho c^2. \tag{1.6}$$

[1]Weyl's postulate states that the world lines of galaxies form a bundle of non-intersecting geodesics orthogonal to a series of spacelike hypersurfaces. This series of hypersurfaces allows for a common cosmic time and the spacelike hypersurfaces are the surfaces of simultaneity with respect to this cosmic time

Here w is called the equation of state parameter. Equation 1.5 and 1.6 can be combined to give the evolution of energy density with the expansion of the Universe:

$$\rho(t) \propto a(t)^{-3(1+w)}. \tag{1.7}$$

1.2.1 Cosmic Expansion

The expansion rate of the Universe is expressed in terms of the Hubble parameter,

$$H(t) = \frac{\dot{a}}{a}. \tag{1.8}$$

The present-day value of $H(t)$, sometimes called the Hubble "constant", is often parameterized in terms of a dimensionless factor h ($= H_0/100\,km^{-1}\ s\ Mpc$), where H_0 is the Hubble constant expressed in units of $km\ s^{-1}\ Mpc^{-1}$. The expansion of the Universe does not only express itself in continuously growing distances between any two objects, it also leads to the increase of the wavelengths of photons. This resulting cosmological redshift z of a presently observed object is given by the relation

$$1 + z = \frac{a(t_0)}{a(t)} = \frac{1}{a(t)} \tag{1.9}$$

where $a(t)$ is the expansion factor of the Universe at the time the observed light was emitted.

1.2.2 Cosmic Constituents

The evolution of the Universe is fully dictated by its energy density ρ and its curvature k. The energy density of the Universe is conveniently expressed in terms of the density needed to produce a geometrically flat Universe, the *critical density*:

$$\rho_c(t) = \frac{3H^2}{8\pi G}. \tag{1.10}$$

The value of critical density at present epoch is thus $\rho_{c,0} = \rho_c(t = 0) = 1.9 \times 10^{-29}[\, h^2 g/cm^3]$. The contribution of any component towards the energy density of the Universe may be expressed in terms of the ratio of its energy density to the critical density. This ratio is denoted by $\Omega(t)$, the *density parameter*, and is expressed as:

$$\Omega(t) = \frac{\rho(t)}{\rho_c(t)} = \frac{8\pi G\rho}{3H^2}. \tag{1.11}$$

The value of $\Omega(t)$ at $t = t_0$ (denoted by Ω) is given by

$$\Omega = \frac{8\pi G\rho_0}{3{H_0}^2}. \tag{1.12}$$

The Universe contains a variety of components. While the contributions of e.g. magnetic fields and gravitational waves may be held negligible, the most important ingredients of the Universe are radiation, baryonic matter, nonbaryonic dark matter and dark energy. The equation of state parameter w for radiation and matter (baryonic as well as non baryonic) is 1/3 and 0 respectively, whereas for dark energy its value is less than $-1/3$. If the dark energy is in the form of a cosmological constant, then $w = -1$. Thus equation 1.7 suggest that radiation ($\rho_r \propto a^{-4}$), matter ($\rho_m \propto a^{-3}$) and dark energy ($\rho_\Lambda = constant$) have evolved differently with the expansion of the Universe.

As the radiation cools off as a result of the expansion of the Universe, its spectrum peaks at microwave wavelengths and is observed today in the form of the **Cosmic Microwave Background** (CMB) with a temperature of $T_0 = 2.725K^\circ$. Since the temperature of radiation scales in inverse proportion to the scale factor ($T \propto a^{-1}(t)$), it must have been very high in the early Universe. The almost perfect blackbody spectrum of CMB defines the strongest evidence for the existence of a very hot and dense phase in the early Universe, i.e. for the Hot Big Bang (see figure 1.2). Technically speaking we should also include cosmic neutrinos in the radiation bill, even though they do not interact with any other cosmic species beyond $z \sim 10^{11}$ and are approximately 4 times less abundant than photons. At very early times radiation was dynamically dominant component of the Universe. Its current density is about $10^{-34} g\ cm^{-3}$ and constitutes

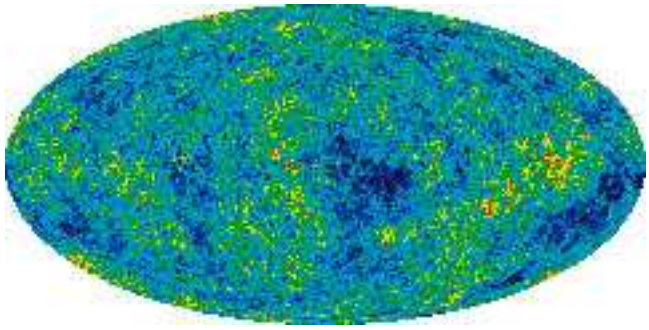


Figure 1.2: Sky projection of the Cosmic Microwave Background (CMB). The shades of gray correspond to temperature fluctuations. Courtesy of the WMAP team.

only a fraction 10^{-5} of the total density.

Baryonic matter Ω_b is the normal matter we ourselves, planets and stars are made of. It is mainly in the form of protons and neutrons (and also electrons). However, it only represents a minor cosmological component and accounts for a mere 4.4% of the energy content of the Universe. Nonbaryonic Dark Matter Ω_{dm} is a very important component for the formation of structures in the Universe. It accounts for $\approx 23\%$ of the energy content of the Universe. The combined contribution of matter (baryonic and non baryonic dark matter) to the energy density is usually expressed as Ω_m. One of the most pressing problems in astrophysics is the identity of this dark matter. While its presence is unmistakably felt through its gravitational attraction, it has as yet escaped direct observation or detection in the laboratory. The commonly accepted view is that it is some unknown weakly interacting particle, presumably some of the particles predicted by supersymmetric theories. Dark matter is pressureless and insensitive to the electromagnetic influence of radiation.

Fluctuations in the dark matter could have started growing as soon as matter began to dominate the dynamics of the Universe at around the epoch of *matter-radiation equality* ($\rho_r = \rho_m$). This occurs at a scale factor of $a(t) \approx 10^{-4}$. The growth of these fluctuations in the dark matter created the gravitational potential wells. After the baryonic matter and radiation decoupled at the epoch of recombination, the baryonic matter started

falling into these gravitation potential wells. This process is believed to have led to the formation of galaxies and stars. Without dark matter it would have been impossible to form the rich structure we observe in today's Universe.

Finally, we now have conclusive evidence to suggest that Universe at the present epoch is undergoing an accelerated expansion (i.e $\ddot{a} > 0$). This could be due to the presence of an elusive medium called *Dark Energy*. Dark Energy (Ω_Λ) is the most dominant component of our Universe at the present epoch. It accounts for $\approx 73\%$ of cosmic energy density. The nature of Dark Energy is even more mysterious than dark matter. All that can be said about dark energy is that it has a negative pressure. This is apparent from equation 1.3 which suggests that for ($\ddot{a} > 0$) we need $p < -\rho/3$. Most observational studies agree with the Dark Energy being equivalent to a cosmological constant although other options are still viable.

The influence of dark energy on the structure formation process is mainly related to its impact on the expansion rate and timescales in the Universe. As soon as the expansion rate of the Universe becomes too high, structure formation comes to a halt. On the other hand, it has stretched the time available in the past to form and evolve structure. It is once again stressed that the evolution of energy density of radiation, matter and dark energy is governed by energy equation given by 1.5.

The cosmological framework of the Hot Big Bang in a spatially homogeneous and isotropic Universe is so widely accepted that it is called the *Standard Hot Big Bang Model*. This model is supported by a number of observations,

- The relation between distance and recession velocity (Hubble Law) as a consequence of its metric and also implies that the Universe has a finite age.

- The almost perfect black-body spectrum of the Cosmic Microwave Background, which is evidence for an extremely hot initial phase of the Universe.

- The excellent match in the observed abundances of light elements and predictions from primordial nucleosynthesis.

- The evident evolution of the appearance of objects as function of their distance from us.

1.2.3 The ΛCDM Model

Our current understanding of the components of the Universe is encoded in the Lambda Cold Dark Matter (ΛCDM) model. In this model we attempt to explain supernova observations in terms of the accelerated expansion of the Universe. This model is also capable of explaining the observed Cosmic Web and the Cosmic Microwave Background. In the acronym ΛCDM, the term Λ refers to the dark energy (Ω_Λ) which is believed to be the driving force behind the accelerated expansion of the Universe at the present epoch. Λ is assumed to have the form of a cosmological constant ($w = -1$). *Cold Dark Matter* refers to a model where the dark matter is explained as being *cold*, i.e., its velocity was non relativistic at an epoch when it decoupled from other constituents of the Universe. This type of dark matter is assumed to be non-baryonic, dissipationless and collisionless. The ΛCDM model has several parameters from which the most important are shown in table 1. In this thesis we base ourselves on the ΛCDM .

Parameter	Value	Description
H_0	$70.4 \pm 2.4 km\ s^{-1}\ Mpc^{-1}$	Hubble parameter
Ω_m	0.277 ± 0.029	Matter Density
Ω_b	0.0459 ± 0.0028	Baryon Density
Ω_Λ	0.723 ± 0.029	Dark Energy Density
ρ_{c0}	$0.94 \pm 0.07 \times 10^{-26} kg\ m^{-3}$	Critical Density
t_0	$13.72 \pm 0.14 Gyr$	Age of the Universe
σ_8	0.811 ± 0.032	Galaxy fluctuation amplitude
n	0.960 ± 0.014	Spectral Index

Table 1: Most recent derived values of cosmological parameters (WMAP5 +SDSS; Komatsu et al., 2008)

1.3 The Gravitation Instability

The fact that at the present time we see structures even at scales of hundreds of Mega-parsecs requires an explanation. In order to understand this fact the primordial Universe is assumed to have been completely homogeneous. Quantum fluctuation created during inflation led to perturbation to this homogeneous background. These fluctuations amplified under the influence of gravitational field, ultimately resulting in the wealth of structures we can see today pervading the Universe at different scales. The theoretical framework that describes the growth of structures from the primordial fluctuations is called the *gravitational instability theory*.

An integral ingredient of today's standard cosmological model is the assumption that origin of fluctuations is to be found in the very early universe during the inflationary phase. Shortly after the Big Bang the Universe entered a phase of extremely rapid expansion. Presumably this phase may be identified with the GUT transition at $\approx 10^{-34}$ seconds after the Big Bang. Small quantum fluctuations present in the first instants of the Universe were blown up to cosmological scales. Not only does this imply a Universe marked by an inhomogeneous matter and energy distribution, it also predicts the fluctuations to have the character of a spatial Gaussian random field. The inhomogeneities in the primordial density field can be conveniently expressed as the fluctuations in density field superimposed on a uniform and isotropic background.

Consider a density field $\rho(\mathbf{x}, \mathbf{t})$. The average density $\bar{\rho}(t)$ for such a field can be defined by taking average over a constant time hypersurface. This can be expressed as,

$$\bar{\rho}(t) = \frac{\int \rho(\mathbf{x}, \mathbf{t}) d^3\mathbf{x}}{\int d^3\mathbf{x}} \tag{1.13}$$

The density fluctuation in such a field can now be defined as

$$\delta\rho(\mathbf{x}, \mathbf{t}) = \rho(\mathbf{x}, \mathbf{t}) - \bar{\rho}(\mathbf{t}) \tag{1.14}$$

In the linear theory, we expand the equation of motion around the homogeneous universe.

To this end, one commonly introduces a dimensionless density contrast given by

$$\delta(\mathbf{x},\mathbf{t}) = \frac{\delta\rho(\mathbf{x},\mathbf{t})}{\bar{\rho}(\mathbf{t})} \tag{1.15}$$

Henceforth, we shall be denoting $\delta(\mathbf{x},\mathbf{t})$ by $\delta(\mathbf{x})$ and $\delta(\mathbf{t})$ by δ just for symbolic convenience. The gravitational acceleration at any position can be described as the contribution from all the matter fluctuations present in the density field,

$$g(\mathbf{x}) = Ga\bar{\rho}(\mathbf{t}) \int \frac{\delta(\mathbf{x}')(\mathbf{x}'-\mathbf{x})}{|\mathbf{x}'-\mathbf{x}|^3} d^3\mathbf{x}' \tag{1.16}$$

where all the symbols have their usual meaning.

The formation of structures is the result of the gravitational growth of the primordial density fluctuations. Gravity has an amplifying effect on the initial fluctuations. Any region with a density higher than its surroundings will collapse and increase its level of density contrast. The increase in density contrast will reflect in the gravitational field attracting even more matter into the initial perturbation. The opposite effect occurs in underdense regions. As matter flows out of them they become less dense. The gravitational force will be weaker and more mass will escape from the underdense region. All in all this will result in a runaway process in which any existing perturbation will be amplified. Overdense regions will collapse until they become bound objects and underdense regions will expand until they are devoid of matter.

After the epoch of matter radiation equality the Universe is matter dominated and hence can be assumed to be pressureless to a good approximation. On cosmological scales one may, to a good approximation, describe the evolution of the cosmic density field by a set of three coupled differential equations involving the density contrast δ, the peculier velocity $\mathbf{v}$ and the gravitational potential ϕ :

- The continuity equation which ensures mass conservation is given by,

$$\dot{\delta} + \nabla.[(1+\delta)\mathbf{v}] = 0 \tag{1.17}$$

- The Euler equation which is the equation of motion of a fluid element can be expressed as

$$\dot{\mathbf{v}} + \frac{\dot{a}}{a}\mathbf{v} + \frac{1}{a}(\mathbf{v}.\nabla)\mathbf{v} = -\frac{1}{a}\nabla\phi \tag{1.18}$$

- The Poisson equation relating the distribution of matter and the gravitational field is represented as

$$\nabla^2\phi = 4\pi G\bar{\rho}a^2\delta \tag{1.19}$$

1.4 The Linear Regime

In the case of small fluctuations ($\delta \ll 1$) and small streaming motions, δ and v can be computed from linear perturbation theory (Peebles, 1980). In the linear approximation the evolution equation of δ is given by

$$\frac{\partial^2\delta}{\partial t^2} + 2\frac{\dot{a}}{a}\frac{\partial\delta}{\partial t} = 4\pi G\bar{\rho}\delta \tag{1.20}$$

This second order differential equation describes the time evolution for the mass fluctuation $\delta = \delta\rho/\rho$ for a pressureless fluid. The solution to this differential equation involves two modes,

$$\delta = A(x)D_1(t) + B(x)D_2(t) \tag{1.21}$$

where D_1 and D_2 are linearly independent function. They correspond to one growing and one decaying solution. Usually, one concentrates on the growing mode because the decaying solution is damped and becomes subdominant. Taking $D_1(t)$ as the growing mode and $D_2(t)$ as the decaying mode we can simplify equation 1.21 as

$$\delta = A(x)D_1(t). \tag{1.22}$$

For a generic FRW Universe in which we ignore the radiation contribution, we may find the following general expression for the growing mode:

$$D_1(z) = \frac{5\Omega_{m,0}H_0}{2}H(z)\int_z^\infty \frac{1+z'}{H^3(z')}dz' \tag{1.23}$$

where $H(z)$ is the Hubble parameter, defined as

$$H(z) = H_0[\Omega_m(1+z)^3 + \Omega_k(1+z)^2 + \Omega_\Lambda]^{1/2}, \tag{1.24}$$

Here $\Omega_k = 1 - \Omega_m - \Omega_\Lambda$. In the Einstein-de Sitter model the expansion parameter varies as $a \propto t^{2/3}$ and the solution of equation 1.20 is

$$\delta = At^{2/3} + Bt^{-1} \tag{1.25}$$

1.4.1 Cosmic Velocity Flow Perturbations

In the linear regime (and also $\delta \ll 1$), using the growing mode solution of δ (i.e. equation 1.22), the continuity equation takes the form

$$\nabla.\mathbf{v} = -a\dot{\delta} = -a\delta\frac{\dot{D_1}(t)}{D_1(t)} \tag{1.26}$$

From the Helmholtz theorem we can express the velocity field as a sum of a divergence free part and an irrotational part. The divergence free part does not contribute to the evolution of the density contrast (δ) and decays as $a^{-1}(t)$ (Peebles, 1980). The solution for the curl free part is given by

$$\mathbf{v}(\mathbf{x}) = a\frac{fH}{4\pi}\int \frac{\mathbf{y}-\mathbf{x}}{|\mathbf{y}-\mathbf{x}|^{\mathbf{3}}}\delta(\mathbf{y})d^3\mathbf{y} \tag{1.27}$$

where

$$f = \frac{a}{\dot{a}}\frac{\dot{D_1}(t)}{D_1(t)} = \frac{1}{H}\frac{\dot{D_1}(t)}{D_1(t)} = \frac{d\log D_1(t)}{d\log a} \tag{1.28}$$

Comparing equation 1.27 with the equation for acceleration i.e. equation 1.16, we see that the peculiar velocity can be written as

$$\mathbf{v} = \frac{fH}{4\pi G\bar{\rho}}\mathbf{g} = \frac{2}{3}\frac{f}{\Omega_m H}\mathbf{g} \tag{1.29}$$

1.4.2 Growth of Cosmic Structure

At early times in a matter-dominated Universe the growth of structure closely resembles that in an Einstein de Sitter Universe at the time $\Omega_m \approx 1$,

$$D_1(t) \approx a(t) \propto t^{2/3}. \tag{1.30}$$

As the Universe evolves and becomes increasingly empty it enters a nearly free expanding phase when the scale factor is given by

$$a_f = \frac{1}{1/\Omega_o - 1}. \tag{1.31}$$

After this time it expands according to

$$a(t) \approx H_0 t \tag{1.32}$$

The growth of structure in such a scenario freezes out as gravity is no longer able to counter the fast cosmic expansion. Hence

$$D_1(t) \approx constant. \tag{1.33}$$

In a Λ-dominated Universe growth of structures comes to a halt in such a situation. The crucial transition time is that where dark energy takes over the dynamics, setting the Universe in a phase of accelerated expansion:

$$a_{m,\Lambda} = \left(\frac{\Omega_m}{2\Omega_\Lambda}\right)^{1/3} \tag{1.34}$$

In the concordance model this corresponds to $z \approx 0.7$.

This, however, does not imply that the the growth of structures freezes out completely. The growth of structures continues on small scales as long as they are embedded in an overdense region detached from the general expansion. The regions in the vicinity of filaments and clusters remain dynamically active and matter still flows into clusters far beyond the time at which the Universe enters free expansion. This results in overdense chunks of matter becoming isolated islands in the expanding Universe.

1.5 Gaussian Random Fields

The primordial perturbations in the cosmic matter and energy density are assumed to constitute a stochastic field of spatially random fluctuations. The density field of the early Universe is assumed to be a near perfect *Gaussian random field*. In addition to the observed near-Gaussianity of the Cosmic Microwave Background temperature anisotropies, the two important rationales behind this expectation are

1. The Gaussian nature of quantum fluctuation arising due to inflation and then expanding into macroscopic fluctuation.

2. The Central Limit Theorem which states that the sum of a sufficiently large number of identically distributed independent random variables each with finite mean and variance is approximately normally distributed

We can think of the description of a spatial random field in terms of its n-point probability distribution (**PDF**) $P^{(n)}\left(\delta_1, \delta_2, \delta_3, \cdots, \delta_n\right)$. The fluctuations in the primordial density field are assumed to be Gaussian, meaning thereby that the PDF is given by

$$P^{(n)}\left(\delta_1, \delta_2, \delta_3, \cdots, \delta_n\right) d\delta_1, d\delta_2, \cdots, d\delta_n = \frac{\exp\left[-\frac{1}{2}\delta_i \left(M^{-1}\right)_{i,j} \delta_j\right]}{\left(2\pi\right)^{n/2} \left(detM\right)^{1/2}} \Pi_{i=1}^{N} d\delta_i \tag{1.35}$$

where $M_{i,j} = \langle \delta_i \delta_j \rangle$ is the covariance matrix. The averaging is performed over ensembles. Under the assumption of ergodicity, averages over space approaches averages over en-

sembles of Universes. The covariance matrix determines the variance of the distribution, and the correlation properties of the fluctuation field. For a homogeneous Universe it is given by :

$$M_{i,j} = \langle \delta_i \delta_j \rangle = \xi \left(\mathbf{x_i} - \mathbf{x_j} \right) \tag{1.36}$$

where $\xi(\mathbf{r})$ is the autocorrelation of the density field. For a discrete point distribution it is usually referred to as the *two-point correlation function* which in the isotropic case is simply $\xi(\mathbf{r}) = \xi(r)$. This reflects the fact that the two point correlation function only depends on the mutual distance between the points. Phase information is lost, limiting our ability to describe the patterns present in the matter distribution. The statistical properties of a Gaussian random field, however, are completely determined by its two-point correlation function which is the inverse Fourier transform of the *power spectrum*:

$$\langle \delta(\mathbf{x}) \delta(\mathbf{x} + \mathbf{r}) \rangle = \int \frac{d^3\mathbf{k}}{(2\pi)^3} P(k) \exp^{-\mathbf{ikr}} \tag{1.37}$$

It also defines the amplitude of density perturbations,

$$\sigma^2 = \frac{1}{(2\pi)}^3 \int d^3k P(k) = \int \frac{d \log k}{2\pi^2} k^3 P(k), \tag{1.38}$$

where $k^3 P(k)$ encapsulates the contribution of fluctuations at wavenumber k to the general fluctuations field. For a simple power-law power spectrum $P(k) \propto k^n$, the corresponding fluctuations on a mass scale are easily shown to be:

$${\sigma_m}^2 \propto M^{-(n+3)} \tag{1.39}$$

In other words, as long as $n > -3$ the fluctuation level is a decreasing function of the mass scale. Such scenarios are called hierarchical clustering scenarios.

1.5.1 The shape of the power spectrum

The initial shape of the power spectrum is governed by those quantum processes which were responsible for the generation of primordial density fluctuation. These fluctuations grew to sizes larger than Hubble radius (cH^{-1})during inflation. In the post inflationary era, these perturbations re-entered the Hubble radius. The perturbation at the epoch of hubble radius exit determine the nature of perturbation at the Hubble radius re-entry from Bardeen's gauge invariant formalism (Seshadri, 1988). In most inflationary models, the primordial power spectrum is scale invariant or has a weak dependence on k when the corresponding mode enters the Hubble radius. After re-entry, to the Hubble radius of the expanding Universe, the fluctuations could start growing. The resulting power spectrum is of the form given by

$$P(k) \propto k^n. \tag{1.40}$$

with $n \approx 1$. This is commonly referred to as the Harrison-Zel'dovich spectrum (Harrison, 1970). This scale-free power spectrum has the property that any perturbation in the metric or gravitational potential are independent of scale

$$\frac{d\sigma^2(\phi)}{d\ln k} = constant. \tag{1.41}$$

Harrison (1970), Zel'Dovich (1970) and Peebles & Yu (1970), all pointed out its importance well before inflation was suggested. The index $n \sim 1$ is now seen as one of the essential predictions of inflation and has been already observed by $WMAP$. There are other possibilities with tilted power spectra $n \neq 1$. In this thesis we will restrict ourselves to the Harrison-Zel'dovich spectrum in a universe with *cold* dark matter.

Once fluctuations have become smaller than the horizon they are affected by gravity and damping processes. Fluctuations in baryonic matter cannot grow as a result of the pressure of the coupled baryon-photon fluid, i.e. as long as they are smaller than the corresponding Jeans length. The fluctuations in dark matter hardly grow as long as the constituents of the Universe is dominated by radiation. Only after matter takes over as

the dynamically dominant component following the epoch of radiation matter equality, the dark matter perturbations begin to grow. These processes give their characteristic shape to the *cold dark matter power spectrum*. This information is encoded in the transfer function

$$P(k,z) = A(z)k^n T^2(k,z). \tag{1.42}$$

where $A(z)$ is a normalization constant determined observationally and T is the transfer function. We follow the expression for T_{cdm} given by Bardeen et al. (1986):

$$T_{cdm} = \frac{\ln(1+2.34q)}{2.34q}\left(1+3.89q+(16.1q)^2+(5.46q)^3+(6.71q)^4\right)^{-1/4}, \tag{1.43}$$

where $q \equiv \frac{k}{\Gamma}\, hMpc^{-1}$ and

$$\Gamma = \Omega_0 h \exp\left(-\Omega_b\left(1+\sqrt{2h}/\Omega_0\right)\right) \tag{1.44}$$

is the shape parameter given by Sugiyama (1995).

The power spectrum at small scales goes as k^{-3} indicating that asymptotically it is a hierarchical scenario. On the large scales it remains as the Harrison-Zel'dovich spectrum set in the inflationary epoch. The horizon scale at the time when matter and radiation densities were equal is reflected in the power spectrum as the turnover point. This marks the point when matter overcame radiation in the dominance of the dynamics of the Universe.

1.6 The nonlinear Regime

The linear regime provides a useful description for the early phases of evolution of the Universe and it ceases to be valid as the density contrast approaches unity. Since the full nonlinear solutions are in general too complex to solve analytically, one must rely on other alternatives such as solutions for simple configurations and numerical methods. N-body computer simulations are the most common tool to study the formation and

evolution of structures in the nonlinear regime. They follow the trajectory of particles sampling the underlying density field. While the primordial linear density field can be well described as a Gaussian random field, in the non linear regime non-gaussianities creep in, making the understanding of the the evolution of density field a lot more complicated. The distribution of matter in the Universe at the present time has three important properties that are the result of the processes that gave it shape:

1. Hierarchical Clustering
2. Anisotropic Collapse into web like structures
3. Appearance of Voids in the Distribution

1.6.1 Hierarchical Clustering

The fluctuations in a Gaussian random field are fully described by their power spectrum. It is assumed to have a power-law behaviour $P(k) \propto k^n$ where the relative amplitude between scales is dictated by the index n. In order to understand the role of the index n in the growth of structures it is useful to study a few simple cases. A density field with power spectrum with index $n = 0$ has same power at all scales. For such a case however, the power over a particular scale when it enters the Hubble radius is not the same as that for another scale when that enters the Hubble radius. Hence for $n = 0$, although the power is same over all scales at a particular time, it will not be the same for different scales at the time when the corresponding scales enter the Hubble radius. Hence $n = 0$ does not correspond to a scale invariant power spectrum. It turns out that for scale invariant power spectrum $n = 1$ when $P(k)$ is measured for all scales at the same time. For $n = 0$, small-scale fluctuations will collapse and virialize well before larger scales. Small clumps of matter will aggregate to form larger systems. An index $n = -2$ will produce an intermediate case where large scale fluctuations will start their collapse while the small-scales will not yet have fully collapsed. The asymptotic case where $n = -3$ represents an extreme scenario in which all scales will undergo collapse at the same

time. Hence we can see that only spectra with $n > -3$ leads to a bottom-up structure formation in which small clumps collapse and aggregate into larger associations. This process of building-up large structures from the merging of smaller structures is called hierarchical structure formation.

The Press-Schechter formalism

Press & Schechter (1974) proposed a formalism to compute the average number of objects that collapsed from the primordial Gaussian density field. They assumed that the dense objects seen at the present time are a direct result of the peaks in the initial density field. These small perturbations collapsed spherically under the action of gravity to form selfbound virilized objects.

In the primordial Gaussian field the probability, that a given point lies in a region with the density contrast δ greater than the critical density for collapse δ_c, is given by

$$p(\delta > \delta_c | R_f) = \frac{1}{2}[1 - erf\left(\frac{\delta_c}{\sqrt{2}\sigma(R_f)}\right)] \tag{1.45}$$

where $\sigma(R_f)$ is the variance of the density field smoothed on the scale R_f. The Press-Schechter formalism assumes that this probability corresponds to the probability that a given point has ever been part of a collapsed object of scale $> R_f$. Then, the comoving number density of halos of mass M at redshift z is given by

$$\frac{dn}{dM}(M,z) = \sqrt{\frac{2}{\pi}}\frac{\bar{\rho}}{M^2}\frac{\delta_c(z)}{\sigma_m} \mid \frac{d\ln\sigma(M)}{d\ln M} \mid \exp\left(-\frac{\delta_c(z)^2}{2\sigma^2(M)}\right) \tag{1.46}$$

where $\sigma(M)$ is the variance corresponding to a radius R_f containing a mass M and $\delta_c(z) = \delta_c^0/D(z)$ is the critical overdensity linearly extrapolated to the present time. Here $\delta_c^0 = \delta_c(z=0)$. For an Einstein-de Sitter universe the critical overdensity is $\delta_c^0 = 1.69$. There are approximations for other models, in general δ_c^0 has a weak dependence on Ω_m (Navarro, Frenk & White , 1997).

One of the limitations of the Press-Schechter formalism is that it assumes overdense

perturbations to be perfectly spherically symmetric. In reality the situation is more complex. Bardeen et al. (1986) extensively studied the statistics of peaks in a random density field. They showed that peaks in the primordial density field have a degree of flattening. This departure from a spherical distribution is amplified under the action of gravity affecting the final collapse of the object.

The original Press-Schechter formalism also does not properly take into account the cloud-in-cloud problem as it ignores underdense regions. This is the origin of the contrived factor of 2 in equation 1.46. An appropriate description in terms of the excursion set barrier crossing led to the formulation of the *extended Press-Schechter formalism* by Bond et al. (1991). Not only did it provide a powerful enough framework to describe the merging of clumps of matter into even larger objects (Lacey & Cole, 1993), but it also allowed a more proper understanding and description of the mass function of galaxies and haloes given their non spherical shape (Sheth et al., 2001; Sheth & Tormen, 2004). Recently Sheth & van de Weygaert (2004) and Shen et al. (2006) provided a viable formalism to describe the hierarchical evolution of voids and elongated filamentary superclusters.

1.6.2 Anisotropic collapse

The distribution of matter in the Universe is not homogeneous over all scales as is clear from galaxy redshift surveys. The Universe has a variety of structures. The nature of these structures like filaments etc. suggest the gravitation collapse to be anisotropic. Early studies focused on the anisotropic nature of the gravitational collapse may be found in Lynden-Bell (1964) and Lin et al. (1965). Icke (1973) investigated the evolution of homogeneous ellipsoidal configurations in an expanding FRW universe and concluded that the predominant final morphologies are flattened and elongated. One of the most important results of the ellipsoidal collapse model is that not only gravity sets any overdense perturbation into a runaway collapse but it also has an amplifying effect on any asphericity present in the initial matter configuration (Icke, 1973; White & Silk, 1979; Eisenstein & Loeb, 1995; Bond & Myers, 1996a).

While nearly all these studies address very specific configurations, the Zel'dovich formalism clarifies the importance of the anisotropic nature of gravitational collapse for more generic cosmological circumstances (Zel'Dovich, 1970). While it formally concerns a linear Lagrangian formalism it has proven to describe the emergence and development of structure to weakly nonlinear stages. Not only it elucidates the first stages of nonlinear clustering but it also has become an essential tool for setting up the initial conditions used as input for N-body computer simulations. The Zel'dovich formalism is based on the mapping between the initial Lagrangian position q to a displaced Eulerian position $\mathbf{x}$. In the weakly non linear regime these two positions are related by

$$x(t) = q + D(t)\nabla\Phi(q), \tag{1.47}$$

where the time dependent function $D(t)$ is the growth rate of linear density perturbations and the time independent spatial function $\Phi(q)$ is related to the linearly extrapolated gravitational potential.

Here we concentrate on the anisotropic collapse of a patch of matter. For a particular structure the force field of the structure hangs together with the flattening of the feature itself. This induces an anisotropic collapse along the main axes of the structure. Applying a simple mass conservation relation $\bar{\rho}d^3q = \rho(x)d^3x$ to equation 1.47, we get:

$$\rho(x) = \frac{\bar{\rho}}{[1 - D_+(t)\lambda_1(q)]\,[1 - D_+(t)\lambda_2(q)]\,[1 - D_+(t)\lambda_3(q)]} \tag{1.48}$$

where $\lambda_1, \lambda_2, \lambda_3$ are the eigenvalues of the deformation tensor:

$$\psi_{i,j} = \frac{\partial^2\Psi}{\partial q_i \partial q_j} \tag{1.49}$$

In order for an object to collapse at least one of the eigenvalues must be positive, so that the density $\rho(x)$ diverges as D_+ increases. The Zel'dovich approximation predicts the collapse of matter into planar sheets or pancakes. The subsequent collapse is determined by the second largest eigenvalue which produces a filament to finally end up

in a spherical clump. This suggest a natural division of the features of the large scale matter distribution based on their morphology. On the basis of the eigenvalues we may distinguish three *final configurations*. If $\lambda_1 > 0$ and λ_2 and λ_3 are both less than 0, the resulting configuration is that of a *pancake*. For a *filament* configuration λ_1 and λ_2 are positive but λ_3 is negative. A *clump* configuration is defined by all λ's being positive.

Each morphology represents a specific evolutionary state in the gravitational collapse. In reality the gravitational collapse is not a sequence of single collapses along λ_1, λ_2 and λ_3. Instead it is a more gradual collapse in all three directions. One can then expect the Universe to contain the three basic morphologies as well as a large number of intermediate cases. The most conspicuous feature of the large scale matter distribution is the existence of a pervading filamentary network and quasi-spherical dense concentrations of matter sitting at the nodes. The planar walls or pancakes can also be seen as slightly overdense regions located between filaments. Most of the space is devoid of matter. Large empty regions extend for several Megaparsecs. These *voids* give the Cosmic Web its characteristic cellular or foamy nature (van de Weygaert, 2002).

1.6.3 The Cosmic Web

Bond, Kofman & Pogosyan (1996) took the analytical description of the hierarchical large-scale matter distribution to a meaningful description of the nonlocal influences on evolving matter structures. They coined the word *cosmic web* in their study of the physical component of structures of Universe. Their peak-patch formalism presented a more complete description involving tidal influences. It provided a basic framework for the Cosmic Web model for more generic cosmological circumstances of a random density field (Bond & Myers, 1996a,b,c). The salient feature of finding of Bond, Kofman & Pogosyan (1996) was that knowledge of the value of the tidal field at a few well-chosen locations in some region is sufficient to determine the overall outline of the web-like pattern in that region.

In the *Cosmic Web Theory* the rare high peaks corresponding to clusters play a fundamental role. They are the nodes that define the cosmic web. This relation may be

traced back to a simple configuration, that of a global quadrupolar matter distribution and the resulting local tidal shear at its central site. Such a quadrupolar primordial matter distribution will almost by default evolve into a canonical cluster-filament-cluster configuration which forms the structural basis of the Cosmic Web.

The Cosmic Web Theory provides a natural explanation to both the elements that form the Cosmic Web as well as their connectivity properties. This intimate connection between the *local* force field and the surrounding global matter distribution can be straightforwardly appreciated on the basis of the *constrained random field* study by van de Weygaert & Bertschinger (1996). They, amongst others, discussed the repercussion of a specified constraint on the value of the tidal shear at some specific location. This expression at a particular position is represented by the following expression.

$$T_{ij}(r,t) = \frac{3\Omega H^2}{8\pi} \int d^3r' \delta(r',t) \left\{ \frac{3(r'_i - r_i)(r'_j - r_j) - |r' - r|^2 \delta_{ij}}{|r' - r|^5} \right\} - \frac{1}{2}\Omega H^2 \delta(r,t)\delta_{ij} \tag{1.50}$$

From the expression 1.50 of the tidal tensor in terms of the generating density distribution, we can immediately observe that any *local* value of T_{ij} has *global* repercussions for the generating density field. Such *global* constraints are in marked contrast to *local* constraints like the value of the density contrast δ or the shape of the local matter distribution. One of the major advantages of their *constrained random field* construction technique (Bertschinger, 1987; Hoffman & Ribak, 1991) is that it offers tools for translating locally specified quantities into the corresponding implied global matter distribution for a given structure formation scenario.

1.7 Ideas about Galaxy Distribution

The *Great Galaxy* view (Kapteyn, 1922) of the distribution of galaxies depicted the Milky Way as a relatively small flattened ellipsoidal system. In this model the Sun is supposed to have been located at the center of milky way. The center was supposed to be surrounded by a halo of globular clusters. However, recognizing the role played by

inter stellar absorption, and also the fact that stars in the Galaxy were orbiting about a distant center, the sun was placed elsewhere instead of the center.

Another view of Galaxy distribution later confirmed by Edwin P. Hubble (Hubble, 1925a,b), was that there are 'field galaxies' largely separated from one another. This view gave rise to the hypothesis of Island Universe. This hypothesis stated that galaxies are building blocks of the Universe. In fact, most galaxies are clustered. The objects which were called nebulae, at that time, were in fact extragalactic system of stars comparable with our own galaxy. The first systematic surveys of the galaxy distribution were undertaken by Shapley and his collaborators (Shapley et al., 1938). It led to the discovery of numerous galaxy clusters and even groups of galaxy clusters. The clustering together of stars, galaxies, and clusters of galaxies in successively ordered assemblies is normally called a hierarchical or multilevel clustering (Charlier, 1908, 1922; de Vaucouleurs, 1970). It has three main consequences. It removes the Olber's paradox (see e.g. Charlier, 1908, 1922). The universe retains a primary center and is therefore nonuniform on the largest cosmic scales. The total amount of matter is much less than in a uniform universe with the same local density. Hierarchical model of clustering also assumes that the visible universe is only one of the series of universes nested inside each other.

More recently still there have been a number of attempts to re-incarnate such a universal hierarchy in terms of fractal models. These models were first proposed by Fournier d' Albe (1907) and subsequently studied by Mandelbrot (1982) and Pietronero (1987). Several attempts have been made to construct hierarchical cosmological models. All these models are, naturally, inhomogeneous. These models have preferred position for the observer, and thus these are unsatisfactory. So the present trend to reconcile fractal models with cosmology is to use the measure of last resort, and to assume that although the matter distribution in the universe is homogeneous on large scales, the galaxy distribution can be contrived to be fractal (Ribeiro, 2001). Numerical models of deep samples as well as data from modern redshift surveys contradict this assumption.

1.7.1 The cosmological Principle

The notion that the Earth is not at the center of the Universe is generally referred to as the Copernican Principle. Einstein (1917) proposed that on the very largest scales the Universe should be homogeneous and isotropic. At that time there could have been no observational support for this assumption. It is a consequence of the notion that we don't have a special place in the Universe. Under this assumption Einstein's field equations have a simple solution. Einstein-de Sitter model of cosmology as well as the famous solution of Einstein's Equation provided by Robertson and Walker use just this principle.

The first demonstration of homogeneity in the galaxy distribution was probably the observation by Peebles that the (projected) two-point correlation function estimated from diverse catalogs probing the galaxy distribution to different depths followed a scaling law that was consistent with homogeneity. The observations of Cosmic Microwave Background Radiation give evidence of the cosmic isotropy of the Universe. The $COBE$ satellite all-sky map of the Cosmic Microwave Background Radiation (Smoot et al., 1992) is isotropic to a high degree, with relative intensity fluctuations only at the level of 10^{-5}.

1.8 Surveys of Cosmic Structures

The first map of the sky came from the Lick survey of galaxies undertaken by Shane & Wirtanen (1967) using large field plates from the Lick Observatory. This map revealed widespread clustering and super clustering of galaxies. With each improvement in telescope and associated back end instruments, we have been able to probe further into the Universe. One of the key impetus in understanding the clustering of galaxies was provided by Palomar Sky survey. Observations were done using a $48''$ Schmidt telescope. A catalog of galaxy redshifts, with information about the clusters to which the galaxies belonged, was published by Humason et al. (1956).

These catalogs simply listed objects as they appeared projected on to the celestial sphere. Only indication of distance to the object came from its brightness or size.

Moreover, these were subject to human selection effects and hence were not sufficiently standardized.

What characterizes more recent surveys is the ability to scan photographic plate digitally (e.g: The Cambridge Automatic Plate Machine APM), or to create the survey in digital format (e.g: IRAS, Sloan Survey etc). It is now far easier to obtain redshifts for large number of objects in these catalogs. Mapping the Universe this way provides information about how structured the universe is now at modest redshift. These structures were generated from initial density perturbations in the early Universe. The perturbations led to the anisotropies in the Cosmic Microwave Background Radiation at the surface of last scattering. The collapse of these tiny fluctuations has given rise to the structures that we observe in the present Universe. Thus observations of Cosmic Microwave Background give us information about the structure of the surface of last scatter. This information can, in turn, serve as the starting point for N body simulations. If we can put these two things (large scale structures and CMBR) together we will have a complete picture of the Universe.

Now we would like to describe briefly some of the recent galaxy redshift surveys that have completed or are under progress.

1.8.1 Cfa and SSRS survey

The first Cfa survey (Huchra et al., 1983, http://tdc-www.harvard.edu/) mapped about 2400 galaxies down to apparent magnitude $m \simeq 14.5$ taken from Zwicky catalog. This survey was too sparse to show definite structures. The Cfa slice was centered on the Coma cluster, hence it was not considered as being representative of the universe as a whole. However, the breadth of the slice sampled a far greater volume, and it was very deep for that time ($\sim 150h^{-1}Mpc$). Subsequent surveys like the following CfA slices and the ESO Southern survey (da Costa et al., 1991) amply confirmed the impression given by the CfA slice.

The Southern Sky Redshift Survey (da Costa et al., 1991, http://vizier.u-strasbg.fr/) was proposed to complement the original CfA survey. It mapped galaxies in the southern

sky taking redshift of about 2400 galaxies. The extended SSRS (da Costa et al., 1998) followed it up with redshifts of about 5400 galaxies mirroring the Second CfA survey for the southern sky.

1.8.2 The Las Campanas Redshift Survey

The Las Campanas Redshift Survey (Shectman et al., 1996) mapped six thin parallel slices ($1.5^\circ \times 90^\circ$). It probed the Universe to a depth of about $750\,h^{-1}$Mpc ($z \approx 0.25$). It measured redshifts of about 24000 galaxies in these slices. This was the first deep survey of sufficient volume of the nearby Universe. The LCRS data can be accessed at http://qold.astro.utoronto.ca/ lin/lcrs.html

1.8.3 2dF galaxy redshift survey

The $2dF$ (Colless et al., 2003) used a multi-fiber spectrograph on the 3.9m Anglo-Australian Telescope. This survey had a field of view of some 2 degrees in diameter, hence the name of the survey. The redshifts measurement was carried out on some $250,000$ galaxies located in extended regions around the north and south Galactic poles. The source catalog is a revised APM survey. The galaxies in the survey go down to magnitude $b_J = 19.45$. The median redshift of the sample is $z = 0.11$ and redshifts extend to about $z \simeq 0.3$. The survey is already complete, and the data can be downloaded from http://www2.aao.gov.au/2dFGRS/

1.8.4 Sloan Digital Sky Survey

The Sloan Digital Sky Survey (SDSS) (York et al., 2000; Stoughton et al., 2002) is the largest galaxy redshift survey to date. It employs a specially designed 2.5 m telescope with a 3° field of view. It uses a mosaic CCD camera, and dual fiber-fed spectrograph, to obtain five band (u, g, r, i, z) digital photometry. The spectroscopic information is obtained over full range of optical wavelengths. The main spectroscopic galaxy sample of the SDSS (Strauss et al., 2002) includes objects having Petrosian magnitude of

$r < 17.77$ after correction for Galactic extinction. It is designed to measure a million galaxy redshifts over $\sim 10^4$ square degrees of sky. The sixth major public release of SDSS data (SDSS DR6; Adelman-McCarthy et al., 2008, www.sdss.org/dr6 and www.cas.sdss.org/dr6/en) in June, 2007 includes 8520 square degrees imaging and 6860 square degrees of spectroscopy. As of now the spectroscopic data includes 1163520 spectra with 792680 galaxy redshift. The survey area covers a single contiguous region in the Northern Galactic Cap and three non-contiguous region in the Southern Galactic Cap. The SDSS surveys to a depth that has been probed previously by earlier surveys like LCRS, however the volume covered by SDSS is enormously greater. The solid angle coverage of the SDSS is almost 14 times that of the LCRS. For a detailed discussion about SDSS we refer the reader to section 5.2 of this thesis.

1.9 Goals and outline of this thesis

The main goal of this thesis is to understand the nature of clustering of matter over large scales in the Universe. There are various methods for the statistical characterization of large scale structures. The traditional approaches include the *two point correlation function, counts in cells, nearest neighbor approximation and N point correlation function.* The approach we use in this thesis for this purpose is the **multifractal analysis** of simulated distribution of points as well as of galaxy distributions from galaxy redshift surveys. Multifractal analysis is a useful tool in this case because the large scale distribution of matter has a scaling behaviour over a range of scales. Galaxy distributions also exhibit self similarity on small scales (Pietronero, 1987; Jones et al., 1988).

Fractals have been invoked to describe many physical phenomena which exhibit self-similarity (Mandelbrot, 1982). A multi-fractal is an extension of the concept of a fractal. It includes the possibility that the self similar behaviour of particle distributions may be different in different density environments. In order to give a complete statistical information about the point distribution the multifractal analysis characterizes scaling properties of moments at all levels. One of the advantages of using this technique over the

traditional approaches is that it does not require *apriori* information about the average density of the Universe. This enables us to use this approach in finding the scale at which the matter distribution in the Universe attains homogeneity. It means we are interested in finding the scale above which the cosmological principle can be assumed to be valid and the Friedman-Robertson-Walker-Lemaitre (FLRW) metric is a correct description of the Universe.

Chapter 2 describes various statistical methods used in the analysis of distribution of galaxies. We start with the standard tool of two point correlation function of the distribution and discuss its merits and demerits. N-point correlation functions and the counts in cells statistics of the number of particles in the distribution are discussed in order to calculate higher moments of the distribution. Fractal analysis as an alternative to the two point correlation function has been extensively described. Different definitions of fractal dimension (e.g Minkowski - Bouligand Dimension) have been discussed which are useful for deterministic as well as statistical fractal distributions.

Chapter 3 deals with the calculation of Minkowski- Bouligand fractal dimension (D_q) for both Homogeneous and weakly clustered distribution of points. We have described the relation between D_q and the probability distribution function of a distribution. We have investigated how the computed dimension changes with the number of particles in the distribution. The fractal dimension has also been calculated for a general mathematical distribution in which the particles are weakly clustered. We also describe the individual contribution of finite number and clustering to the Minkowski Bouligand Dimension and derive an analytical expression to quantify the deviation of D_q from Euclidean dimension due to these two contributions.

In chapter 4 the application of our model of calculating Minkowski Bouligand Dimension developed in chapter 3 has been discussed. For this purpose various distribution of points have been considered. To test the correctness of our model the application to *Multinomial Multifractal* distribution has been studied. We have also discussed the application of our model to the concordance model of cosmology. We describe the scale at which the unbiased distribution of L_* type galaxies is homogenously distributed. Ap-

plication of our model to biased distribution of Large Redshift Galaxies (LRG) has also been discussed. Contribution of clustering term to the Minkowski-Bouligand Dimension has been discussed for the distribution of points having a feature (like the Baryon Acoustic Oscillation) in the correlation function.

Chapter 5 tests the large scale homogeneity of the galaxy distribution in the Sloan Digital Sky Survey Data Release One (SDSS-DR1) using volume limited subsamples extracted from two equatorial strips. The two dimensional multifractal analysis of the galaxy distribution projected on the equatorial plane has been studied. The galaxy distribution has also been compared with the distribution generated from random catalog and also from N-Body simulations. The effect of bias to the scale of homogeneity of the galaxy distribution has also been discussed in this chapter.

Chapter 6 gives a summary of the thesis along with the future scope of our work.

Chapter 2

Statistical tools to analyze Distribution of Galaxy

2.1 Introduction

One of the goals of modern cosmology is to understand and quantify the nature of large scale matter distribution of the Universe. An accurate empirical description of large scale clustering of matter, derived from systematic observations of visible matter in the Universe, is essential to achieve this goal. Efforts in this directions have vastly improved due to better instruments that have been available in recent times for astronomical data acquisition as well as better statistical techniques of analysis of the acquired data. It is as a result of these efforts that an enormous amount of data about the observable universe has been accumulated in the form of the now well-known *redshift surveys*, and some widely accepted conclusions drawn from these data have created a certain confidence in many researchers that an accurate description of the large scale matter distribution is just about being achieved.

In statistical analysis of galaxy distribution, we are not interested in the number of galaxies in a particular region of the sky but we are rather interested only in the average properties of number distribution of galaxies. We are *e.g.* interested in knowing whether or not distribution of galaxies is clumpy, and if so, how we can quantify the nature

of clumpiness. In the literature (Martínez & Saar, 2002), various statistical methods of analysis of galaxy clustering have been discussed. The broad feature of all these methods is to discuss the nature of clumpiness of the galaxy distribution. Among all these methods the historical favorites have been variants of two point correlation function (see equation 2.1). This function measures the excess probability, relative to a Poisson distribution, of finding an object near another object. Bok's statistic (the dispersion of the counts N in cells), is an integral over two point correlation function. Zwicky's index of clumpiness is the ratio of variance of N to what would be expected for a uniform random distribution. From the two point correlation function of the counts of galaxies in the Lick survey, Limber showed that there is a linear integral equation relating the angular correlation function to the corresponding spatial correlation function. Neyman and Scott devised a *priori* statistical model of clustering and then adjusted the parameters to fit model statistics to estimates from data. A recent program in a similar vein is called the halo model. Recently there have been precise estimates of two point correlation function from redshift surveys like Two Degree Field Galaxy Redshift Survey (2dFGRS) and the Sloan Digital Sky Survey (SDSS).

The Fourier or spherical harmonic transform of the two point correlation function is the power spectrum (see equation 2.5). It is the description of clustering in terms of wavenumbers k that separates the effects of different scales. Other descriptors of statistics have been the N point correlation function of the distribution of points, moments and counts in cells, void probability function and nearest neighbor distances etc. However all these methods are based on the idea of eventual homogenization of the matter distribution within the sample size itself. A group of researcher feels that this idea of homogenization is flawed and the distribution of matter in the Universe is intrinsically inhomogeneous to largest observed scales and, perhaps, indefinitively.

The debate of homogeneous versus non homogeneous distribution of matter has taken a new vigor with the arrival of a new method for describing the clustering of galaxies. This method is based on the ideas of a new geometrical perspective for the description of irregular patterns in nature. We generally refer to it as *the fractal geometry*. In this

chapter we intend to show the basic idea behind this geometrical approach.

The plan of this chapter is as follows. In section 2.2 we briefly present the basic tools used in statistical analysis of the large scale distribution of galaxies, its estimations, difficulties and answers given to these difficulties. The subsection 2.2.3 describes Higher order statistics of the distribution. Section 2.3 describes various other methods of statistical analysis. Section 2.4 presents a brief, but general, introduction to fractals, which emphasizes their empirical side and applications. The discussion on various fractal dimensions along with their merits (and demerits) follow in section 2.5 and 2.6. We conclude the chapter with a small discussion on Lacunarity of the point distribution in section 2.7.

2.2 The Standard Correlation Function Analysis

The standard statistical analysis assumes that the objects under discussion (galaxies) can be regarded as point particles. These particles are assumed to be distributed homogeneously on a sufficiently large scale within the sample boundaries. This means that we can meaningfully assign an average number density to the distribution. Therefore, we can characterize the galaxy distribution in terms of the extent of the departures from uniformity on various scales. The correlation function as introduced by Peebles (1980) is basically the statistical tool that permits the quantitative study of this departure from homogeneity.

Consider a set of N galaxies contained in a volume V. The average number density of galaxies is defined by $\bar{n} = N/V$. It implies that we have to go on an average a distance of $(\bar{n})^{-1/3}$ from a given galaxy before another is encountered. This means that local departures from uniformity can be described if we specify the distance we actually go from any particular galaxy before encountering another. This will sometimes be larger than average, but sometimes less. Specifying this distance in each case is equivalent to giving the locations of all galaxies. This is an awkward way of doing things and does not solve the problem. What we require is a statistical description giving the probability of

finding the nearest neighbor galaxy within a certain distance.

As we know the probability of finding a galaxy closer than, say, 50 kpc to the Milky Way is zero, and at a distance greater than this value is one. This sort of probability information is not useful to us. What is necessary is some sort of average. We can view the actual universe to be a particular realization of some statistical distribution of galaxies. The departure from randomness due to clustering of these galaxies is expressed by the fact that the average separation of galaxies over the statistical ensemble of this separation is less than $(\bar{n})^{-1/3}$.

For a completely random and homogeneous distribution of galaxies, the probability dP_1 of finding a galaxy in an infinitesimal volume dV_1 is proportional to dV_1 and to $\bar{n}$, and is independent of position. So we have

$$dP_1 = \frac{\bar{n}}{N} dV_1,$$

where N is the total number of galaxies in the sample. The sample space is divided into cells of volumes dV_1 and we count the ratio of those cells which contain a galaxy to the total number. The probability of finding two galaxies in a cell is of order $(dV_1)^2$, and so can be ignored in the limit $dV_1 \to 0$. It is important to state once more that this procedure only makes sense if the galaxies are distributed randomly on some scale less than that of the sample.

Similarly the joint probability dP_{12} of finding galaxies in volumes dV_1 and dV_2 at positions $\vec{r}_1$, $\vec{r}_2$ respectively is just the product of probabilities of finding each of the galaxies, i.e.

$$dP_{12} \propto dP_1 dP_2,$$

This is because in a random distribution the positions of galaxies are uncorrelated. On the other hand, if the galaxies are correlated we would have a departure from the random distribution. In that case the joint probability is different from a simple product. The *two-point correlation function* $\xi(\vec{r}_1, \vec{r}_2)$ is by definition a function which determines this

difference from a random distribution. So we have

$$dP_{12} = \left(\frac{\bar{n}}{N}\right)^2 [1 + \xi(\vec{r}_1, \vec{r}_2)]\, dV_1 dV_2 \tag{2.1}$$

as the probability of finding a pair of galaxies in volumes dV_1, dV_2 at positions $\vec{r}_1$, $\vec{r}_2$. Obviously, the assumption of randomness on sufficiently large scales means that $\xi(\vec{r}_1, \vec{r}_2)$ must tend to zero if $|\vec{r}_1 - \vec{r}_2|$ is sufficiently large. In addition, the assumption of homogeneity and isotropy implies that ξ cannot depend on the location of the galaxy pair, but only on the distance $|\vec{r}_1 - \vec{r}_2|$ that separates them, as the probability must be independent of the location of the first galaxy. If ξ is positive we have an excess probability over a random distribution and, therefore, clustering. If ξ is negative we have anti-clustering. Obviously $\xi > -1$.

The two-point correlation function can be generalized to define n-point correlation functions, which are functions of $n-1$ relative distances, but in practice computations have not been carried out beyond the four-point correlation function.

It is a common practice to replace the description above using point particles by a continuum description. So if galaxies are thought to be the constituent parts of a fluid with variable density $n(\vec{r})$, and if the averaging over a volume V is carried out over scales large compared to the scale of clustering, we have

$$\frac{1}{V}\int_V n(\vec{r}) dV = \bar{n}, \tag{2.2}$$

where dV is an element of volume at $\vec{r}$. The joint probability of finding a galaxy in dV_1 at $\vec{r} + \vec{r}_1$ and in dV_2 at $\vec{r} + \vec{r}_2$ is given by

$$\left(\frac{1}{N}\right)^2 n(\vec{r} + \vec{r}_1) n(\vec{r} + \vec{r}_2) dV_1 dV_2.$$

Averaging this equation over the sample gives

$$dP_{12} = \frac{1}{N^2 V}\int_V n(\vec{r} + \vec{r}_1) n(\vec{r} + \vec{r}_2) dV dV_1 dV_2. \tag{2.3}$$

Now if we compare the equation 2.3 with equation (2.1) we obtain

$$\bar{n}^2 \left[1 + \xi(\vec{\tau})\right] = \frac{1}{V} \int_V n(\vec{R}) n(\vec{R} + \vec{\tau}) dV, \tag{2.4}$$

where $\vec{\tau} = \vec{r}_2 - \vec{r}_1$, $\vec{R} = \vec{r} + \vec{r}_1$ and dV is the volume element at $\vec{R}$.

It is worth mentioning that in statistical mechanics the correlation function normally used is $g(r) = 1 + \xi(r)$ which is called the radial distribution function. Statisticians call this quantity the pair correlation function. The number of galaxies, on average, lying between r and $r + dr$ is $4\pi r^2 n g(r)$ with n being the average number density.

Related to the correlation function is the so-called *power spectrum* of the distribution, defined by the Fourier transform of the correlation function.

$$\xi(r) = \frac{1}{2\pi^2} \int dk\ k^2\ P(k) \frac{sin(kr)}{kr} \tag{2.5}$$

The scale or wavelength λ of a fluctuation is related to the wavenumber k by $k = \frac{2\pi}{\lambda}$. As explained in chapter 1 the power spectrum describes the way that large, intermediate and small structures combine to produce the observed distribution of luminous matter. It is also possible to define an *angular correlation function* which will express the probability of finding a pair of galaxies separated by a certain angle, and this is the appropriate function to studying catalogs of galaxies which contain only information on the positions of galaxies on the celestial sphere. It means that the angular correlation function is used to study the projected galactic distribution when the galaxy distances (i.e. the redshift information) are not available. Further details about these two functions can be found at various places in the literature (Peebles, 1980; Martínez & Saar, 2002). Finally, for the sake of easy comparison with other works it is useful to write equation (2.4) in a slightly different notation:

$$\xi(r) = \frac{\langle n(\vec{r_0}) n(\vec{r_0} + \vec{r}) \rangle}{\langle n \rangle^2} - 1. \tag{2.6}$$

The usual interpretation of the correlation function obtained from the data is as

follows: when $\xi \gg 1$ the system is strongly correlated and for the region when $\xi \ll 1$ the system has small correlation. From direct calculations from catalogs it was found that at small values of r the function $\xi(r)$ can be characterized by a power law (Pietronero, 1987; Davis et al., 1988):

$$\xi(r) = \left(\frac{r}{r_0}\right)^{-\gamma} \approx Ar^{-\gamma}, \quad (\gamma \approx 1.7), \tag{2.7}$$

where A is a constant. This power law behavior holds for galaxies and clusters of galaxies. The distance r_0 at which $\xi = 1$ is called the *correlation length*, and this implies that the system becomes essentially homogeneous for lengths appreciably larger than this characteristic length. This also implies that there should be no appreciable overdensities (superclusters) or underdensities (voids) extending over distances appreciably larger than r_0.

In the calculation of two point correlation function we have assumed an average value for the density of matter on the scales well within the sample size. In practice however, we do not have a statistical ensemble from which the average value can be derived. So what we can do is to take a spatial average over the visible universe, or as much of it as has been cataloged, in place of an ensemble average. This only makes sense if the departure from homogeneity occurs on a scale smaller than the depth of the sample, so that the sample will statistically reflect the properties of the universe as a whole. In other words, we need to have a *fair sample* of the Universe in order to fulfill this program. This fair sample ought to be homogeneous, by assumption. If, for some reason, the sample we have is not a fair sample in the above sense, we can not construct an average density of the Universe with this sample. In that case this whole program breaks down.

2.2.1 Estimators of Two point Correlation Function

The two-point correlation function $\xi(r)$ can be estimated in several ways from a given galaxy sample. At small distances, nearly all the estimators provide very similar performance. However at large distances, their performance is not equivalent any more and

some of them could be biased. Considering the galaxy distribution as a point process, the two-point correlation function at a given distance r is estimated by counting and averaging the number of neighbors each galaxy has within a given scale. It is clear that the boundaries of the sample have to be taken into account, because as no galaxies are observed beyond the boundaries, the number of neighbors is systematically underestimated at larger distances. If we do not make any assumption regarding the kind of point process that we are dealing with, the only solution is to use the so-called minus-estimators, the kind of estimators favored by Pietronero and co-workers (Sylos Labini et al. , 1998). In this estimation the averages of the number of neighbors at a given distance are taken omitting those galaxies lying closer than r to the sample boundary. Thus at large scales only a small fraction of the galaxies in the sample enter in the estimation. This increases the variance. To make full use of the surveyed galaxies, the estimator has to incorporate an edge-correction.The most widely used estimators in cosmology are the Davis and Peebles estimator (ξ_{DP}, Davis & Peebles, 1983), the Hamilton estimator (ξ_{HAM}, Hamilton, 1993) and the Landy-Szalay estimator (ξ_{LS}, Landy & Szalay, 1993). Here we provide their formulae.

Consider a complete galaxy sample in a given volume with N objects. A Poisson catalog generated by a binomial process with N_{rd} points has also to be produced within the same volume. Then the three estimators are represented by

$$\xi_{DP}(r) = \frac{N_{rd}}{N}\frac{DD(r)}{DR(r)} - 1 \tag{2.8}$$

$$\xi_{HAM}(r) = \frac{DD(r).RR(r)}{[DR(r)]^2} - 1 \tag{2.9}$$

$$\xi_{LS}(r) = 1 + \left(\frac{N_{rd}}{N}\right)^2 \frac{DD(r)}{DR(r)} - 2\frac{N_{rd}}{N}\frac{DD(r)}{DR(r)}. \tag{2.10}$$

Here $DD(r)$ is the number of pairs of galaxies with separation within the interval $r - \frac{dr}{2}$ to $r + \frac{dr}{2}$ and $RR(r)$ is the number of pairs with separation in the same interval in the

Poisson catalog. In order to calculate $DR(r)$ we use a combination of points in the galaxy sample as well as in Poisson catalog. From a point in the poisson catalog, we find the the number of galaxies that are within $r - \frac{dr}{2}$ to $r + \frac{dr}{2}$ of the point. It is this number that we call $DR(r)$. At large scales the performance of the Hamilton and Landy-Szalay estimators has been proved to be better.

Now that we have obtained the explicit form of the two-point correlation function, it is important to emphasize at this point two essential aspects of this method. First that this analysis fits very well in the standard Friedmannian cosmology which *assumes* spatial homogeneity, but it does not take into consideration any effect due to the curvature of the spacetime. In fact, this method overlooks this problem altogether under the assumption that the scales under study are relatively small. However, it is important to keep in mind that beyond some scales curvature effects become significant. Secondly, if Universe is inhomogeneous, this analysis is *inapplicable*. Moreover, since this analysis starts by assuming the homogeneity of the distribution within the sample size, *it does not offer any kind of test for the hypothesis itself*. In other words, *this correlation analysis cannot disprove the homogeneous hypothesis*.

2.2.2 Difficulties of the Standard Analysis

The first puzzling aspect found using the method just described is the difference in the amplitude A of the observed correlation function (see equation 2.7) when measured for galaxies and clusters of galaxies. While the exponent γ is approximately 1.7 in both cases, for galaxies $A_G \simeq 20$ and for clusters $A_C \simeq 360$. Its value for superclusters of galaxies is found to be $A_{SC} \simeq 1000 - 1500$. The correlation length was found to be $r_0 \simeq 5$ h^{-1} Mpc for galaxies and $r_0 \simeq 25$ h^{-1} Mpc for clusters.

Since $A_C \simeq 18 A_G$, clusters appear to be much more correlated than galaxies. This dicripency in the value of A is puzzling because cluster themselves are made of galaxies. Similarly superclusters will then appear to be more correlated than clusters. From the interpretation of $\xi(r)$ described above, the galaxy distribution becomes homogeneous at the distance $\simeq$ 10-15 h^{-1} Mpc where $\xi(r)$ is found to become zero, while clusters and

superclusters are actually observed at much larger distances.

The second problem of the standard analysis has to do with the homogeneity assumption itself and the possibility of achieving a fair sample, which should not be confused with a homogeneous sample as the standard analysis usually does. A fair sample is one in which there exists enough points from where we are able to derive some unambiguous statistical properties of the entire distribution. Improvements in astronomical detection techniques, in particular the new sensors and automation, have enabled astronomers to obtain a large amount of galaxy redshift measurements per night. With these improvements, it is now possible to map the distribution of galaxies in three dimensions. The picture that emerges from these surveys appears to be far from the expected homogeneity. We can clearly see clusters of galaxies, voids and superclusters appearing at all scales, with no clear homogenization of the distribution. The first 'slice' of the universe shown by de Lapparent, Geller & Huchra (1986) confirmed this inhomogeneity with very clear pictures. Inhomogeneities are more perceptible in the observed slices of the Universe when we compare with a randomly generated distribution. Of course, with the modern galaxy redshift surveys it may be possible to demonstrate that the survey is a fair sample of the universe by showing that the values of $\bar{\rho}$ derived from sub-samples of the survey are consistent with each other, or that the value of $\bar{\rho}$ computed at different scales converges to a definite value at scales much smaller than the size of the survey. However, to verify and hence validate the cosmological principle, it is useful to consider a statistical test which does not presuppose the premise being tested.

Some people think that third difficulty of the standard analysis is related to the correlation length (see e.g. Einasto et al., 1986; Davis et al., 1988; Calzetti et al., 1987; Coleman, Pietronero & Sanders, 1988; Pietronero, Montuory & Sylos Labini, 1997). They found that the correlation length r_0 *increases with the sample size*. However, this interpretation is also not supported by data from modern galaxy redshift survey (e.g. Martinez et al., 1990).

2.2.3 Higher Order Correlation Function

The two-point correlation function is not the only method to quantify clustering. It is merely the first of an infinite hierarchy of such descriptors describing the distribution of galaxies taken N at a time. Two quite different distributions can have the same two-point correlation function. In particular, the fact that a point distribution generated by any random walk (e.g., as a *Lévy* flight as proposed by Mandelbrot (1975)) has the correct two-point correlation function does not convey much information unless other statistical measures of clustering are tested.

The present day galaxy distribution is manifestly not a gaussian random process: there is, for example, no symmetry about the mean density. Even this fact alone tells us that there is more to clustering of galaxies than two point correlation function. The higher order correlation functions provide a much more detailed description of galaxy clustering probing the low and high count tails of the distribution. The simplest higher order correlation function is the 3-point correlation function. It is defined in terms of probability of finding three points inside the infinitesimal volume elements dV_1, dV_2 and dV_3 respectively placed at the vertices of a triangle with sides r_{12}, r_{23},and r_{31}. This probability, of occurrence of three points nearby, is given by

$$dP_{123} = \left(\frac{\bar{n}}{N}\right)^3 \left[1 + \xi(r_{12}) + \xi(r_{23}) + \xi(r_{31}) + \zeta(r_{12,r_{23},r_{31}})\right] dV_1 dV_2 dV_3 \tag{2.11}$$

where $\zeta(r_{12}, r_{23}, r_{31})$ is the reduced or connected three point correlation function, while the full three-point correlation function is given by the sum of last four terms in the square brackets. The reduced three point correlation function appears to be simply related to the two-point function through a Kirkwood-like relationship:

$$\zeta(r_{12}, r_{23}, r_{31}) = Q[\xi(r_{12})\xi(r_{23}) + \xi(r_{23})\xi(r_{31}) + \xi(r_{31})\xi(r_{12})] \tag{2.12}$$

where $Q \sim 1$ is a constant, and the equality is due to the usual assumption of homogeneity and isotropy. This scaling law is called the hierarchical model in cosmology, and it agrees

rather well with observations. The full Kirkwood law would require an additional term on the right-hand side of this equation, proportional to $\xi(r_{12})\xi(r_{23})\xi(r_{31})$. Equation 2.12 can be generalized to any order n by the expression

$$\xi_n(r_1, \cdots, r_n) = \sum_{t=1}^{T(n)} Q_{n,t} \sum_{L_{n,t}} \Pi^{n-1} \xi(r_{ij}). \tag{2.13}$$

where $Q_{n,t}$ are known as structure constants. $T(n)$ are the number of distinct structures formed by linking of n galaxies and $L_{n,t}$ is the number of possible relabelings for each distinct structure. A simplification of equation 2.13 is the scale invariant model proposed by Balian & Schaeffer (1989)

$$\xi_n(kr_1, \cdots, kr_n) = k^{-(n-1)\gamma} \xi_n(r_1, \cdots, r_n)$$

2.3 Other Statistical Measures

2.3.1 Moments of Counts in Cells and Void Probability

The probability that a randomly placed cell A of volume $V(A)$ contains exactly N objects of the point process is denoted by $P(N, V(A))$. For a Poisson process with intensity λ, these quantities are completely known

$$P(N, V(A)) = \frac{(\lambda V(A))^N}{N!} exp(-\lambda V(A)). \tag{2.14}$$

When $N = 0$, the above quantity quantifies a region of space which has no particles in the cell. Such regions of space is called a *void* and the corresponding probability $P(0, V(A))$ is known as the emptiness or void probability. The moments of order n of the counts are defined by

$$\mu^n(A^n) = E(\phi(A^n)) = \sum_{N=0}^{\infty} N^n P(N, V(A)). \tag{2.15}$$

N-point volume averaged correlation function can now be related to the n^{th} moment of the counts in cells by

$$\bar{\xi}_n(V) = \frac{\mu^n(A^n)}{\bar{N}^n} \tag{2.16}$$

As we have seen previously in subsection 2.2.3 that higher-order correlation functions depend on a large number of arguments, indicating that they are rather difficult to estimate. However, since counts in cells are easy to estimate, they are frequently used to study higher order correlations in the galaxy distribution using equation 2.16.

2.3.2 Nearest Neighbor Distances

In this statistical method the distribution function $G(r)$ is chosen in a way so that $G(r)$ is the probability that the distance between a randomly chosen galaxy and its nearest neighbor is less than or equal to r. If the measure of this function $G(r)$ for the given distribution of galaxies is greater than its counterpart for a Poisson distribution, the galaxy distribution is said to be clustered. Likewise, for a regular distribution the measure of $G(r)$ is smaller than that for a Poisson distribution. This is because a point in a regular distribution is, on average, farther away from its nearest neighbor than in Poisson distribution.

2.3.3 Need of fractal Hypothesis

The problems of combinatorial explosions of terms in N point correlation function together with the power law behavior of $\xi(r)$ clearly pose difficulties in their calculation. While many solutions to these issues have been proposed they usually deal with each of these issues separately. As we shall see, the fractal hypothesis, on the other hand, deals with all these problems as a whole and offers an explanation to each of them within the fractal picture. We, however, do not intend to claim that the fractal hypothesis is the only possible explanation to these problems, whether considering them together or separately. From now on in this thesis we shall take the point of view that fractals offer an attractively simple description of the large scale distribution of galaxies. Therefore

the analysis offered by them deserves a deep, serious and unprejudiced investigation.

From its basis, the fractal hypothesis in many ways represents a radical departure from the orthodox traditional view of an *observationally* homogeneous universe. By using tools of fractal analysis we will investigate if the distribution of large scale structures *actually* behaves as a fractal to arbitrary large scales, or if there is a transition to homogeneity. Fractal analysis is going to be used as the main statistical tool, to quantify the clustering in the distribution of large scale structures, in this thesis. Keeping this in mind Section 2.4 introduces a brief background on fractals necessary in this thesis.

2.4 On the "Definition" of Fractals

Fractal geometry deals with the objects which are highly irregular and can not be handled by the tools of differential geometry. A geometric object can in general be described in terms of its topological dimension which is an integer that defines the number of coordinates needed to specify the geometric object. A *fractal* is defined to be a set of points for which the Hausdorff-Besicovitch dimension strictly exceeds the topological dimension. We shall discuss later the Hausdorff dimension, but the important point here is that this original tentative definition is very abstract. It is often too difficult to be used in practice. This definition also excludes some sets which ought to be regarded as fractals (e.g. space filling (Hilbert) curve).

Loosely speaking a fractal is a shape that tends to have a *scaling* property, implying that degree of its irregularity and/or fragmentation is identical at all scales. Time and again the definition of fractal has been modified by arguing that a single definition of fractal would be restrictive and, perhaps, it would be best to consider fractals as a collection of techniques and methods applicable in the study of the irregular, broken and self-similar geometrical patterns.

It seems best to regard a fractal as a set that has properties such as those described below : when we refer to a set as a fractal, we will typically keep in mind that this set has a fine structure, i.e., one has to look for detail on arbitrarily small scales. It

is too irregular to be described in traditional geometrical language, both locally and globally. This set which we call a fractal, often has some form of self-similarity, perhaps approximate or statistical. The 'fractal dimension' of such a set (defined in some way) is greater than its topological dimension. And in most cases of interest this set of points is defined in a very simple way, perhaps recursively.

With the above description of fractals, we have kept open the possibility that a given fractal shape can be characterized by more than one definition of fractal dimension, and they do not necessarily need to coincide with each other, although they have in common the property of being able to take fractional values. Therefore, an important aspect of studying a fractal structure (once it is characterized as such by, say, at least being recognized as self-similar in some way) is the choice of a definition for fractal dimension that best applies to, or is derived from, the case in study.

Fractal geometry has been considered a revolution in the way we are able to mathematically represent and study figures, sets and functions. In the past, sets or functions that are not sufficiently smooth or regular tended to be ignored as "pathological". Nowadays, there is a realization that a lot can and is worth being said about non-smooth sets. Another interesting points is that the irregular and broken sets provide a much better representation of many phenomena than do figures of classical geometry.

2.4.1 Application of fractals

The concept of scale invariance is of key importance in the characterization of many physical system. It has long been recognized that scale invariance are usually associated with the complexity displayed by a given structure, for which the differentiable geometry based techniques are completely inadequate. A classic example is that of Brownian motion, where the concepts of non differentiable manifolds were used to describe the random motions of particles in liquid or gaseous medium. Although the concept of non differentiable geometry has been subsequently used in many physical and mathematical application, the concept of fractal object has been explicitly introduced and formalized only recently by Mandelbrot. A description in terms of fractal gives a good representation

of wide spectrum of phenomena, not only in physics, but also in biology, geology etc.

The application of fractal techniques to the study of chaotic dynamical system has been quite fruitful. Fractal techniques have been used to describe geometric structures which have completely unpredictable trajectories in the configuration space. Such structures, which are generally termed as *strange attractor*, can not be represented by means of usual geometric tools. Fractal techniques have been extensively applied in the statistical characterization of the study of turbulence.

In this thesis we are going to apply the fractal techniques to statistically describe the distribution of gravitationally evolved Large Scale Structures of the Universe. Despite the great difference existing between the dissipative dynamics of fully developed turbulence and the non- dissipative gravitational dynamics, several common aspects can be identified. First of all, both the Navier-Stokes equation of fluidodynamics and the BBGKY equation which describe the gravitational dynamics, do not contain intrinsic scales. Further numerical simulation of both non linear gravity and the turbulent flows are seen to generate small scale coherent structures arising from a large scale smooth background. On the ground of these similarities, we feel that the fractal description, that is so successful in describing the statistics of dissipative eddies of turbulent flows, to be equally useful in describing the statistics of gravitational clustering. The following discussion starts on the mathematical aspects associated with fractals, but gradually there is a growing emphasis on applications.

2.4.2 The Hausdorff Dimension

An important step in the understanding of fractal dimensions is for one to be introduced to the *Hausdorff-Besicovitch dimension* (often known simply as *Hausdorff dimension* (Falconer, 1990)). It can take non-integer values and was found to coincide with many other definitions. In obtaining the dimension that bears his name, Hausdorff used the idea of defining measures using covers of point sets (first proposed by C. Carathéodory). We shall offer an *illustration* of the Hausdorff measure whose final result is the same as achieved by the formal mathematical proof.

Consider a set F of points. In order to give a measure of the size of this set in space we have taken a test function $h(\delta) = \gamma(d)\delta^d$, where $\gamma(d) = [\Gamma(1/2)]^d/\Gamma(1 + d/2)$. For lines, squares and cubes we have the geometrical factor $\gamma(d)$ equal to $2, \pi$ and $\frac{4}{3}\pi$ respectively. Here δ is the length of the line segment needed to cover the point set completely. Hausdorff proposed a *measure* $H_d(F) = \sum h(\delta)$ of such a point set. In general we find that, as $\delta \to 0$, the measure $H_d(F)$ is either infinite or zero depending on the value of d, the dimension of the measure. The Hausdorff dimension D of the set F is the *critical dimension* for which the measure $H_d(F)$ jumps from infinity to zero (see figure 2.1):

$$H_d(F) = \sum \gamma(d)\delta^d = \gamma(d)N(\delta)\delta^d \underset{\delta\to 0}{\to} \begin{cases} 0, & d > D, \\ \infty, & d < D. \end{cases} \tag{2.17}$$

The quantity $H_d(F)$ is called the d-measure of the set and its value for $d = D$ is often

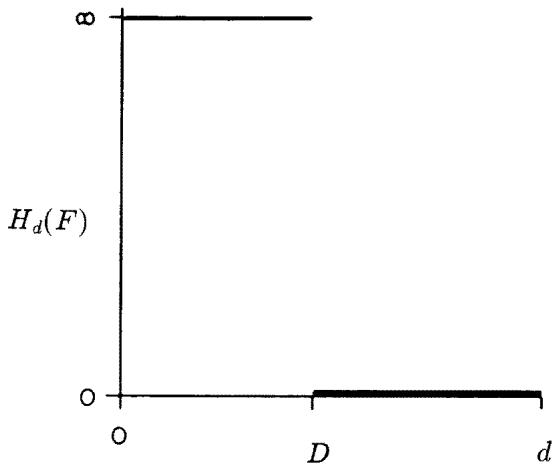


Figure 2.1: Graph of $H_d(F)$ against d for a set F. The Hausdorff dimension D is the critical value of d at which the jump of Hausdorff measure from ∞ to 0 occurs. It can be an integer (for line, plane and sphere etc.) as well as a fractional number(e.g. for irregular shapes and clustered point set)

finite, but may be zero or infinity. It is the position of the jump in H_d as function of d that is important. Note that this definition means the Hausdorff dimension D is a local property in the sense that it measures properties of sets of points in the limit of

a vanishing diameter of size δ of the test function used to cover the set. It also follows that the D may depend on position.

The familiar cases are $D = 1$ for lines, $D = 2$ for planes and surfaces and $D = 3$ for spheres and other finite volumes. There are many sets, however, for which the Hausdorff dimension is non integer and is said to be fractal. In other words, because the jump of the measure $H_d(F)$ can happen at non integer values of d, when $H_d(F)$ is calculated for irregular and broken sets the value D where the jump actually occurs is usually non integer.

2.4.3 Fractal Dimension of orthogonal projections and intersections

We briefly present the properties of orthogonal projections and intersections of fractal structures. This discussion is useful in the interpretation of angular and one dimensional (pencil beams) catalogs.

Orthogonal projections preserve the sizes of objects in the perpendicular direction. If an object of fractal dimension D, embedded in a space of dimension $d = 3$, is projected on a plane (of dimension $d' = 2$) it is possible to show that the projection has dimension D' such that

$$D' = \begin{cases} D, & \text{if } D < d' = 2 \\ d', & \text{if } D > d' = 2 \end{cases} \tag{2.18}$$

This explains, for example, why clouds which have fractal dimension $D \approx 2.5$, give rise to a compact shadow of dimension $D' = 2$. The angular projection represents a more complex problem due to the mix of very different length scales. Nevertheless the theorem given by Equation 2.18 can be extended to the case of angular projections in the limit of small angles.

We discuss now a different but related problem. We investigate the properties of the structure that comes out from the intersection of a fractal with dimension D, embedded in the $d = 3$ Euclidean space, with an object of dimension D' ? The later can be for

example a line ($D' = 1$ - schematically a pencil beam survey), a plane ($D' = 2$) or a random distribution ($D' = 3$). Then the *co-dimension* of the intersection is equal to the sum of the *co-dimensions* of the two intersecting structures. We can represent this as

$$d - D_I = (d - D) + (d - D') \tag{2.19}$$

where D_I is the fractal dimension of the intersection set. Hence we can write for the dimension D_I:

$$D_I = D + D' - d \tag{2.20}$$

If $D_I \leq 0$, in the intersection it is not possible to recover any correlated signal. Hence, e.g., the intersection of a stochastic fractal with a random distribution has the same dimension $D_I = D$ of the original structure. Such a property is useful in the discussion of surveys in which a random sampling has been applied.

2.5 Other Fractal Dimensions

The illustration of the Hausdorff dimension shown previously may be a good description from a mathematical point of view, but it is hard to get an intuitive feel about significance of the fractal dimension from it. Moreover, we do not have a clear picture of what this fractional value of dimension means. In order to try to answer these questions let us see different definitions of fractal dimension and some examples.

2.5.1 Similarity Dimension

The fractals we discuss may be considered to be sets of points embedded in space. This space has the usual topological dimension which we are used to, and from a physicist's point of view it coincides with degrees of freedom defined by the number of independent variables. So the location of a point on a given line is determined by one real number and a set of two independent real numbers is needed to define a plane. If we define dimension by the number of degrees of freedom in this way, we are in a position to

consider a d-dimensional space for any non-negative integer d. In fact, in mechanics it is conventional to consider the motion of m particles in 3 dimensions as being the motion of one particle in a $6m$-dimensional space if we take each particle's position and momentum as independent.

The dimension defined by degrees of freedom seems very natural but contains a serious flaw. In practice we can have a curve (e.g. a Peano Curve) that folds so wildly that it nearly 'fills' a plane. In this way we are able to define the position of any point on the plane by a single real number. Hence the degree of freedom, or the dimension, of *this* plane becomes 1, which contradicts the empirical value 2. In order to explain such structures we have to define a new dimension based on similarity.

Let us consider dividing a unit line segment into N parts. As we decrease the size (say δ) of each part, the N will correspondingly increase. This results in $N(\delta) \propto 1/\delta$, implying for a straight line segment of unit length we have $N\delta^1 = 1$. Similarly, if we divide a unit square into N similar parts, each one is scaled by a factor $\delta = 1/N^{1/2}$ (if $N = 4$ the square is scaled by half the side length); so $N\delta^2 = 1$. Now if a unit cube is divided in N parts, each scaled by $\delta = 1/N^{1/3}$ (again if $N = 8$ the cube is scaled by half the side length), we have $N\delta^3 = 1$. Note that the exponents of δ correspond to the space dimensions in each case. Generalizing this discussion we may say that for an object of N parts, each scaled down from the whole by a ratio δ, the relation $N\delta^D = 1$ defines the *similarity dimension* D of the set as

$$D = \lim_{\delta \to 0} \frac{d \log N}{d \log 1/\delta}. \tag{2.21}$$

The calculation of similarity dimension of sets can be better viewed with the example of a strictly self similar fractal called "Koch Curve". Figure 2.2 shows the construction of the von Koch curve, and any of its segments of unit length is composed of 4 sub-segments each of which is scaled down by a factor 1/3 from its parent. Therefore, its similarity dimension is $D = \log 4 \,/\, \log 3 \cong 1.26$. This non-integer dimension, greater than one but less than two, reflects the properties of the curve. It somehow fills more

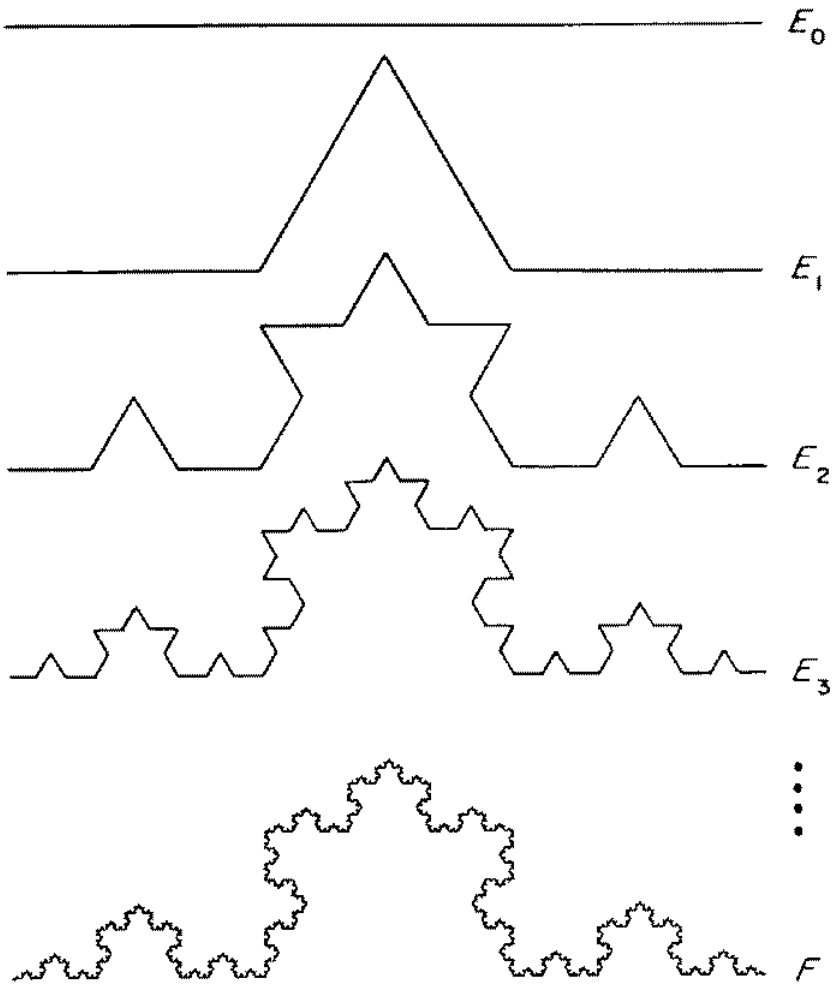


Figure 2.2: Construction of the von Koch curve F. At each stage, the middle third of each interval is replaced by the other two sides of an equilateral triangle. We can see that the length of the curve E_k goes to infinity as k tends to infinity. The von Koch curve occupies almost zero area implying that geometric measures like length and area are not well defined for fractal structures.

space than a simple line ($D = 1$), but less than a Euclidean area of the plane ($D = 2$). Figure 2.2 also shows that the von Koch curve has a finite structure which is reflected in irregularities at all scales; nonetheless, this intricate structure stems from a basically simple construction. Whilst it is reasonable to call it a curve, it is too irregular to have tangents in the classical sense. A simple calculation on the von Koch curve (Figure 2.2) shows that at k^{th} step E_k is of length $\left(\frac{4}{3}\right)^k$; letting k tend to infinity implies that the curve F has infinite length. On the other hand, curve F occupies almost zero area in the plane. So neither length nor area provides a very useful description of the size of the von Koch curve F.

After this discussion we start to have a better idea of what those fractal dimensions mean. Roughly, a fractal dimension provides a description of how much space a set fills. It is a measure of the prominence of the irregularities of a set when viewed at very small scales. We can therefore expect that a shape (or point set) with a high fractal dimension will be more complicated (or clustered) than another shape with a lower fractal dimension. The Hausdorff dimension described previously can be seen as a generalization of this similarity dimension. Unfortunately, similarity dimension is only meaningful for a small class of strictly self-similar sets. For non self similar fractals we need to introduce more general measures like box counting dimensions discussed below.

2.5.2 Box Counting Dimension

The Hausdorff and similarity dimensions defined so far provide definitions of fractal dimension for deterministic fractals, i.e., classical fractal sets in a mathematically idealized way. Although some of these classical fractals can be used to model physical structures, what is necessary now is to discuss structures that are statistically self similar, which are encountered in natural phenomena. Hence, we need to apply as far as possible the mathematical concepts and tools developed so far in the study of such statistically self similar fractal structures. One such tool is called the box counting dimension. In this approach the irregular curve or the distribution of particles is covered with a set of boxes of size δ and the number of boxes are counted which contain the part of the fractal. This

size δ is varied over a range and the resulting number of boxes required to cover the distribution of points gives the number $N(\delta)$. Obviously $N(\delta)$ will increase as the size δ decreases. If we proceed this way and find $N(\delta)$ for smaller values of δ, we are able to plot a graph of $N(\delta)$ versus δ, for different grid sizes. Now it follows from equation (2.17) that asymptotically in the limit of small δ the following equation is valid:

$$N(\delta) \propto \frac{1}{\delta^D}. \tag{2.22}$$

So the fractal dimension D of the distribution can be determined by finding the slope of $\log N(\delta)$ plotted as a function of $\log \delta$. We get the expression for the box counting dimension D_b as

$$D_b := \lim_{\delta \to 0} \frac{d \log N(\delta)}{d \log(1/\delta)}. \tag{2.23}$$

If the limit does not exist then one must talk about the upper box dimension and the lower box dimension which correspond to the upper limit and lower limit respectively in the expression above. In other words, the box-counting dimension is strictly defined only if the upper and lower box dimensions are equal. The upper box dimension is sometimes called the entropy dimension, Kolmogorov dimension, Kolmogorov capacity or upper Minkowski dimension, while the lower box dimension is also called the lower Minkowski dimension. Box counting dimension D_b is, in essence, a scaling rule comparing how a pattern's detail changes with the scale at which it is considered. According to equation (2.22), for a space filling distribution we expect that $N(\delta)$ should decrease as δ^{-3}, so that fractal dimension for such a distribution is equal to the dimension of the ambient space *i.e.* $D_b = 3$. In a similar way for a filamentary structure it is $N(\delta) \sim \delta^{-1}$, while for a planer point distribution $N(\delta) \sim \delta^{-2}$, with resulting box counting dimensions $D_b = 1$ and $D_b = 2$ respectively. In more general cases, non integer dimensions can also be expected. By means of equation (2.22) we can obtain the expression for the length L of irregular curve as

$$L = N(\delta) \ \mathbf{x} \ \delta \propto \delta^{1-D},$$

which shows its explicit dependence on the yardstick chosen.

The box counting dimension proposes a systematic measurement which applies to any structure in the plane, and can be readily adapted for structures in the space. It is perhaps the most commonly used method of calculating dimensions. Its advantage lies in the easy and automatic computability provided by the method, as it is straightforward to count boxes and maintain statistics allowing dimension calculation. The program can be carried out for shapes with and without self-similarity and, moreover, the objects may be embedded in higher dimensional spaces.

Note that the above two definitions of dimension (i.e. Hausdorff and Box counting) deal with the number of required coverings.These definitions have no regard to the number of points contained inside each of the covering boxes. In this sense, such dimensions depend on the 'shape' of the distribution. In this way they provide a purely geometrical description, while no information is given about the clumpiness, as correlation functions do. In order to extend the description in terms of fractal dimensions, so as to include the clustering properties of a distribution, we need to introduce a probability measure, so that adequate information about the clustering of the distribution is available.

2.6 Probability and Probability Measure

The probability of an event is not just a property of an individual experiment. It is a joint property of the number of different possible outcomes of the experiment performed under similar conditions. If an experiment is performed N times, and a certain outcome A occurs in M of these cases, the ratio M/N approaches a limiting value as $N \to \infty$. This ratio is defined as the probability $P(A)$ of A. In other words probability of an event is a measure of how likely the event is to occur when the random experiment within a sample space is run. In a sample space S, a measure $d\mu$ is said to be a probability measure if $d\mu(A) \geq 0$ for any event A within the sample space. The probability measure has also got to satisfy $d\mu(S) = 1$. While analyzing the clustering properties of distribution of points, the coarse grained probability, $p_i(r)$, in terms of the probability measure $d\mu$ is

given by

$$p_i(r) = \int_{\Lambda_i} d\mu(x) \tag{2.24}$$

It provides the measure of "mass" contained inside the hypercube Λ_i of side r, with $i = 1, 2, \cdots, N(r)$. Accordingly, the set $P_r = \{p_i; i = 1, \cdots, N(r)\}$ is the probability distribution over the $N(r)$ different states. In this way the information content of the distribution can be defined as

$$J(r, P(r)) = \log_2 N(r) + \sum_{i=1}^{N(r)} p_i \log_2 p_i \tag{2.25}$$

This is characterized in terms of Information Dimension of the distribution which we discuss below.

2.6.1 Information Dimension

For a homogenous distribution, all the boxes are expected to be equally populated, that is, all the states are equally probable (maximum entropy configuration). Correspondingly, the quantity $J(r, P(r))$ vanishes, thus indicating the absence of any information carried by unclustered structures. Conversely, the maximum information content is obtained when one single state has unity probability, while it is vanishing for all the other states (minimum entropy configuration). In this case, $J(r, P(r)) = \log_2 N(r)$, while in general $0 \leq J(r, P(r)) \leq \log_2 N(r)$.We define the Shannon information (or entropy),

$$I(r, P(r)) = -\sum_{i=1}^{N(r)} p_i \log_2 p_i \tag{2.26}$$

as the difference between the maximum information content and the actual information provided by the P_r distribution. Therefore, the information dimension,

$$D_I = \lim_{r \to 0} \frac{I(r, P(r))}{\log_2(1/r)} = -\lim_{r \to 0} \frac{\langle \log p_i \rangle}{\log \frac{1}{r}} \tag{2.27}$$

is related to the rate of information loss as the resolution scale increases.

2.6.2 Correlation Dimension

A further important characterization of the scale-invariant properties of a fractal set is given in terms of the correlation dimension, originally introduced by Grassberger & Procaccia . For a given point $\mathbf{x_i}$ belonging to A, let

$$C_i(r) = \frac{1}{N} \sum_{j=1 \neq i}^{N} \Theta(r - |\mathbf{x_i} - \mathbf{x_j}|) = \frac{n_i(r)}{N} \tag{2.28}$$

is the probability of finding $n_i(< r)$ points out of the N points of the set within a distance r from $\mathbf{x_i}$. In equation 2.28, Θ is the Heaviside step function with the following property:

$$\Theta(x) = \begin{cases} 1, & x > 0, \\ 0, & x < 0. \end{cases} \tag{2.29}$$

We, then, introduce the correlation integral

$$C(r) = \frac{1}{N} \lim_{N \to \infty} \sum_{i=1}^{N} C_i(r) \tag{2.30}$$

whose scaling in the limit $r \to 0$ defines the correlation dimension, D_ν, according to

$$C(r) \sim r^{D_\nu} \tag{2.31}$$

Note that for a structure that behaves like a fractal at all the scales it is not possible to define an average density, since it turns out to depend on the dimension of the fractal itself. In fact, since equation 2.31 gives the scaling of the number of neighbors, the density around the i^{th} point will scale as r^{3-D_ν}, and, thus, unless $D_\nu = 3$, it decreases for increasing scales. Note that this kind of behavior is not expected for the distribution of cosmic structures, which, on grounds of the Cosmological Principle, should reach homogeneity at sufficiently large scales. However, we can define fractal dimensions in a finite scale range, while taking homogeneity at large scales. In this case, following the definition of the 2-point correlation function given in subsection 2.2, it is easy to see that

it is related to the correlation integral of equation 2.30 according to

$$C(r) = \int_0^r d^3r'[1 + \xi(r')] = \bar{N}\left[1 + (\frac{r_c}{r})^\gamma\right] \tag{2.32}$$

Here, $\bar{N} = \frac{4}{3}\pi r^3 \bar{n}$ is the number of neighbors within a radius r expected for a homogeneous distribution, while the clustering scale r_c is related to the correlation length r_o as $r_c = [3/(3-\gamma)]^{1/\gamma} r_o$. Thus, according to the definition 2.31 of correlation dimension, the observed power law shape of the 2-point correlation function implies that at $r \ll r_c$ the galaxy distribution behaves like a fractal with $D_\nu \neq 3$, while assuming large scale homogeneity gives $D_\nu = 3$ at $r \gg r_c$.

As we have seen in subsection 2.2.3, a complete statistical description of a given points distribution requires the knowledge of correlations or moments of any order. In a similar way, a complete characterization of the scaling properties of a fractal set should require the introduction of a hierarchy of scaling indices, that generalize those already introduced and that account for the scaling of correlation functions of different orders. This will be realized in the following subsection by introducing the concept of the multifractal spectrum of generalized dimensions.

2.6.3 The Generalized Dimension

The various definitions of fractal dimension that we have introduced represent particular cases of a continuous sequence of scaling indices, known as multifractal spectrum of generalized dimensions (see e.g. Borgani, 1995). A first definition can be given in terms of the generalized Hausdorff dimensions, which represents the extension of the classical Hausdorff dimension of equation (2.17). Consider p_i to be the measure associated with a given set Λ_i (as defined by equation 2.24). We can introduce a partition function $\Gamma(q,\tau)$ as

$$\Gamma(q,\tau) = \begin{cases} \lim_{r\to 0} \inf_{\Gamma_A^r} \sum_i \frac{{p_i}^q}{{r_i}^\tau}, & \tau \leq 0, \quad q \leq 1, \\ \lim_{r\to 0} \sup_{\Gamma_A^r} \sum_i \frac{{p_i}^q}{{r_i}^\tau}, & \tau \geq 0, \quad q \geq 1. \end{cases} \tag{2.33}$$

For each value of q, the respective $\tau(\equiv \tau_q)$ is defined as the unique value which makes $\Gamma(q,\tau)$ a finite constant. Then, the generalized Hausdorff dimensions are defined as

$$D(q) = \frac{\tau(q)}{(q-1)} \tag{2.34}$$

For $q = 1$, $D(1) = \lim_{q\to 1} D(q)$. From this definition, it is easy to recognize that Hausdorff Dimension, $D_H = D(0) = -\tau(0)$.

A further set of scaling indices is given by the *Renyi dimensions*. Let us consider a covering, of a point set, formed by $N(r)$ cells of the same size r. Then, if n_i is the number of points in the cell i, the probability $p_i = n_i(r)/\sum_j n_j$ is the measure associated to the i^{th} box. The Renyi dimensions are defined as

$$D_q = \frac{1}{q-1} \lim_{r\to 0} \frac{\log \sum_i {p_i}^q}{\log r} \tag{2.35}$$

In this case, the capacity dimension corresponds to the $q = 0$ case, while the information dimension is recovered in the limit $q \to 1$. In general, it can be proved that $D(q) \leq D_q$, while in most cases of practical application the two definitions (2.34) and (2.35) of generalized dimensions can be considered as completely equivalent.

A slightly different definition is represented by the Minkowski-Bouligand dimensions. In this case, the covering of the fractal set is obtained by means of spheres of radius r, that are centered each at a point belonging to the fractal. If $n_i(< r)$ is the number of points within r from the i^{th} point, the Minkowski-Bouligand dimensions are defined as

$$D'_q = \lim_{N\to\infty} \frac{1}{N^2} \lim_{r\to 0} \frac{1}{q-1} \frac{\log \sum_i {n_i}^{q-1}}{\log r} \tag{2.36}$$

and generalize the correlation dimension of equation 2.31 . Further, it can be proved that the Renyi and Minkowski-Bouligand dimensions are completely equivalent (Dressler, 1980).

An important class of fractals is represented by self-similar monofractals. These fractal sets are characterized by the fact that every part of the set represents an exact

replica of the whole set (in a statistical sense), so that the scaling properties are the same around each point. For these fractals $D_q = D_H$ for any q, so that a single dimension gives a complete characterization of the whole set. More complex fractal sets are represented by multifractals. In this case, the entire spectrum of generalized fractal dimensions D_q is required to describe the local character of the scaling properties. For a multifractal, it can be shown that $D_q \leq D_{q'}$ for $q \geq q'$. According to the definitions (2.33) of the Γ partition function and (2.35) of Renyi dimensions, in the case $q \gg 0$ the summations are dominated by the densest regions in the set, while for $q \ll 0$ the least dense regions give the largest contribution. In this sense, for positive q's the generalized dimensions provide information about the scaling properties of the distribution inside the regions of high density, as correlation functions do, while for $q \ll 0$ they account for the scaling inside the underdense regions, thus providing a comprehensive statistical description of the entire point distribution. We are going to characterize both homogeneous as well as slightly clustered distribution of points using Minkowski-Bouligand Dimension in chapter 3.

2.7 Lacunarity

So far we have quantified fractal structures by their dimension. That this is not a sufficient characterization can be illustrated by the fact that we can have two points sets (one deterministic and one stochastic Cantor set) with the same fractal dimension D but with different *morphological properties*. In order to distinguish such sets, Mandelbrot has introduced the concept of *lacunarity* F as

$$Nr(\lambda > \Lambda) = F\Lambda^{-D} \tag{2.37}$$

where $Nr(\lambda > \Lambda)$ is the number of voids with a size $\lambda > \Lambda$. The scaling behavior of $Nr(\lambda)$ is the same for both Cantor sets. However the lacunarity F, i.e. the prefactor of the distribution, takes different values for the two Cantor sets.

In order to define lacunarity for random fractals we need a probabilistic form of Equation 2.37. This can be done by introducing $P(\lambda)$, which is the conditional probability that, given a box of size ϵ containing points of the set, this box is neighbored by a void of size $\lambda > \Lambda$. Lacunarity is defined as the prefactor of the void distribution

$$P(\lambda > \Lambda) = F\Lambda^{-D} \, . \tag{2.38}$$

It is easy to show that in the case of deterministic fractals this definition gives the same value of the lacunarity defined in Equation 2.37. Lacunarity plays a very important role in the characterization of voids distribution in the available galaxy catalogs.

Chapter 3

Fractal Dimensions of a Homogeneous and Weakly Clustered Distribution

Homogeneity and isotropy of the universe at *sufficiently* large scales is a fundamental premise on which modern cosmology is based. Fractal dimensions of matter distribution is a parameter that can be used to test the hypothesis of homogeneity. In this method, galaxies are used as tracers of the distribution of matter and samples derived from various galaxy redshift surveys are used to determine the scale of homogeneity in the Universe. Ideally, for homogeneity, the distribution should be a mono-fractal with the fractal dimension equal to the ambient dimension. While this ideal definition is true for infinitely large point sets, this may not be realized, as in practice, we have only a finite point set. The correct benchmark for realistic data sets is a homogeneous distribution of a finite number of points and this should be used in place of the mathematically defined fractal dimension for infinite number of points (D) as a requirement for approach towards homogeneity. We derive the expected fractal dimension for a homogeneous distribution of a finite number of points. We show that for sufficiently large data sets the expected fractal dimension approaches D in the absence of clustering. It is also important to take the weak, but non-zero amplitude of clustering at very large scales into account. In this

chapter[1] we also compute the expected fractal dimension for a finite point set that is weakly clustered. Clustering introduces departures in the Fractal dimensions from D and in most situations the departures are small if the amplitude of clustering is small. Features in the two point correlation function, like those introduced by Baryon Acoustic Oscillations (BAO) can lead to non-trivial variations in the Fractal dimensions where the amplitude of clustering and deviations from D are no longer related in a monotonic manner. We show that the contribution of clustering and finite numbers to the fractal dimension is given by two separate terms in the expression.

3.1 Introduction

We expect the Universe to be homogeneous and isotropic on the largest scales. Indeed, one of the fundamental postulates in cosmology is that the Universe is spatially homogeneous and isotropic. It is this postulate, generally known as the Cosmological Principle (CP)(Einstein, 1917), that allows us to describe the geometry of the space time over large scales in terms of the Friedman-Robertson-Walker-Lemaitre (FLRW) metric. The standard approach to cosmology assumes that the universe can be modeled as a perturbed FLRW universe. The large scale structures (LSS) in the universe are believed to have been formed due to the collapse of small inhomogeneities present in the early Universe (Peebles, 1980; Peacock, 1999; Padmanabhan, 2002; Bernardeau et al., 2002). Thus it is of paramount importance to test whether the observed distribution of galaxies approaches a homogeneous distribution at large scales.

The primary aim of galaxy surveys (Colless et al., 2001; York et al., 2000; Shectman et al., 1996) is to determine the distribution of matter in our Universe. Redshift surveys of galaxies have revealed that the universe consists of a hierarchy of structures starting from groups and clusters of galaxies to superclusters and interconnected network of filaments spread across the observed Universe (van de Weygaert & Schaap, 2007; Colombi,

[1]This chapter is based on *Fractal Dimensions of a Weakly Clustered Distribution and the Scale of Homogeneity* (J.S. Bagla, Jaswant Yadav & T.R. Seshadri), Monthly Notices of Royal Astronomical Society **390**, 829

Pogosyan & Souradeep, 2000a; de Lapparent, Geller & Huchra, 1986; Kim et al., 2002).

Fractal dimensions can be used as an indicator to test whether or not the distribution of galaxies approaches homogeneity. One of the reasons that make the Fractal dimensions an attractive option is that one does not require the assumption that an average density of matter in the sample region is the same as that of the Universe as a whole (Mandelbrot, 1982). In other words one does not have to assume that the matter distribution in the Universe has achieved homogeneity within the sampled region itself (Martínez & Saar, 2002). Ideally one would like to work with volume limited samples in order to avoid corrections due to a varying selection function. Redshift surveys of galaxies can be used to construct such sub-samples from the full magnitude limited sample but this typically leads to a sub-sample that has a much smaller number of galaxies as compared to the full sample. This limitation was found to be too restrictive for the earliest surveys and corrections for the varying selection function were attempted in order to determine the scale of homogeneity: (for example see Bharadwaj, Gupta & Seshadri, 1999) With the large surveys available today, this limitation is no longer very serious. Fractal dimensions are computed for the given sample or sub-sample and the scale beyond which the fractal dimension is close to the physical dimension of the sample is identified as the scale of homogeneity. We expect that at scales larger than the scale of homogeneity, any fluctuation in density is small enough to be ignored. Thus at larger scales, CP can be assumed to be valid and it is at these scales that the FLRW metric is a correct description of the Universe.

Fractal Dimension is defined in the mathematically rigorous way only for an infinite set of points. Given that the observational samples are finite, there is a need to understand the relation between the fractal dimension and the physical dimension for such samples. In this chapter, we compute the expected fractal dimension for a finite distribution of points (see e.g. Borgani et al., 1993; Borgani & Murante, 1994) The early work on these effects has focused on small scales where the amplitude of clustering is large. In this work, we calculate fractal distribution for a uniform distribution, as well as for a weakly clustered distribution of a finite number of points. This is of interest at

larger scale where fractal dimensions are used as a tool to find the scale of homogeneity.

catalogs of different extra-galactic objects have been studied using various statistical methods. One of the important tools in this direction has been the use of two point correlation function $\xi(r)$ (Peebles, 1980) and its Fourier transform the power spectrum $P(k)$. We have precise estimates of $\xi(r)$ (Kulkarni et al., 2007; Ross et al., 2007; de Lapparent & Slezak, 2007) and the power spectrum $P(k)$ (Cole et al., 2005; Percival et al., 2007b) from different galaxy surveys. Different measurements appear to be consistent with one another once differences in selection function are accounted for (Cole, Sanchez & Wilkins , 2006) (but also see Sánchez & Cole, 2008) On small scales the two point correlation function is found to be well described by the form

$$\xi(r) = \left(\frac{r_0}{r}\right)^{\gamma} \tag{3.1}$$

where $\gamma = 1.75 \pm 0.03$ and $r_0 = 6.1 \pm 0.2\ h^{-1}$Mpc for the SDSS (Zehavi et al., 2002) and $\gamma = 1.67 \pm 0.03$ and $r_0 = 5.05 \pm 0.26\ h^{-1}$Mpc for the 2dFGRS (Hawkins et al., 2003). Recent galaxy surveys have reassured us that the power law behavior for $\xi(r)$ does not extend to arbitrarily large scales. The breakdown of this behavior occurs at $r > 16h^{-1}$Mpc for SDSS and at $r > 20h^{-1}$Mpc for 2dFGRS, which appears consistent with the distribution of galaxies being homogeneous at large scales. A note of caution here is that though the $\xi(r)$ determined from redshift surveys appear to be consistent with the universe being homogeneous at large scales in that $|\xi(r)| \ll 1$ at large r, it does not actually imply that the universe is necessarily homogeneous. This is because the two point correlation function given by,

$$\xi(r) =< \delta(x+r)\delta(x) > \tag{3.2}$$

where

$$\delta(x) = \frac{\rho(x) - \bar{\rho}}{\bar{\rho}} \tag{3.3}$$

presupposes that galaxy distribution that we are analyzing is homogeneous on the

scales within our survey region. This is implicit in the fact that $\bar{\rho}$, which is assumed to be the spatial average density of matter in the universe, is computed by averaging the density from within the survey volume. Of course, it may be possible to demonstrate that the survey is a fair sample of the universe by showing that the values of $\bar{\rho}$ derived from sub-samples of the survey are consistent with each other, or that the value of $\bar{\rho}$ computed at different scales converges to a definite value at scales much smaller than the size of the survey. However, to verify and hence validate the cosmological principle, it is useful to consider a statistical test which does not presuppose the premise being tested, In other words the survey region need not be assumed to represent a fair sample of the whole Universe. In this chapter we consider one such test, the "multi-fractal analysis" and apply it to distribution of particles in random as well as clustered distributions.

Fractal dimension, which is generally a fractional number, is characterized by the scaling exponent. A single exponent is sufficient to characterize a monofractal distribution. However, in many physical situations, we need to use a set with an invariant measure characterized by a whole spectrum of scaling exponents, instead of a single number. Such a system is called a multi-fractal and we need to do a multifractal analysis of a point set to study the system.

In this chapter we calculate the fractal dimension for a distribution of finite number of points which are distributed homogeneously as well as for those which are weakly clustered. For this purpose we use the multi-fractal analysis to study the scaling behavior of uniform as well as weakly clustered distributions in turn finding the relationship between the fractal dimension and the two point correlation function. We find deviations of fractal dimension D_q from the D arising due to a finite number of points for a random distribution with uniform density, these deviations arise due to discreteness. In this case we can relate the deviation (of D_q from D) to the number density of points. We further show that for a distribution of points with weak clustering, there is an additional deviation of D_q from D. This deviation can be related to the two point correlation and the intuitive relation between the amplitude of clustering and deviation from homogeneity can be quantified. We then apply the derived relation to cosmology and compute the

expected deviations in a model that fits most observations.

A brief outline of this chapter is as follows. In §3.2 we describe briefly the method of calculation of fractal dimension from various measures. §3.3 contains the expression of Minkowski Bouligand dimension for a homogeneous distribution of points. The fractal dimension of a weakly clustered distribution has been calculated in §3.4. The appendices A.1 and A.2 contain the detailed derivation of the expression for fractal dimension.

3.2 Fractal Dimensions

Fractal dimension is a basic characterization of any point distribution. There are many different methods that can be used to calculate the fractal dimension. Box counting dimension of fractal distribution is defined in terms of non empty boxes $N(r)$ of radius r required to cover the distribution. Cosider a distribution of points in a region. We start by covering this distribution with certain number of spheres $N(r)$ of radius r. As the radius of the sphere increases, we note, that the number of the spheres required to cover the distribution of point decreases. Hence their is a scaling relation between the number of spheres and the radius of the sphere. This relation can be represented as

$$N(r) \propto r^{-D_b} \tag{3.4}$$

where D_b is defined to be the box counting dimension of the distribution of particles. One of the difficulties with such an analysis is that it does not depend on the number of particles inside the boxes and rather depends only on the number of boxes. As such it provides limited information about the degree of clumpiness of the distribution and is a purely geometrical measure. To get more detailed information on clustering of the distribution we need to use higher order moments of the distribution. The simplest of these moments is the correlation dimension. Instead of using the formal definition of correlation dimension, which demands that the number of points in the distribution approach infinity, we choose a 'working definition' which can be applied to a distribution

of a finite number of points.

We consider a distribution of N points. Out of these N points we choose M points and put spheres centered on these M points. Let the number of points lying inside the sphere of radius r centered on i^{th} point be $n_i(r)$. Correlation integral for such a system of points is then given by

$$C_2(r) = \frac{1}{NM} \sum_{i=1}^{M} n_i(r) \tag{3.5}$$

In general the number of points and spheres are different as one cannot use points near the edge of the sample where a sphere of radius r is not completely inside the sample.

The term $n_i(r)$ denotes the number of particles within a distance r from a particle at the point i :

$$n_i(r) = \sum_{j=1}^{N} \Theta(r - \mid \mathbf{x}_i - \mathbf{x}_j \mid) \tag{3.6}$$

where $\mathbf{x}_i$ is the position coordinate of the i^{th} particle. $\Theta(x)$ is the Heaviside function given by equation 2.29.

An alternative way of defining correlation integral $C_2(r)$ is in terms of the probability distribution of particles. In this method we define C_2 in terms of the probability of finding particles in a sphere of radius r centered on one of the particles in the distribution. Let $P(n; r, N)$ represent the probability of finding n neighbours inside a radius r to any particle in a distribution of N particles. Then correlation integral C_2 can be defined as,

$$C_2(r) = \frac{1}{N} \sum_{n=0}^{N} nP(n; r, N) \tag{3.7}$$

For a homogeneous distribution of points, the probability for any point to fall within a sphere is proportional to the ratio of the volume of the sphere to the total volume of the sample. In such a case C_2 reduces to the product of the volume of a sphere of radius r and the total number of particles, divided by the total volume. As the total number and total volume are fixed quantities, C_2 for a homogeneous distribution of points scales as r^D at sufficiently large scales, where as before D is the dimension of the ambient space in which the particles are distributed.

For a general point distribution the power law scaling of correlation integral i.e. $C_2(r) \propto r^{D_2}$ defines the correlation dimension D_2 of the distribution.

$$D_2(r) = \frac{\partial \log C_2(r)}{\partial \log r} \tag{3.8}$$

Depending on the scaling of C_2, the value of correlation dimension D_2 can vary with scale r. For the special case of a homogeneous distribution, we see that $D_2(r) = D$ at sufficiently large scales and this matches the intuitive expectation that the correlation dimension of a homogeneous distribution of points should equal the mathematically defined fractal dimension for infinite number of points.

We see from equation 3.7 that the correlation integral is defined in terms of probability of finding n point out of a distribution of N points within a distance r. This makes it a measure of one of the moments of the distribution. We need all the moments of the distribution to completely characterize the system statistically. The multifractal analysis used here does this with the generalized dimension D_q, the Minkowski-Bouligand dimension, which is defined for an arbitrary q and typically computed for a range of values. It is different from Renyi dimension only in the aspect that in this case the spheres of radius r have been centered at the point belonging to the fractal whereas in Renyi dimension the sphere need not be centered on the particle in the distribution (Borgani, 1995). However, it can be proved that these two definitions are completely equivalent (Dressler, 1980).

The definition of generalized dimension D_q is a generalization of the correlation dimension D_2. In stead of taking the first moment of the distribution as in case of correlation integral, we need to take the $(q-1)^{th}$ moment in order to define the generalized integral $C_q(r)$. Consider $n_i(r)$ to be the number of neighbours within r of the particle i. The correlation integral for such a distribution of particles can now be generalized to define $C_q(r)$ as

$$C_q(r) = \frac{1}{NM} \sum_{i=1}^{M} n_i^{q-1}(r) \tag{3.9}$$

Alternatively, in terms of probability distribution function (equation 3.7) this can be

written as

$$\begin{aligned} C_q(r) &= \frac{1}{N}\sum_{n=0}^{N} n^{q-1} P_c(n) \\ &= \frac{1}{N}\langle \mathcal{N}^{q-1} \rangle_c \end{aligned} \tag{3.10}$$

The subscript c denotes that spheres have been centered on points within the distribution. Thus the q^{th} order generalized integral (i.e. $C_q(r)$) is related to the $(q-1)^{th}$ order moment of the distribution. Equation 3.10 can now be used to define the Minkowski-Bouligand dimension as

$$D_q = \frac{1}{q-1}\frac{d\log C_q(r)}{d\log r} \tag{3.11}$$

As is obvious from equation 3.11, the generalized dimension corresponds to the correlation dimension for $q = 2$. For the case $q = 1$ we can see from equation (3.10) that $C_q(r)$ does not contain any information about the number of neighbours of the particle which has been taken as center. If we place the center of the sphere randomly, as is done in calculating the Renyi Dimension , then q=1 corresponds to box counting dimension. For $q > 2$ the contribution to C_q comes from a range of correlation function ranging from 2 point correlation function to q point correlation function. If the distribution of points is a monofractal then we have $D_q = D_2$ for all q and at all scales. However, a multifractal distribution of points can only be described by the full spectrum of D_q.

By construction , the positive values of q in the generalized integral (see equation 3.9) give more weightage to regions with a high number density whereas the negative values of q give more weightage to underdense regions. Thus we may interpret D_q for $q \gg 0$ as characterizing the scaling behavior of the galaxy distribution in the high density regions like clusters whereas $q \ll 0$ characterizes the scaling in voids. In the situation where the galaxy distribution is homogeneous and isotropic on large scales, we intuitively expect $D_q \simeq D = 3$ independent of the value of q at the relevant scales.

3.3 Fractal Dimension for a Homogeneous Distribution

In our analysis, we first compute the expected values for C_q and D_q for a homogeneous distribution in a finite volume. The volume V_{tot} over which the points are distributed is taken to be much larger than volume of spheres (V). The points are distributed randomly and hence we can use a set of points generated from the Binomial distribution. The conditional probability of finding n points in a sphere of volume V centered on a point, if V_{tot} contains N particles is:

$$P_c(n) = \binom{N-1}{n-1} p^{n-1} (1-p)^{N-n} \tag{3.12}$$

where p is the probability that a given point (out of N) is located in a randomly placed sphere. This p, however, is not the same as the probability of finding only one particle in such a sphere. If we place a sphere of volume V inside a distribution which is contained in volume V_{tot} then $p = \frac{V}{V_{tot}}$. . Recalling that we have taken $V_{tot} \gg V$, we shall assume in our calculations that $p \ll 1$. The above expression 3.12 follows from the fact that with the sphere centered on one point, this point is already in the sphere and we need to compute the probability of $n-1$ points out of $N-1$ being in the sphere. For comparison, the probability of finding n particles in a randomly placed sphere of volume V is:

$$P(n) = \binom{N}{n} p^{n} (1-p)^{N-n} \tag{3.13}$$

The average number of points in a randomly placed sphere which we define by $\bar{N}$ is Np and we assume that this is much larger than unity. Thus we work in the limit where $1 \ll Np \ll N$.

In order to calculate the generalized correlation integral we need to calculate the higher order moments of the distribution. Moments of the distribution for spheres centered at points (denoted by$\langle \mathcal{N}^m \rangle_c$) can be related to moments for randomly placed

spheres (denoted by $\langle \mathcal{N}^m \rangle$). We start with the expression for the conditional moment given by

$$\begin{aligned}
\langle \mathcal{N}^m \rangle_c &= \sum n^m P_c(n) \\
&= \sum n^m \binom{N-1}{n-1} p^{n-1} (1-p)^{N-n} \\
&= \sum (n-1+1)^m \binom{N-1}{n-1} p^{n-1} (1-p)^{N-n} \\
&\simeq \sum (n-1)^m \binom{N-1}{n-1} p^{n-1} (1-p)^{N-n} \\
&\quad + \sum m (n-1)^{m-1} \binom{N-1}{n-1} p^{n-1} (1-p)^{N-n}
\end{aligned} \tag{3.14}$$

In the limit $1 \ll Np \ll N$ we can replace $N-1$ by N in the above expression 3.14. So we get the following approximation

$$\langle \mathcal{N}^m \rangle_c \simeq \langle \mathcal{N}^m \rangle + m \langle \mathcal{N}^{m-1} \rangle \tag{3.15}$$

It is once again stressed that subscript c on the angle brackets denotes that the average is for spheres centered on points within the distribution. A specific application of the above expression is to compute the average number of points in a spherical region. The average number of points in a sphere centered at a point is $1+(N-1)p \simeq Np+1 = \bar{N}+1$. $\bar{N}$, here, is the average number of points in the randomly placed sphere in the binomial distribution. The difference between the two expressions for average number of particles arises due to fluctuations that are present in an uncorrelated distribution of points.

The generalized correlation integral can now be expressed in terms of the moments of this probability distribution. In the limit $1 \ll Np \ll N$ we can write down a leading order expression for the generalized correlation integral for $q > 1$ as:

$$NC_q(r) \simeq \bar{N}^{q-1} + \frac{(q-1)(q-2)}{2} \bar{N}^{q-2} + (q-1)\bar{N}^{q-2} + \cdots \tag{3.16}$$

(See Appendix A.1 for a detailed discussion on how we arrived at this expression.) Here we have ignored terms that are of lower order in $\bar{N}$ and terms of the same order in $\bar{N}$

with powers of p multiplying it.

The Minkowski-Bouligand dimension corresponding to this generalized integral(3.16) has contribution from the fluctuations in the distribution due to discreetness and also from preferential placing of the spheres on the points in the distribution. We can quantify these contributions by:

$$D_q(r) = D - \frac{(q-2)}{2}\frac{D}{\bar{N}} - \frac{D}{\bar{N}} \tag{3.17}$$

to the same order as for equation 3.16. The last two terms in the intermediate expression for $D_q(r)$ have a different origin: the first of the two terms arises due to fluctuations present in a random distribution and the second term arises due to the spheres being centered at points within the distribution and this leads to weak clustering. A few points of significance are:

- We do not expect $D_q(r)$ to coincide with the D even if the distribution of points is homogeneous. Thus the benchmark for a sample of points is not D but $D_q(r)$ given by expression 3.17, and if the Minkowski-Bouligand dimension for a distribution of points coincides with $D_q(r)$ then it may be considered as a homogeneous distribution of points.

- For $q > 1$, the correction due to a finite size sample always leads to a smaller value for $D_q(r)$ than the D.

- The correction is small if $\bar{N} \gg 1$, as expected. The correction arises primarily due to discreteness and has been discussed by Borgani (1995). The major advantage of our approach is that we are able to derive an analytic expression for the correction.

3.4 Fractal dimension of a Weakly Clustered Distribution

In a weakly clustered distributions of points, the counts of number of neighbours, for spheres whose centers are randomly placed and for those whose centers are placed on

the points in the distribution, differ by a significant amount. Also there is no simple way of relating the two and hence we cannot use the approach we followed in section 3.3 for estimating the generalized correlation integral.

In order to make further progress, we note that we can always define an average density for a distribution of a finite number of points in a finite volume. This allows us to go a step further and also define $n-$point correlation functions. It is well known that this can be used to relate the generalized correlation integral with $n-$point correlation functions (e.g. see Borgani, 1995). We shall show in Appendix A.2 that it is possible to considerably simplify this relation, between the generalized correlation integral and two point correlation function, in the limit of weak clustering. We can show that the correlation integral may be written as follows (see Appendix A.2 for details).

$$\begin{aligned} NC_q(r) &\simeq \bar{N}^{q-1}\left(1+\frac{(q-1)\,(q-2)}{2\bar{N}}+\frac{q(q-1)}{2}\bar{\xi}\right. \\ &\left.+\mathcal{O}\left(\bar{\xi}^2\right)+\mathcal{O}\left(\frac{\bar{\xi}}{\bar{N}}\right)+\mathcal{O}\left(\frac{1}{\bar{N}^2}\right)\right) \end{aligned} \tag{3.18}$$

Here we have used the assumption that $|\bar{\xi}| \ll 1$ (*weak clustering limit*) and that higher powers of $\bar{\xi}$ as well as higher order correlation functions can be ignored when compared to terms of order $\bar{\xi}$ and $1/\bar{N}$. This assumption is over and above the limit $1 \ll Np \ll N$. The first two terms on the right hand side of equation 3.18 are same as the first two terms in the expression 3.16 for C_q that we derived for a homogeneous distribution of points. The third term encapsulates the contribution of clustering. This differs from the last term in the corresponding expression for a homogeneous distribution as in that case the "clustering" is only due to spheres being centered at points whereas in this case the locations of every pair of points has a weak correlation. It is worth noting that the highest order term of order $\mathcal{O}\left(\bar{\xi}^2\right)$ has a factor $\mathcal{O}\left(q^3\right)$ and hence can become important for sufficiently large q. *This may be quantified by stating that* $q\bar{\xi} \ll 1$ *is the more relevant small parameter for this perturbative expansion.*

The Minkowski-Bouligand dimension for such a system can now be expressed in the

form

$$\begin{aligned} D_q(r) &\simeq D - \frac{D\,(q-2)}{2\bar{N}} + \frac{q}{2}\frac{\partial\bar{\xi}}{\partial\log r} \\ &= D - \frac{D\,(q-2)}{2\bar{N}} - \frac{Dq}{2}\left(\bar{\xi}(r) - \xi(r)\right) \\ &= D - (\Delta D_q)_{\bar{N}} - (\Delta D_q)_{clus} \end{aligned} \tag{3.19}$$

It is interesting to see that the departure of D_q from D due to a finite sample and weak clustering is given by distinct terms at the leading order. This expression allows us to compute D_q for a distribution of points if the number density and $\bar{\xi}$ are known.

Recall that D is the mathematically defined fractal dimension for an infinite set of points with a homogeneous distribution. We have already noted some aspects of the correction due to a finite number of points in the previous section, here we would like to highlight aspects of corrections due to clustering.

- For hierarchical clustering, the last two terms in equation 3.19 have the same sign and lead to a smaller value for D_q as compared to D.

- Unless the correlation function has a feature at some scale, smaller correlation corresponds to a smaller correction to the Minkowski-Bouligand dimension. The expression given above quantifies this intuitive expectation.

- Note that for $q = 2$, the expression given here is exact. For this case, the contribution of clustering has also been discussed by Martinez et al. (1998).

- If the correlation function has a feature then it is possible to have a small correction term $(\Delta D_q)_{clus}$ for a relatively large ξ. The relation between ξ and $(\Delta D_q)_{clus}$ is not longer one to one.

Our results as given in equation 3.17 and 3.19 are completely general and apply to any distribution of points with weak clustering. In chapter 4 we shall be using the example of galaxy clustering in concordance model of cosmology to illustrate our calculations.

Appendix A

A.1 Derivation of D_q for Homogeneous Distribution

In a homogeneous distribution of points the probability for a point to be found in a sphere of volume V enclosed within a total volume of V_{tot} is $p = V/V_{tot}$. In an uncorrelated distribution of points, the probability of finding a point is independent of the location of other points in the distribution and hence the probability of n out of N points falling in a sphere of volume V is:

$$P(n, N) = \binom{N}{n} p^n (1-p)^{N-n} \tag{A.1}$$

The distribution function determined by the probability function $P(n, N)$ is called a Binomial distribution. As discussed in the text, the probability distribution for occupation number of spheres centered at points (i.e. $P_c(n, N)$), as given by equation 3.12) is different from the one given in equation A.1. However, moments of the distribution in both these cases can be related in the limit $N \gg Np \gg 1$ as shown by expression 3.15. We will be interested in the description being accurate to first order in $1/\bar{N}$.

We start with the moment generating function for the Binomial distribution given by

$$G(t) = \sum_{n=0}^{N} e^{tn} \binom{N}{n} p^n (1-p)^{N-n} = (pe^t + 1 - p)^N \tag{A.2}$$

The m^{th} moment of this distribution can then be calculated by differentiating G, m

times with respect to t, and then setting t to zero. The m^{th} derivative of $G(t)$, at $t = 0$ can be written as:

$$G^{(m)}(t) \mid_{t=0} = \sum_{l=1}^{m} H_{m,l} \frac{N!}{(N-l)!} p^l \tag{A.3}$$

where H satisfies the following recurrence relation

$$H_{m,l} = l H_{m-1,l} + H_{m-1,l-1} \tag{A.4}$$

with the assumption that $H_{1,1} = 1$ and $H_{m,l} = 0$ for $l > m$ and $l < 1$. It can now be shown that for all l,

$$H_{l,l} = 1$$

The m^{th} moment of the distribution is thus given by:

$$\begin{aligned} \langle \mathcal{N}^m \rangle &= G^{(m)}(t) \mid_{t=0} \\ &= \sum_{l=1}^{m} H_{m,l} \frac{N!}{(N-l)!} p^l \end{aligned}$$

On the face of it this expression has a large number of terms for $m \gg 1$ and is difficult to analyze. But if we assume that $p \ll 1$ and $\bar{N} = Np \gg 1$ then we can rewrite the expression in the following form:

$$\begin{aligned} \langle \mathcal{N}^m \rangle &= H_{m,m} \frac{N!}{(N-m)!} p^m + H_{m,m-1} \frac{N!}{(N-m+1)!} p^{m-1} + \cdots \\ &= \bar{N}^m + \mathcal{O}(p\bar{N}^{m-1}) + H_{m,m-1}\bar{N}^{m-1} + \mathcal{O}(p\bar{N}^{m-2}) + \mathcal{O}(\bar{N}^{m-2}) \\ &\simeq \bar{N}^m + \frac{m\,(m-1)}{2} \bar{N}^{m-1} \end{aligned} \tag{A.5}$$

Here we have retained terms up to $\mathcal{O}(\bar{N}^{m-1})$ and have dropped all other lower order terms. We have also used the recurrence relation A.4 and find that $H_{m,m-1} = m(m-1)/2$.

We can now write the expression for the generalized correlation integral with the help of equation 3.10, 3.15 and A.5 as:

$$NC_q(r) = \langle \mathcal{N}^{q-1} \rangle + (q-1) \langle \mathcal{N}^{q-2} \rangle$$

$$\simeq \bar{N}^{q-1} + \frac{(q-1)(q-2)}{2}\bar{N}^{q-2} + (q-1)\bar{N}^{q-2} + \cdots \tag{A.6}$$

The Minkowski-Bouligand dimension for a homogeneous distribution is then given by

$$\begin{aligned} D_q(r) &= \frac{1}{q-1}\frac{\partial \log C_q(r)}{\partial \log r} \\ &\simeq \frac{1}{q-1}\frac{\partial}{\partial \log r}\log\left[\bar{N}^{q-1}\left(1+\frac{(q-1)\,(q-2)}{2\bar{N}}\right)+\frac{(q-1)}{\bar{N}}\right] \\ &\simeq D\left(1-\frac{(q-2)}{2\bar{N}}-\frac{1}{\bar{N}}\right) \end{aligned} \tag{A.7}$$

where D is the dimension of the space in which particles are distributed. This is the relation we have used in equation 3.17 to describe a homogeneous distribution of points. In this calculation, we have again made use of the fact that $\bar{N} \gg 1$ and that it scales as the D^{th} power of scale r for a random distribution such that

$$D = \frac{\partial \log \bar{N}}{\partial \log r} \tag{A.8}$$

A.2 Derivation of D_q for a Weakly Clustered Distribution

In this section we will derive the form of the correlation integral for a weakly clustered distribution of points. Consider a sphere of volume V contained within the sample of volume V_{tot}. We follow the approach given in §36 of Peebles (1980) for estimating the correlation integral. In order to estimate the correlation integral, we divide the sphere into small elements such that each element contains at most one point. This is a useful construct because in such a case we have $n_i^m = n_i$ for all $m \geq 0$, where n_i is the number of points occupying the i^{th} infinitesimal volume element. If the occupancy of the i^{th}

volume element is n_i then we have the total number of particle in this volume given by:

$$\mathcal{N} = \sum_i n_i \tag{A.9}$$

We can also define the mean count of such a distribution as:

$$\langle \mathcal{N} \rangle = \left\langle \sum_i n_i \right\rangle = \bar{N} \tag{A.10}$$

Knowing the mean, the m^{th} moment of the distribution is given by:

$$\langle \mathcal{N}^m \rangle = \left\langle \left(\sum_i n_i \right)^m \right\rangle \tag{A.11}$$

Since we are not interested in number of galaxies in a region, but are rather interested in the number of galaxies around a galaxy, we have to take care that the spheres that we throw in the sample are centered on the points of the sample. If the sphere is centered at a point in the distribution then the average number of points, and hence the different order moments of the distribution, are denoted as $< \mathcal{N}^m >_c$. This is what we are interested in for the purpose of computing the correlation integral.

$$\langle \mathcal{N}^m \rangle_c = \left\langle \left(\sum_i n_i \right)^m \right\rangle_c \tag{A.12}$$

Averaging the sum raised to a positive integral power will lead to averaging of terms of type $n_i n_j$, $n_i n_j n_k$, etc. and the expression for such terms involves n-point correlation functions, n being the number of terms being multiplied. With this insight, we can write

$$\begin{aligned} \langle \mathcal{N}^m \rangle_c &= \left\langle \sum n_1^m \right\rangle_c + m \left\langle \sum n_1^{m-1} n_m \right\rangle_c + \cdots + \frac{m(m-1)}{2} \left\langle \sum n_1^2 n_3 \ldots n_m \right\rangle_c \\ &\quad + \left\langle \sum n_1 n_2 n_3 \ldots n_m \right\rangle_c \\ &= \left\langle \sum n_1 \right\rangle_c + m \left\langle \sum n_1 n_m \right\rangle_c + \cdots + \frac{m(m-1)}{2} \left\langle \sum n_1 n_3 \ldots n_m \right\rangle_c \\ &\quad + \left\langle \sum n_1 n_2 n_3 \ldots n_m \right\rangle_c \end{aligned} \tag{A.13}$$

Here the terms in the expansion correspond to all indices being equal for the first term, only one of the indices differing from the rest for the second term and so on. The last term in this series is for all the m indices being different. We have shifted the notation in order to write down the explicit form for arbitrary m. It is interesting to see that for 2^{nd} order moment of the distribution, the expression A.13 reduces to

$$\begin{aligned}
\langle \mathcal{N}^2 \rangle_c &= \langle \sum_i n_i^2 \rangle_c + \langle \sum_{i,j} n_i n_j \rangle_c \\
&= \langle \sum_i n_i \rangle_c + \langle \sum_{i,j} n_i n_j \rangle_c \\
&= \bar{n} V + \bar{n} \int \xi(r) \delta v + \bar{n}^2 \int \delta v_1 \delta v_2 (1 + \xi(r_1) + \xi(r_2) + \xi(r_{12}) + \zeta(r_1, r_2))
\end{aligned}$$

here ζ is the reduced three point correlation function given by equation 2.11. V and δv represent the total sample volume and the volume of the sphere that has been thrown in the sample. $\bar{n}$ is the average number density (i.e. $\bar{n} = \bar{N}/V$).

For a weakly clustered set of points with statistical isotropy and homogeneity, we can safely assume that on large scales the magnitude of the two point correlation function is small compared to unity, and higher order correlation functions are even smaller. Keeping this in mind we get the second moment of this weakly clustered distribution as

$$\begin{aligned}
\langle \mathcal{N}^2 \rangle_c &= \bar{n} V + \bar{n}^2 V^2 + \bar{n} \int \xi(r) \delta v + 3 \bar{n}^2 \int \delta v_1 \delta v_2 (\xi(r)) \\
&= \bar{N}^2 \left(1 + \frac{3}{V} \int \xi(r) \delta v + \frac{1}{\bar{N} V} \int \xi(r) \delta v + \frac{1}{\bar{N}} \right) \qquad \text{(A.14)}
\end{aligned}$$

Further, we continue to use the assumption that $\bar{N} \gg 1$ and hence we need to retain only terms of the highest and the next highest order in this parameter. Thus we have two small parameters in the problem: ξ and $1/\bar{N}$ and our task is to compute the leading order terms in $\langle \mathcal{N}^m \rangle_c$. Here ξ is the two point correlation function.

It can be shown that the leading order contribution to $\langle \mathcal{N}^m \rangle_c$ comes from the last term in the series in Equation (A.13), and the next to leading order contribution is from the last two terms. We should note that these terms also contain several terms that are

smaller than the leading and next to leading order within them.

The foremost contribution comes from the uncorrelated component of the last term, i.e., $\bar{n}^m \int \delta v_1 \delta v_2 \ldots \delta v_m = \bar{N}^m$. The integral here is over m independent volumes and $\bar{n}$ is the average number density. The corresponding term for $m = 2$ is the first term in expression A.14.

The next contribution comes from components of this term that include the effect of pairwise correlations. As there are m distinct points in the last term of expression A.13, the number of distinct pairs is $m(m+1)/2$. It implies that the contributing term due to the effect of pairwise correlation has the form:

$$\bar{N}^m \frac{m(m+1)}{2} \bar{\xi}(r) \tag{A.15}$$

where r is the radius of the sphere with volume δv and $\bar{\xi}$ is given by:

$$\bar{\xi}(r) = \frac{3}{r^3} \int_0^r x^2 \xi(x) dx \qquad . \tag{A.16}$$

The corresponding term for $m = 2$ is the second term in expression A.14. It can be shown that all other components of the last term involve higher order correlation functions, or higher powers of ξ.

Further, it can be shown that the contributions that contain only a single power of ξ from other terms in the series in Equation (A.13) contain a lower power of $\bar{N}$ *i.e.* it is of $\bar{N}^{m'} \bar{\xi}$ form where m' ranges from 0 to $m-1$. Lastly, the only other term that we need to take into account comes from the penultimate term in the series in Equation (A.13). The uncorrelated component of this term is:

$$\frac{m(m-1)}{2} \bar{N}^{m-1} \tag{A.17}$$

Thus we have for the m^{th} moment of the counts of neighbors:

$$\langle \mathcal{N}^m \rangle_c = \bar{N}^m + \frac{m(m+1)}{2} \bar{N}^m \bar{\xi} + \frac{m(m-1)}{2} \bar{N}^{m-1}$$

$$
\begin{aligned}
&+\bar{N}^m\left(\mathcal{O}\left(\bar{\xi}^2\right)+\mathcal{O}\left(\frac{\bar{\xi}}{\bar{N}}\right)+\mathcal{O}\left(\frac{1}{\bar{N}^2}\right)\right)\\
\simeq\ & \bar{N}^m\left(1+\frac{m(m+1)}{2}\bar{\xi}+\frac{m(m-1)}{2\bar{N}}\right) \qquad \text{(A.18)}
\end{aligned}
$$

The largest term of order $\mathcal{O}\left(\bar{\xi}^2\right)$ arises from the contribution of correlated triangles in the last term of Equation (A.13). The number of triangles scales as m^3 and hence can become important for sufficiently large m. This may be codified by stating that $m\bar{\xi} \ll 1$ is the more relevant small parameter.

Hence the correlation integral (3.10) can be written as

$$
NC_q(r) \simeq \bar{N}^{q-1}\left(1+\frac{q(q-1)}{2}\bar{\xi}+\frac{(q-1)(q-2)}{2\bar{N}}\right) \qquad \text{(A.19)}
$$

From this we can calculate the Minkowski-Bouligand dimension using equation A.7 as

$$
\begin{aligned}
D_q(r) &= \frac{1}{(q-1)}\frac{\partial \log C_q(r)}{\partial \log r}\\
&\simeq D-\frac{D\,(q-2)}{2\bar{N}}+\frac{q}{2}\frac{\partial\bar{\xi}}{\partial\log r}\\
&= D-\frac{D\,(q-2)}{2\bar{N}}-\frac{Dq}{2}\left(\bar{\xi}(r)-\xi(r)\right) \qquad \text{(A.20)}
\end{aligned}
$$

This is the required expression for the fractal dimension of a weakly clustered distribution and has been used in text as equation 3.19.

Chapter 4

Fractal Dimension as a measure of Homogeneity

There are various observational probes which test the cosmological principle. The near isotropicity of Cosmic Microwave background Radiations (CMBR) tell us that our space time locally is very well described by FRW metric. Similarly the CMBR anisotropies at large angular scales (10°) imply that density fluctuations in the distribution of matter in the Universe is very small on large scales ($\delta\rho/\rho \sim 10^{-4}$ on $1000\,h^{-1}Mpc$). The absence of big voids in the distribution of Lyman α absorbers is also consistent with the Universe being Homogeneous on large scales. In this chapter[1] we have tested the large scale homogeneity of the homogeneous as well as slightly clustered distribution of points using *multifractal analysis* developed in chapter 3. The distribution is said to be homogeneous when the multifractal dimension of the point distribution is same for all moments and is equal to the ambient dimension of the space in which the points are distributed. We have also applied our analysis to the distribution of various types (L_* as well as LRG) of galaxies in the concordance model of cosmology. We see that in the concordance model, the fractal dimension makes a rapid transition to values close to 3 at scales between 40 and 100 Mpc.

[1]This chapter is based on *Fractal Dimensions of a Weakly Clustered Distribution and the Scale of Homogeneity* (J.S. Bagla, Jaswant Yadav & T.R. Seshadri), Monthly Notices of Royal Astronomical Society **390**, 829

4.1 Introduction

Various groups have used the concept of fractals to analyze catalogues of extra-galactic objects. See Jones et al. (2005) for an excellent review of quantitative measures used for describing distributions of points. Based on the scale invariance of galaxy clustering, Pietronero (1987) suggested that the distribution of galaxies is a fractal to arbitrarily large scales. In a later analysis of different samples of galaxies Coleman & Pietronero (1992) obtained results consistent with this argument. On the other hand Borgani (1995) showed that the distribution is a fractal only on small scales and on large scales there is a transition to homogeneity. If the distribution of galaxies is found to be a fractal then the average number of galaxies in a volume of radius r centred on a galaxy should scale as r^d, where d is the fractal dimension. Hence, the number density of neighboring galaxies would go as $\rho = r^{d-D}$ in a D dimensional distribution. This, when calculated for higher values of r will show a decrease compared to its value for lower scales. This effect led Sylos Labini et al. (1998) to believe that the value of correlation length r_0 (see equation 3.1) increases with the increase in size of the sample. However, this interpretation is not supported by volume limited samples of various galaxy redshift surveys (Benoist et al., 1996; Martínez, López-Martí, & Pons-Bordería, 2001).

A number of authors (e.g. Cappi et al., 1998; Hatton, 1999; Best, 2000; Amendola & Palladino, 1999; Baryshev & Bukhmastova, 2004) have shown the distribution of galaxies to be a mono-fractal up to the largest scales that they were able to analyze. On the other hand homogeneity has been seen at large scale in other analysis (see *e.g.* Guzzo, 1997; Bharadwaj, Gupta & Seshadri, 1999; Martinez, 1999; Kurokawa, Morikawa & Mouri, 2001; Pan & Coles, 2000; Hogg et al., 2005). The best argument in favour of large scale homogeneity stems from the near isotropy of radio sources or background radiation in projection on the sky (Wu, Lahav & Rees, 1999).

We have developed a model (equation 3.17 and 3.19) which predicts the scale of homogeneity for a homogeneous distribution of points as well as for a slightly clustered distribution of points. In order to test our model we have applied it to a multifractal

multinomial distribution of points for which the fractal dimension is analytically known. We have also applied our model to the concordance model of cosmology. In this case we have considered unbiased (e.g. L_* galaxies) as well as biased (e.g. Large Redshift Galaxies (LRG)) tracers of the underlying dark matter distribution, to test the scales at which these distributions attain homogeneity. For this purpose we have taken the large scale two point correlation function for a flat ΛCDM model with a power law initial power spectrum that best fits the observations. We have used this correlation function to see how the clustering in the distribution of galaxies is going to affect the scale of homogeneity. We have also studied the effect of the bump in the correlation function on the behaviour of the fractal dimension of a clustered galaxy distribution.

A brief outline of this chapter is as follows. In section 4.2 we discuss the application of our model to the multifractal multinomial distribution. The discussion about the scale of homogeneity of different types of galaxies follows in section 4.3. We end this chapter with a list of conclusions in section 4.4.

4.2 Multifractal Multinomial Distribution

We have applied our method to the multinomial multifractal model discussed in literature (See e.g. Martínez & Saar, 2002). The set of points for this model can be generated by starting with a square and dividing it into four parts. We assign a probability $\{f_i\}$ to each of these subsquares $\left(\sum_{i=1}^{4} f_i = 1\right)$. At the second step each of the small squares is again subdivided into 4 parts thus getting 16 squares. The probability attached to each one of these 16 squares is the product of the probability of the individual square (one of the f_i's) multiplied by the probability of its parent square. This construction can be continued iteratively by dividing each smaller square further and assigning probability by multiplying the corresponding number f_i by all its ancestors. We performed this construction to $L = 8$ levels, thus getting a 256^2 lattice with the corresponding probability measures associated with each pixel of lattice. As an illustration we have performed several realisations of this process for different choices of the initial parameters :

Model	f_1	f_2	f_3	f_4
I	0.25	0.25	0.25	0.25
II	0.23	0.27	0.25	0.25
III	0.15	0.20	0.30	0.35
IV	0.05	0.50	0.35	0.15

Table 1: Generation of various multinomial multifractal Distribution

These realisations are shown in figure 4.1 on page 89. For such models we have an analytical expression for the generalized dimension (Falconer, 1990; Martinez et al., 1990) given by

$$D_q = \frac{1}{q-1} \log_2 \left(\sum_{i=1, f_i \neq 0}^{4} {f_i}^q \right) \tag{4.1}$$

As equation 4.1 is an analytical expression, it can be used to check whether our model for finite number and correlation work correctly or not.

We have calculated the generalized dimension for this model taking four different combination of f_i. In one of the cases all four f_i's are 0.25 so that the distribution is homogeneous. In this case the expected $D_q = 2$ for all q using the above expression. Our model in this case gives a scale dependent correction to this due to a finite number of particles. Figure 4.2 on page 90 shows $\Delta D_q = D_q - D$, as a function of $\langle N \rangle \equiv \bar{N}$ for $q = 2$ and 6 for this distribution. ΔD_q measured from a realization are plotted as points, and our model is shown as a curve. It is clear that for $\bar{N} \leq 10^3$, there is a visible deviation of D_q from the expected value and that our model correctly estimates this deviation.

We now simulate a weakly clustered distribution of points by taking the values of f_i slightly different from one another. More specifically, we present here, an example where the f_i's are close to 0.25 but not exactly equal to 0.25. This construction provides us a slightly clustered distribution. We used parent f_i to be $0.23, 0.27, 0.25$ and 0.25 and generated five realizations of this fractal. In this case, the expected $D_q = 1.986$ for $q = 6$. As this differs from $D = 2$, the difference in our model must come from clustering present in this fractal. Figure 4.3 on page 91 shows $\Delta D_q \equiv D_q - D_{q\,exp}$ as a function of

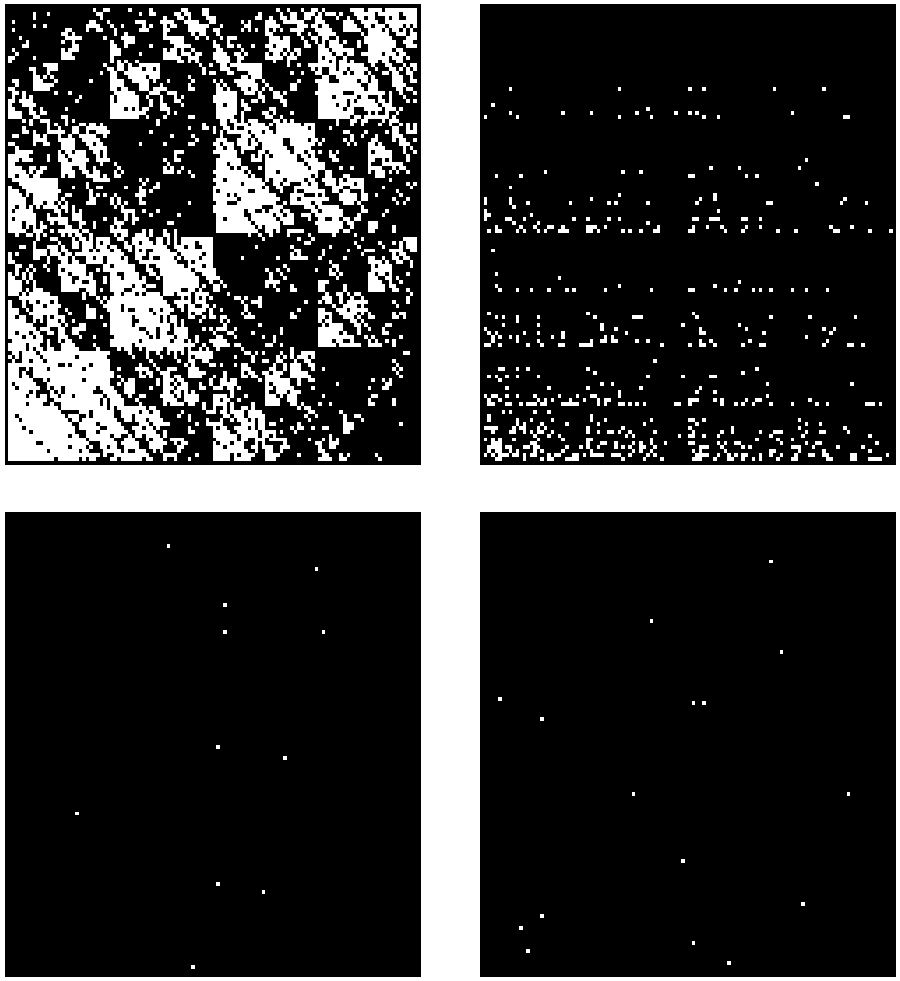


Figure 4.1: Multifractal multiplicative cascades with parameters given in table 1. Models are I, II, III and IV from bottom to top and left to right

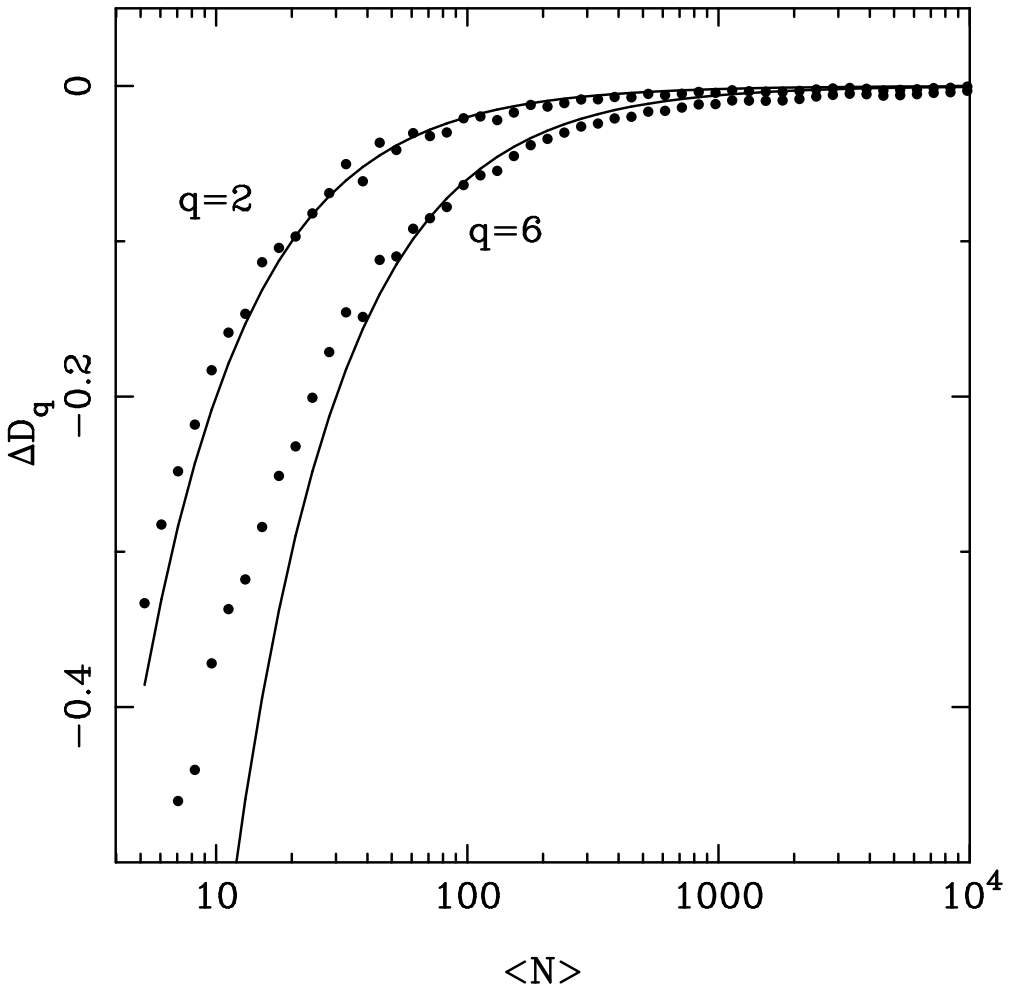


Figure 4.2: Our model is compared with the observed Fractal dimensions for a random distribution of points in the special case of the multinomial model (model I). ΔD_q is shown as a function of $\langle N \rangle \equiv \bar{N}$ for $q = 2$ and 6 for this distribution. ΔD_q measured from a realization are plotted as points, and our model is shown as a curve.

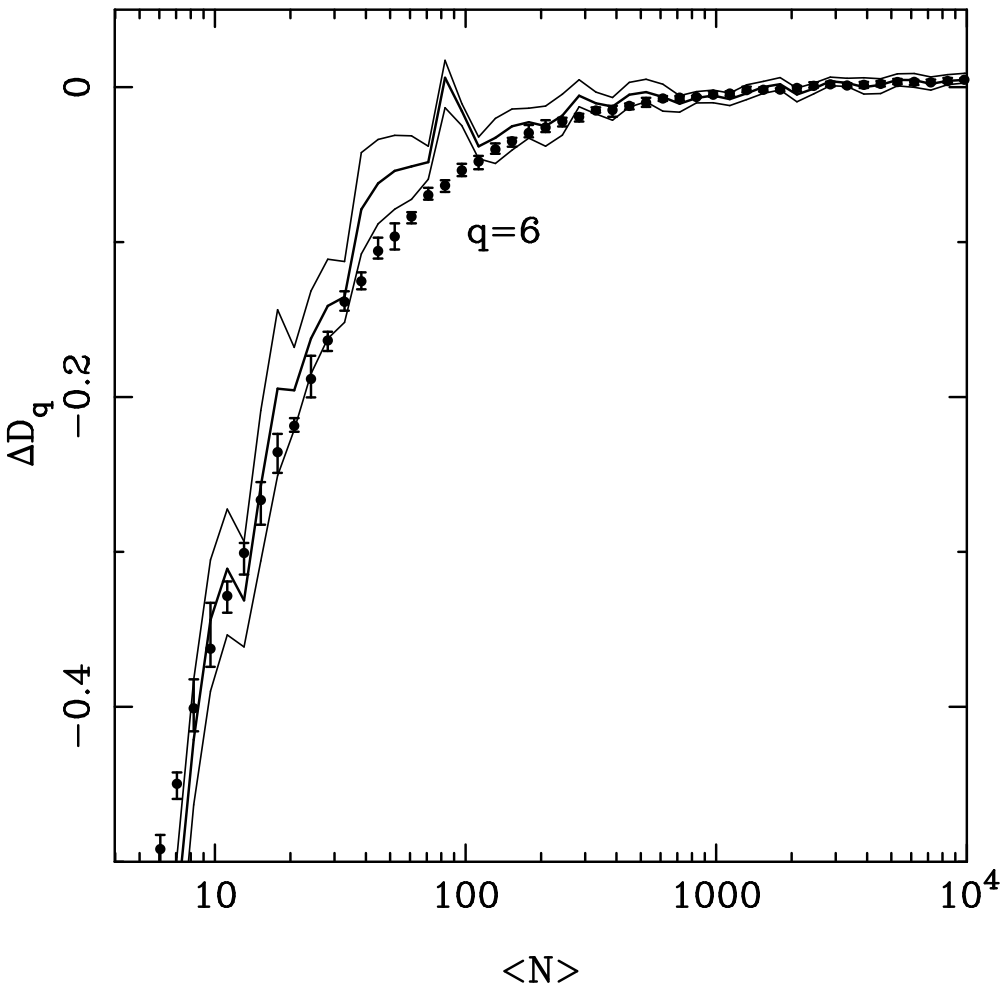


Figure 4.3: Our model is compared with the observed Fractal dimensions for a multinomial fractal with $f_i = 0.23, 0.27, 0.25, 0.25$ (model II). $\Delta D_q \equiv D_q - D_{q\,exp}$ is shown as a function of $\langle N \rangle$ for $q = 6$. We have plotted ΔD_q measured in the five realizations as points with error bars. The error bars mark the extreme values of ΔD_q seen in these realizations whereas the central point marks the average value. Predictions of our model based on correlation function measured in these realizations is shown as a thick line. Thick line corresponds to the average value of ξ and $\bar{\xi}$ measured in simulations, and thin lines mark the predictions of our model based on extreme values seen in these simulations.

$\langle N \rangle$ for $q = 6$, where $D_{q\,exp}$ follows from Equation 4.1.

We have plotted ΔD_q measured in the five realizations as points with error bars. The error bars mark the extreme values of ΔD_q seen in these realizations whereas the central point marks the average value. Predictions of our model (Equation 3.19) based on correlation function measured in these realizations is shown as a thick line. This line corresponds to the average value of ξ and $\bar{\xi}$ measured in simulations, and thin lines mark the predictions of our model based on extreme values seen in these simulations. At $\langle N \rangle \ll 100$, where the effect of a finite number is dominant, our model matches the measured ΔD_q very well. At $\langle N \rangle \gg 100$ where the effect of clustering is dominant we again find a good match between the model and measured values. It is significant that at very large $\langle N \rangle$, the deviation of D_q from $D = 2$ is correctly accounted for in our model.

However, there appears to be a mismatch in the transition region around $\langle N \rangle \simeq 100$. On inspection, we find that $\xi - \bar{\xi}$ has an oscillatory behavior up to this scale and the discrepancy corresponds to the last oscillation. At the scale of maximum discrepancy, $\xi - \bar{\xi} \simeq 0.05$ and perhaps we cannot ignore values of this order.

In summary we can say that our model works very well for the multinomial model and we find that the correction due to clustering as well as a finite number of points matches with the observed behavior of D_q.

4.3 Discussion

The expressions of D_q derived in chapter 3 in section 3.3 and 3.4 have a rich structure and we illustrate some of the features here. We would also like to discuss the application to the concordance model here. The two point correlation function for the model that fits best the WMAP-3 data (Spergel et al., 2007) is shown in Figure 4.4 on page 93. We have used the flat ΛCDM model with a power law initial power spectrum that best fits the WMAP-3 data here. Parameters of the model used here are: $H_0 = 73$ km/s/Mpc, $\Omega_b h^2 = 0.0223$, $\Omega_c h^2 = 0.105$, $n_s = 0.96$ and $\tau = 0.088$. For this model, $\sigma_8 = 0.76$. The two point correlation has been shown at large scales where the clustering can be assumed

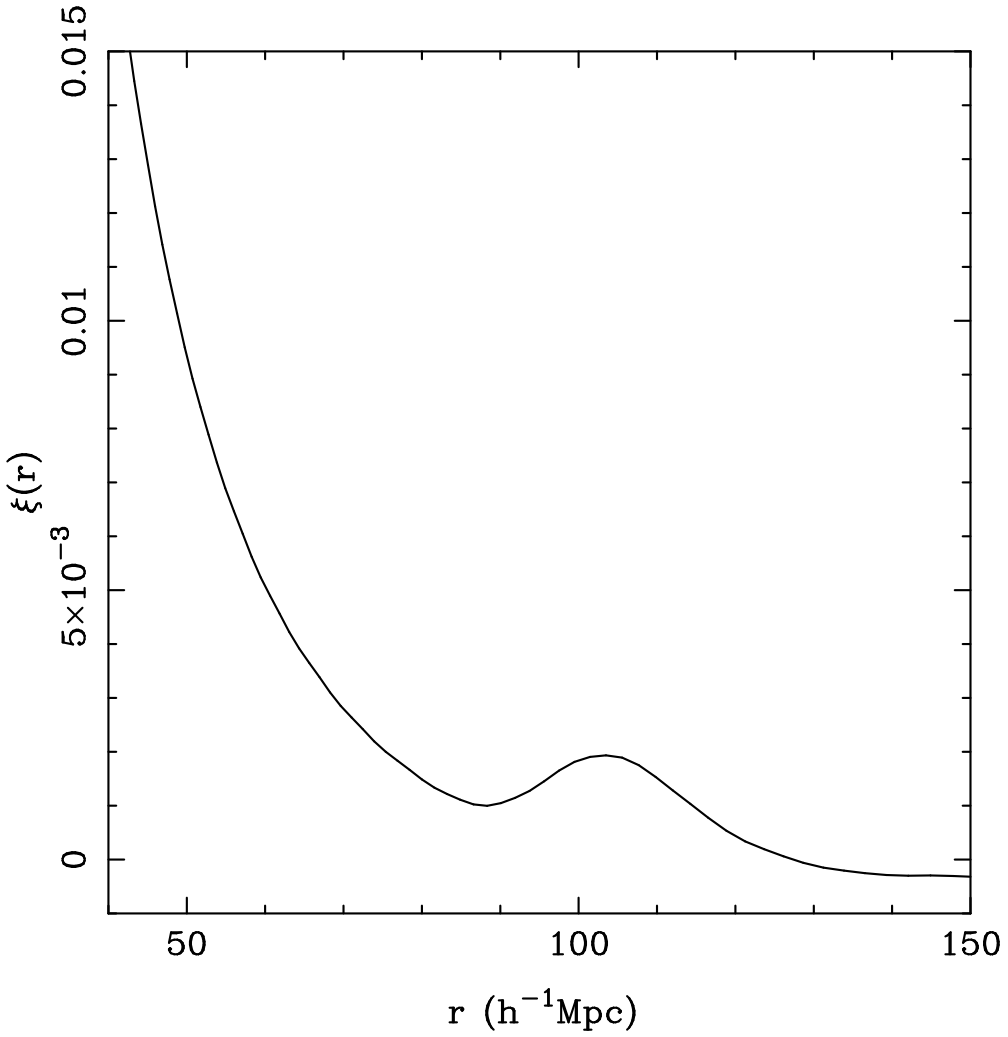


Figure 4.4: The linearly extrapolated two point correlation function is shown as a function of scale for the best fit model for WMAP-3 (see section 4.3 for details). This has been used, for calculation of $(\Delta D_q)_{clus}$.

to be weak. The most prominent feature here is the peak near 100 Mpc. This peak is caused by baryon acoustic oscillations (BAO) prior to decoupling (see, e.g., Eisenstein & Hu, 1998). Apart from this peak, the two point correlation function declines from small scales towards larger scales at length scales shown here. All observations of galaxies are carried out in redshift space. Therefore we must use the correlation function in redshift space. At large scales, redshift space distortions caused by infall lead to an enhancement of the two point correlation function. The enhancement is mainly along the line of sight but the angle averaged two point correlation function is also amplified by some amount (Kaiser, 1987).

Further, we must also take into account the *bias* in the distribution of galaxies while using the correlation function shown in Figure 4.4. This has been discussed by many authors (e.g. Kaiser, 1984; Bardeen et al., 1986; Brainerd & Villumsen, 1994; Fry, 1996; Mo & White, 1996; Bagla, 1998a,b; Dekel & Lahav , 1999). At large scales, we may assume that the linear bias factor b is sufficient for describing the redshift space distortions and clustering.

Lastly, we should mention that we are working with the linearly extrapolated correlation function at these scales even though there is some evidence that perturbative effects lead to a slight shift in the location of the peak in ξ (For example, see Smith et al., 2008). The only change caused by such a shift in the location of the peak is to in turn shift the scale where there appears to be a transition from large values of ΔD_q towards small and constant values. As the shift does not alter our key conclusions, we will ignore such effects in the following discussion.

We plot the expected departure of D_q from D for an unbiased sample of galaxies in Figure 4.5 on page 95. We assumed that typical (L*) galaxies have an average number density of 0.02 $\mathrm{h^3Mpc^{-3}}$ (Peebles, 1980)and a bias factor of unity. ΔD_q for such a population is shown as a function of scale by black curves for $q = 2$, 4 and 6. Red curves show the same quantity for a sample of galaxies similar to Luminous Red Galaxies (LRGs). We used a bias factor $b = 2$ and a number density of 5×10^{-5} $\mathrm{h^3Mpc^{-3}}$ that is representative of such a population (Percival et al., 2007b). ΔD_q is negative at all scales

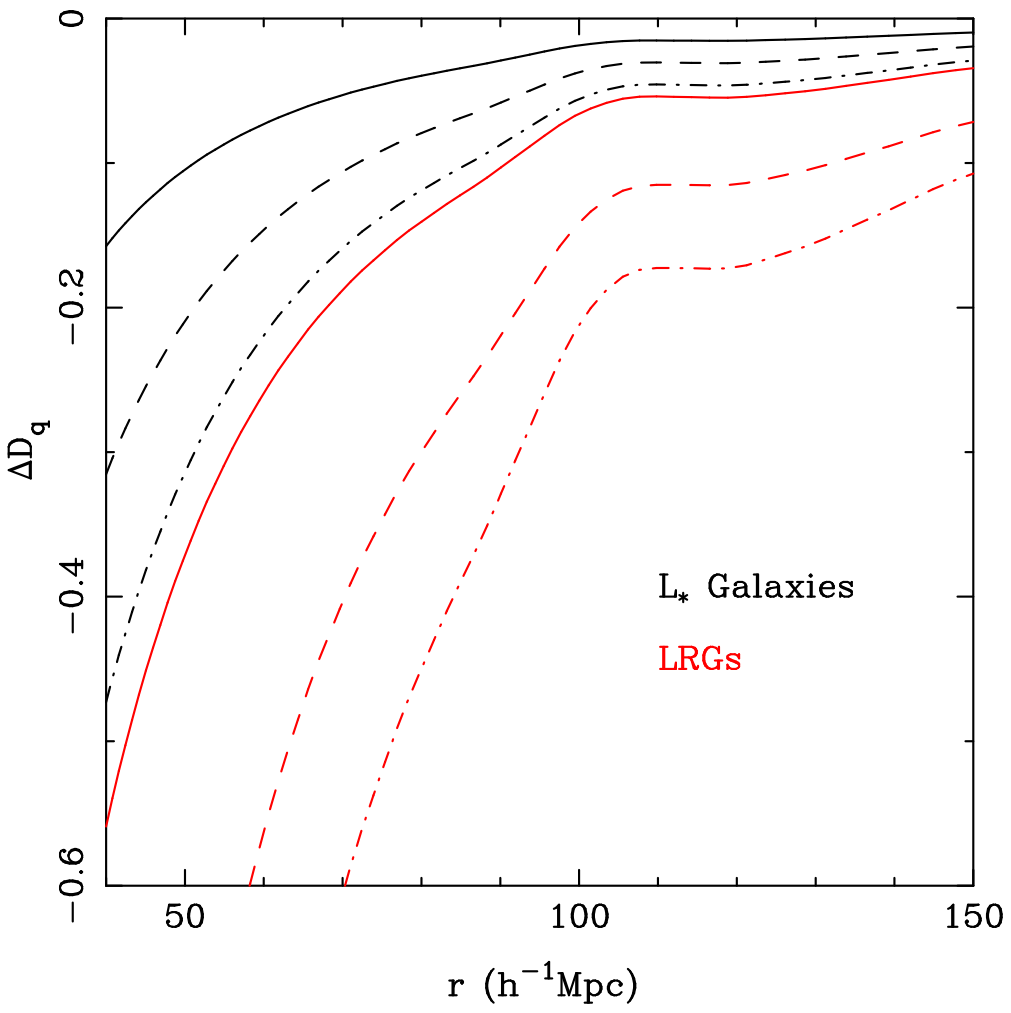


Figure 4.5: Estimated deviation of the Minkowski-Bouligand dimension from the physical dimension is shown here for two types of populations. In black we have plotted ΔD_q for an unbiased sample of points, distributed in redshift space with the real space correlation function as shown in Figure 4.2. The solid curve shows ΔD_2, whereas ΔD_4 and ΔD_6 are shown with a dashed curve and a dot-dashed curve respectively. Curves in red correspond to an LRG like population with a number density of 5×10^{-5} h^{-3}Mpc^3 and a linear bias of 2.

shown here, as expected from the expression (see Eqn.(3.19)) for hierarchical clustering. The behavior of ΔD_q as a function of scale has two distinct regimes on either side of 100 h^{-1}Mpc. The magnitude of ΔD_q decreases rapidly as we go from smaller scales towards 100 h^{-1}Mpc. At scales larger than 100 h^{-1}Mpc, magnitude of ΔD_q either stays constant or decreases at a very slow rate. The behavior of ΔD_q around 100 h^{-1}Mpc is dictated largely by the BAO peak in ξ at this scale. Although there is no peak in $\bar{\xi}$, $\partial\bar{\xi}/\partial \log r$ which is given by $-0.5D(\bar{\xi}(r) - \xi(r))$ has a minima and a maxima near the scale of the peak in $\xi(r)$. This results in a corresponding minima and maxima for ΔD_q as the contribution of a finite number of galaxies is subdominant at such large scales. We illustrate this in Figure 4.6 on page 97 where ΔD_4 is plotted for an LRG like sample, and the two contributions (from a finite sample and weak clustering) are also shown. If ξ has a power law form then there are no extrema for $\partial\bar{\xi}/\partial \log r$ and the magnitude of both ξ and ΔD_q becomes progressively smaller as we get to larger scales. There is a one to one relation between ξ and ΔD_q for a given model of this type. However, a feature like the peak introduced by BAO leads to the non-trivial behavior illustrated in Figure 4.5. Here we find that D_q can be smaller at scales with a larger ξ. For example, the scale with the local maxima of ξ is very close to the scale with the local minima of D_q. The intuitive correspondence of a small ξ implying a smaller deviation of D_q from D does not apply in this case.

The difference between the unbiased galaxy population, and an LRG like sample is stark. The LRG like sample has a Minkowski-Bouligand dimension that differs from $D = 3$ by a significant amount. The main reason for this difference is the high bias factor associated with the LRG population, although a smaller number density also makes some difference. Different clustering properties for different types of galaxies imply that these will have not have the same Minkowski-Bouligand dimension. This has no impact on determination of the scale of homogeneity for the universe, where we must use unbiased tracers.

The calculations presented in the section 3.3 and 3.4 allow us to estimate the offset of the Minkowski-Bouligand dimension from the physical dimension due to weak clustering

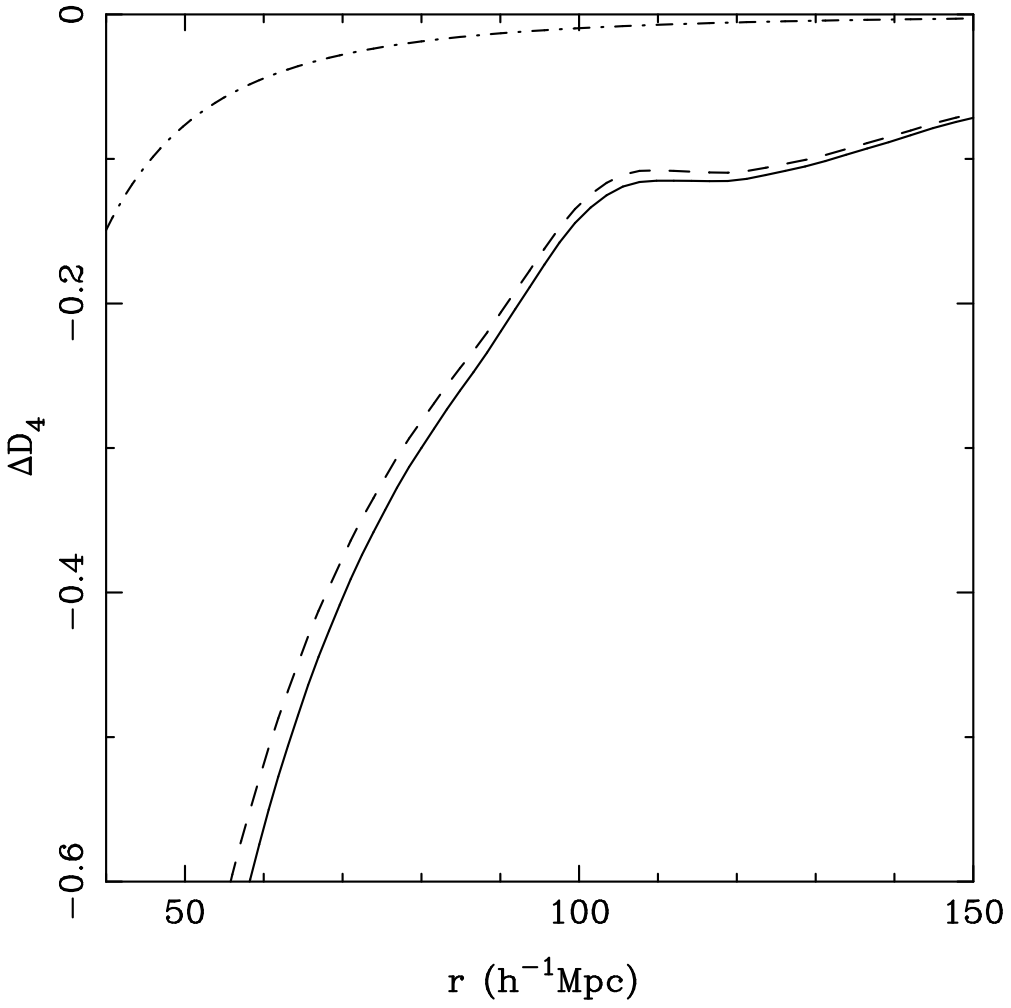


Figure 4.6: This figure shows the components of ΔD_q for an LRG like population of galaxies for $q = 4$. This value of q was chosen as the contribution of a finite number of galaxies does not vanish in this case. The solid line shows ΔD_4, the dashed line shows the contribution of clustering to ΔD_q and the dot-dashed line is the correction due to a finite number of galaxies. Clearly, the correction due to clustering is the dominant reason for departure of D_q from D.

and a finite sample. This has to be accompanied by a calculation of the dispersion in the expected values (Szapudi, Colombi, & Bernardeau, 1999; Colombi et al., 2000b). The natural estimate for the scale of homogeneity is the scale where the offset of the Minkowski-Bouligand dimension from the physical dimension becomes smaller than the dispersion in a sufficiently large survey. Given that the offset is dominated by the effect of clustering, we have $\Delta D_q \simeq 0.5Dq(\xi - \bar{\xi}) \sim q(\xi - \bar{\xi})$. The offset scales with q. Further, it is apparent that the dispersion in ΔD_q must also scale with q. This implies that the requirement of dispersion being greater than the offset leads to the same scale for all q. This is a very satisfying feature of this approach in that the scale of homogeneity does not depend on the choice of q as long as the effect of a finite number of points is subdominant.

Alternatively, we may argue that the scale of homogeneity should be identified with the scale above which the variation of ΔD_q is very small. While this is an acceptable prescription for typical galaxies where $\Delta D_q \leq 0.06$ at scales above 100 h^{-1}Mpc, it does not appear reasonable for an LRG like population. The scale of homogeneity for the latter population is clearly much larger than 100 h^{-1}Mpc.

4.4 Conclusions

We have studied the problem of the expected value of the Minkowski-Bouligand dimension for a finite distribution of points. For this purpose, we have studied a homogeneous distribution as well as a weakly clustered distribution. In our study, $q/\bar{N}$ and $q\bar{\xi}$ are taken to be small parameters and the deviation of D_q from D is estimated in terms of these quantities. In both cases we find that the expected values of the Minkowski-Bouligand dimension D_q are different from D for the distribution of points. For generic distributions, the value of D_q is less than the dimension D. We have derived an expression for D_q in terms of the correlation function and the number density in the limit of weak clustering. We see that the dimension of the ambient space (i.e. D) is not the correct benchmark for defining a homogeneous distribution and instead the minkowski bouli-

gand dimension of the distribution should match with equation 3.17 for the distribution to be homogeneous.

We find that $\Delta D_q = D_q - D$ is non-zero at all scales for unbiased tracers of mass in the concordance model in cosmology. For this model ΔD_q is a large negative number at small scales but it rapidly approaches zero at larger scales. ΔD_q is a very slowly varying function of scale above 100 h^{-1}Mpc and hence this may be tentatively identified as the scale of homogeneity for this model. A more quantitative approach requires us to estimate not only the systematic offset ΔD_q but the dispersion in this quantity. The scale of homogeneity can then be identified as the scale where the offset is smaller than the expected dispersion.

Although we have used the example of galaxy clustering for illustrating our calculations, the results as given in Equation (3.17) and Equation (3.19) are completely general and apply to any distribution of points with weak departures from homogeneity. A detailed derivation of the relations presented here, with verification using mock distributions of points will be presented in a future publication, where we also expect to highlight other applications.

We have obtained the scale of homogeneity of the galaxy distribution in the volume limited samples obtained from first data release of Sloan Digital Sky Survey. We will discuss this in detail in chapter 5.

Chapter 5

Testing homogeneity on large scales in the Sloan Digital Sky Survey

One of the most important assumption on which modern cosmology is based is the Cosmological Principle. It states that the Universe is homogeneous and isotropic on large scales. We[1] have tested the large scale homogeneity of the galaxy distribution in the Sloan Digital Sky Survey Data Release One (SDSS-DR1) using volume limited subsamples extracted from the two equatorial strips. These strips are nearly two dimensional (2D). The galaxy distribution is projected on the equatorial plane and we have carried out a 2-dimensional multi-fractal analysis by counting the number of galaxies inside circles of different radii r in the range $5\,h^{-1}$Mpc to $150\,h^{-1}$Mpc. The circles have been centred on galaxies. Different moments of the count-in-cells have been analyzed to identify a range of length-scales ($60 - 70\,h^{-1}$Mpc to $150h^{-1}$Mpc) where the moments show a power law scaling behavior. It has helped us to determine the scaling exponent which gives the spectrum of generalized dimension D_q. If the galaxy distribution is homogeneous, D_q does not vary with q and is equal to the Euclidean dimension which in our case is 2. We find that D_q varies in the range 1.7 to 2.2. We also constructed mock data from random, homogeneous point distributions and from ΛCDM N-body simulations with

[1]This chapter is based on *Testing homogeneity on large scales in Sloan Digital Sky Survey Data Release One*, (Jaswant Yadav, S. Bharadwaj, B. Pandey & T.R. Seshadri), Monthly Notices of Royal Astronomical Society, 2005, **364**, 601

bias $b = 1, 1.6$ and 2, and analyzed these in exactly the same way. The values of D_q in the random distribution and the unbiased simulations show much smaller variations and these are not consistent with the actual data. The biased simulations, however, show larger variations in D_q and these are consistent with both the random and the actual data. Interpreting the actual data as a realization of a biased ΛCDM universe, we conclude that the galaxy distribution is homogeneous on scales larger than $60 - 70\,h^{-1}$Mpc.

5.1 Introduction

The collapse of small scale inhomogeneities created due to some quantum process in the early Universe gave rise to Large Scale Structures that we observe in the Universe at present epoch. The primary aim of all galaxy redshift surveys which have completed or are still underway is to determine the distribution of large scale structures in the universe. Though the galaxy distribution exhibits a large variety of structures starting from groups and clusters, extending to superclusters and an interconnected network of filaments which appears to extend across the whole universe, we expect the galaxy distribution to be homogeneous on large scales. The assumption that the universe is homogeneous and isotropic on large scales is known as the Cosmological Principle and this is one of the fundamental pillars of cosmology today. In addition to determining the large scale structures, galaxy redshift surveys can also be used to verify if the galaxy distribution does indeed become homogeneous on large scales and thereby validate the Cosmological Principle. Further, the galaxy redshift surveys can also be used to investigate the scales at which this transition to homogeneity takes place. In this chapter we test using multifractal analysis whether the galaxy distribution in the SDSS-DR1 (Abazajian et al., 2003) is *actually* homogeneous on large scales and if so what is the scale at which the transition to homogeneity takes place.

A large variety of methods have been developed and used to quantify the galaxy distribution in redshift surveys. Prominent among these methods are the two-point correlation function $\xi(r)$ (Peebles, 1980) and its Fourier transform the power spectrum

$P(k)$. There now exist very precise estimates of $\xi(r)$ (e.g. Zehavi et al., 2002; Hawkins et al., 2003) and the power spectrum $P(k)$ (e.g. Percival et al., 2001; Tegmark et al., 2004b) determined from different large redshift surveys. As has been pointed out in chapter 3, the two point correlation function is found to be well described by a power law (equation 3.1) on small scales.

The power law behavior of $\xi(r)$ suggests a scale invariant clustering pattern in the distribution of galaxies. This pattern would violate homogeneity if this power-law behavior were to extend to arbitrarily large length-scales. Reassuringly, the power law form for $\xi(r)$ does not hold on large scales and it breaks down at $r > 16h^{-1}$Mpc for SDSS and at $r > 20h^{-1}$Mpc for 2dFGRS. The fact that the values of $\xi(r)$ fall off sufficiently fast with increasing r is consistent with the galaxy distribution being homogeneous on large scales. A point to note is that though the $\xi(r)$ determined from redshift surveys is consistent with the universe being homogeneous at large scales it does not actually test this. This is because the way in which $\xi(r)$ is defined and determined from observations refers to the mean number density of galaxies and therefore it presupposes that the galaxy distribution is homogeneous on large scales. Further, the mean density which we compute is only that on the scale of the survey. It will be equal to the mean density in the universe only if the transition to homogeneity occurs well within the survey region. To verify the large scale homogeneity of the galaxy distribution it is necessary to consider a statistical test which does not presuppose the premise which is being tested. Here we consider one such test, the "multi-fractal dimension" and apply it to the SDSS-DR1.

The fact that the galaxy clustering is scale-invariant over a range of length-scales led Pietronero (1987) to propose that the galaxies had a fractal distribution. The later analysis of Coleman & Pietronero (1992) seemed to bear out such a proposition whereas Borgani (1995) claimed that the fractal description was valid only on small scales and the galaxy distribution was consistent with homogeneity on large scales. A purely fractal distribution would not be homogeneous on any length-scale and this would violate the Cosmological Principle. Further, the mean density would decrease if it were to be evaluated for progressively larger volumes and this would manifest itself as an increase

in the correlation length r_0 (equation 3.1) with the size of the sample. However, this simple prediction of the fractal interpretation is not supported by data, instead r_0 remains constant for volume limited samples of CfA2 redshift survey with increasing depth (Martínez, López-Martí, & Pons-Bordería, 2001).

The analysis of the ESO slice project by Guzzo (1997) confirms large scale homogeneity whereas the analysis of volume limited samples of SSRS2 by Cappi et al. (1998) is consistent with both the scenarios of fractality and homogeneity. A similar analysis (Hatton, 1999) carried out on APM-Stromlo survey exhibits a fractal behavior with a fractal dimension of 2.1 ± 0.1 on scales up to $40\,h^{-1}$Mpc. Coming to the fractal analysis of the Las Campanas Redshift Survey (LCRS), Amendola & Palladino (1999) find a fractal behavior on scales less than $\sim 30h^{-1}\,$Mpc but are inconclusive about the transition to homogeneity. A multi-fractal analysis by Bharadwaj, Gupta & Seshadri (1999) shows that the LCRS exhibits homogeneity on the scales 80 to $200\,h^{-1}\,$Mpc. The analysis of Kurokawa, Morikawa & Mouri (2001) shows this to occur at a length-scale of $\sim 30\,h^{-1}\,$Mpc, whereas Best (2000) fails to find a transition to homogeneity even on the largest scale analyzed. The fractal analysis of the PSCz (Pan & Coles, 2000) shows a transition to homogeneity on scales of $30\,h^{-1}$Mpc. Recently Baryshev & Bukhmastova (2004) have performed a fractal analysis of SDSS EDR and find that a fractal distribution continues to length-scales of $200\,h^{-1}$Mpc whereas Hogg et al. (2005) analyze the SDSS LRG to find a convergence to homogeneity at a scale of around $70\,h^{-1}$Mpc.

In this chapter we use the multi-fractal analysis to study the scaling properties of the galaxy distribution in the SDSS-DR1 and test if it is consistent with homogeneity on large scales. The SDSS is the largest galaxy survey available at present. For the current analysis we have used volume limited subsamples extracted from the two equatorial strips of the SDSS-DR1. This reduces the number of galaxies but offers several advantages. The volume limitedness of the samples ensures that the variation in the number density in these samples are independent of the details of the luminosity function and is caused only by clustering. The larger area and depth of these samples provide us the scope to investigate the scale of homogeneity in greater detail .

The ΛCDM model with $\Omega_{m0} = 0.3$, $\Omega_{\Lambda 0} = 0.7$, $h = 0.7$ and an adiabatic, scale invariant primordial power spectrum is currently believed to be the minimal model which is consistent with most cosmological data (Efstathiou et al., 2001; Percival et al., 2002; Tegmark et al., 2004a). Estimates of the two point correlation function $\xi(r)$ (Tucker et al. , 1997; Zehavi et al., 2002; Hawkins et al., 2003) and the power spectrum $P(k)$ (Lin et al. , 1996; Percival et al., 2001; Tegmark et al., 2004b) are all consistent with this model. In this chapter we use the particle position inferred from N-body simulations (see subsection 5.2.3) to determine the length-scale where the transition to homogeneity occurs in the ΛCDM model and test if the actual data is consistent with this.

Galaxy surveys provide us information about the visual part of the matter distribution only. We should also keep in mind the fact that the models of structure formation primarily predict the clustering of the *dark matter* which dominates the dynamics. The process of galaxy formation and the exact relation between the distribution of the galaxies and the dark matter is far from well understood. The fact that the galaxies are a biased tracer of the dark matter distribution is now well accepted (e.g. Kaiser, 1984; Mo & White, 1996; Dekel & Lahav , 1999; Taruya & Suto , 2001; Yoshikawa et al., 2001). Further, on large scales one expects the fluctuations in the galaxy and the dark matter distribution to be linearly related through the linear bias parameter b. Determining the bias b is an important issue in cosmology. Not only will it allow the dark matter distribution to be determined, but it is also expected to throw light on galaxy formation. There currently exist several ways to determine the bias. Measuring the redshift space distortion parameter $\beta = {\Omega^{0.6}}_m/b$ (e.g. Hawkins et al., 2003; Tegmark et al., 2004a) in combination with an independent determination of Ω_{m0} allows b to be determined. The bispectrum (Verde et al., 2002) provides a technique to determine the bias from redshift surveys without the need of inputs from other observations. A combination of weak lensing and the SDSS galaxy survey has been used by Seljak et al. (2005) to determine the bias. The multifractal nature of the galaxy distribution from the N-body simulations is very sensitive to the bias parameter and holds the possibility of giving accurate estimates for this. We apply this test to the volume limited samples analyzed in this chapter.

There are various other probes which test the cosmological principle. The fact that the Cosmic Microwave Background Radiation (CMBR) is nearly isotropic ($\Delta T/T \sim 10^{-5}$) can be used to infer that our spacetime is locally very well described by the Friedmann-Robertson-Walker metric (Ehlers, Green & Sachs, 1968). Further, the CMBR anisotropy at large angular scales ($\sim 10^o$) constrains the *rms* density fluctuations to $\delta\rho/\rho \sim 10^{-4}$ on length-scales of $1000\,h^{-1}$Mpc (e.g. Wu, Lahav & Rees, 1999). The analysis of deep radio surveys (e.g. FIRST, Baleises et al., 1998) suggests the distribution to be nearly isotropic on large scales. By comparing the predicted multipoles of the X-ray Background to those observed by HEAO1 (Scharf et al., 2000) the fluctuations in amplitude are found to be consistent with the homogeneous universe (Lahav, 2002). The absence of big voids in the distribution of Lyman-α absorbers is inconsistent with a purely fractal model (Nusser & Lahav, 2000).

A brief outline of this chapter follows. In Section 5.2 we describe the data collected from SDSS as well as N-body simulations. The method of analysis of the acquired data has been discussed in section 5.3. We conclude in Section 5.4 with results and conclusions.

5.2 Galaxy Sample : The Sloan digital Sky Survey

The results presented in this chapter are based on a galaxy sample selected from the largest galaxy survey to date, the Sloan Digital Sky Survey (SDSS). The SDSS is a wide-field photometric and spectroscopic survey carried out with a dedicated 2.5 meter telescope (Figure 5.1) at Apache Point, New Mexico (York et al., 2000). The SDSS telescope uses the drift scanning technique in which the telescope is fixed and the earth's rotation is made use of to record small strips of the sky. The telescope scans continuously the sky on five photometric bandpasses namely u, g, r, i and z . For our analysis, we have used the $r-$band result. The wavelength range for this band is $5500\mathring{A} - 7000\mathring{A}$, which is better for low-redshift galaxy. The telescope scans to a limiting r-band apparent



Figure 5.1: The Sloan Digital Sky Survey Telescope

magnitude[2] of 22.5 (Fukugita et al., 1996; Smith et al., 2002). All the data obtained from the telescope is processed by dedicated software for astrometry (Pier et al., 2003), identification of sources and candidates (Lupton et al., 2002), candidate selection for the spectroscopy sample (Eisenstein et al., 2001; Strauss et al., 2002), adaptive tiling (Blanton et al., 2003) and photometric calibration (Hogg et al., 2001; Smith et al., 2002). An extensive analysis of possible systematics uncertainties present in the data is described in Scranton (2002)

When finished the SDSS will cover approximately 10^4 square degrees of the sky. The main part of the survey is located in the Northern Galactic sky, with an additional small area in the Southern Galactic sky. In total it will provide $\sim 10^8$ optical images in five bands and $\sim 10^6$ spectra of galaxies with apparent magnitude $m_r < 17.77$ (Gunn et al., 1998; York et al., 2000). SDSS is also recording the redshifts to $\sim 100,000$ quasars (the most distant objects known) giving us unprecedented knowledge of the distribution of matter to the edge of the visible universe. The spectroscopic targets in the SDSS are divided into three categories.

- The main galaxy sample (Strauss et al., 2002).
- The luminous red sample (Eisenstein et al., 2001).

[2]The apparent magnitude (m) of a celestial body is a measure of its brightness as seen by an observer on Earth, normalized to the value it would have in the absence of the atmosphere. The brighter the object appears, the lower the value of its magnitude

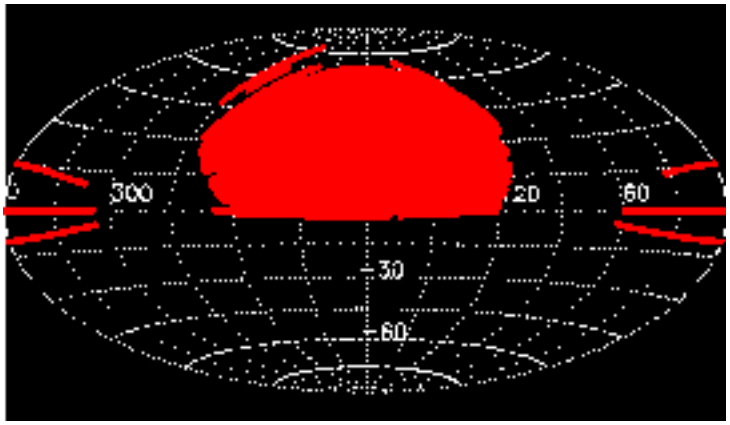


Figure 5.2: Projection on the sky of the **SDSS-DR6** Imaging (Aitoff projection of Equatorial coordinates). The relation between Equatorial Coordinates and the survey coordinates is given in appendix B.1. Figure courtesy the SDSS team

- The quasar sample (Richards et al., 2002).

The main galaxy sample is complete down to an apparent r-band Petrosian magnitude limit of $m_R < 17.77$. The galaxy sample used in this work was obtained from the sky server[3] using the SDSS CasJobs site[4]. The website is based on SQL queries which can perform a large number of pre-processing tasks (see appendix B.2). All galaxies with r band apparent magnitude of $r < 20$ were extracted from the spectroscopic main sample. For each galaxy we obtained the position in the sky (ra, dec) and redshift z as well as many other properties such as apparent magnitudes in the five bands (u, g, r, i and z), isophotal radius, position angle in the sky, petrosian radius enclosing 90% and 50% of the total flux, etc. The detailed list of properties queried can be found in appendix B.2.

Figure 5.2 and 5.3 show the projection on the sky of the imaging and spectroscopic sample respectively, taken from the latest data release to date[5](DR6). There are five large patches. There are also several smaller ones corresponding to the last observed fields as well as many holes inside the large areas. The holes are the result of bright stars,

[3]http://www.sdss.org/
[4]http://casjobs.sdss.org/CasJobs/
[5]by the time of thesis submission

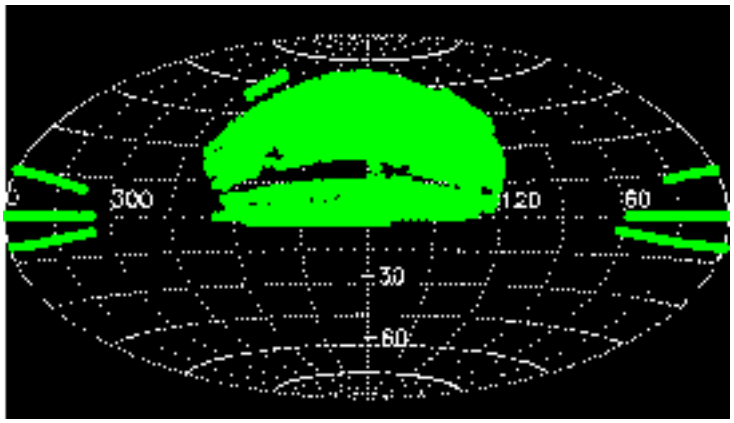


Figure 5.3: Projection on the sky of the **SDSS-DR6** spectroscopic sample. The center of the plot is in the direction $\alpha = 180$, $\delta = 0$. Contour lines delineate the edges of the survey. Courtesy the SDSS team

telescope artefacts and failures in sky coverage. When finished the SDSS will completely cover the area in the center of the map in figure 5.3, covering almost a quarter of the sky.

In order to analyze a galaxy sample from the survey only redshift information is not going to suffice. We have to assume a cosmological model in order to get physical distance from the observer to the object in the sample.

5.2.1 Redshift-Distance Formula

The expansion of the universe and its (assumed) isotropic nature provides a convenient way to determine the distance to galaxies by means of their recession velocity:

$$r_{gal} = \frac{v_{rec} - v_{pec}}{H_0} \tag{5.1}$$

where r_{gal} is the distance to the galaxy. v_{rec} is the recession velocity of the unperturbed Hubble flow and v_{pec} is the line of sight component of the peculiar velocity of the galaxy. The peculiar velocity is the velocity of a galaxy with respect to the Hubble flow. H_0 is

the Hubble parameter, parameterized by h:

$$H_0 = 100\,h\left[kms^{-1}Mpc^{-1}\right]. \tag{5.2}$$

We can artificially produce a 'redshift space' by setting each galaxy at distance r_{gal} obtained by considering $v_{pec} = 0$ in equation 5.1. The 'redshift space' is thus distorted representation of the 'real space'.

The recession velocity can be inferred from the spectra of the galaxy by measuring the shift in frequency of emission or absorption lines compared to that in the rest frame. This shift in the frequency is produced by the expansion of the Universe:

$$\nu_e = (1+z)\nu_o \tag{5.3}$$

where ν_e is the frequency of a photon when it was emitted, ν_o is the observed frequency and z is the redshift. More generally, we can compute the distance to a galaxy given its observed redshift according to:

$$R = a_0 r(z)(1+z) \tag{5.4}$$

where a_0 is the present value of scale factor of expansion of the Universe and $r(z)$ is the redshift dependent radial coordinate distance given by (Weinberg, 2008):

$$r(z) = S\left[\frac{1}{a_0 H_0}\int_{1/(1+z)}^{1}\frac{dx}{x^2\sqrt{\Omega_\Lambda + \Omega_m x^{-3} + \Omega_{rad}x^{-4} + (1-\Omega_\Lambda-\Omega_m-\Omega_{rad})x^{-2}}}\right] \tag{5.5}$$

where the function $S[x]$ for different geometries of Universe is given by:

$$S[x] = \begin{cases} \sin(x) & k=+1 \quad (Spherical\ \ Universe) \\ x & k=\ 0 \quad (Flat\ \ Universe) \\ \sinh(x) & k=-1 \quad (Hyperbolic\ \ Universe) \end{cases} \tag{5.6}$$

We have assumed the standard ΛCDM model for the value of different cosmological parameters.[See table 1 in chapter 1]

5.2.2 SDSS-DR1

Our analysis of multifractal nature of galaxy distribution is based on the publicly available SDSS-DR1 data (Abazajian et al., 2003). In this work we have analyzed two equatorial strips which are centred along the celestial equator ($\delta = 0°$), one in the Northern Galactic Cap (NGP) spanning 91° in *r.a.*(from $145° < \alpha < 236°$) and the other in Southern Galactic Cap (SGP) spanning 65° in *r.a.* (from $351° < \alpha < 56°$), their thickness varying within $\mid \delta \mid \leq 2.5°$ in *dec.* These regions contains 38,838 galaxies having redshift in the range $0.02 \leq z \leq 0.2$ with the selection criteria that the extinction corrected Petrosian r band magnitude is $r_p < 17.77$.

For the current purpose we have selected only the galaxies lying within $-1° < \delta < 1°$ as both the equatorial strips have complete coverage in this declination range. We have constructed volume limited subsamples of the data. In this case we have to select the maximum limiting radius D_{lim} of the sample. We also have to find the limiting absolute magnitude M_{lim} of a galaxy that corresponds to the apparent magnitude limit m_{lim} of the survey. The cosmological magnitude-distance relation that connects the three values is given by

$$m = M + 5\log_{10}(D_L/1Mpc) + 25 \tag{5.7}$$

These volume limited subsamples, used here, extend from $z = 0.08$ to 0.2 in redshift (*i.e.* $235\,h^{-1}$Mpc $\leq R \leq 571\,h^{-1}$Mpc comoving in the radial direction in the standard ΛCDM model). They have been formed by restricting the extinction corrected Petrosian r band apparent magnitude in the range $14.5 \leq m_r \leq 17.5$ and the absolute magnitude range to $-22.6 \leq M_r \leq -21.6$. Even though the number of galaxies are reduced this way, there are several advantages on offer. The radial selection function is nearly uniform in this case. So the variation in number density of galaxies in the subsample is caused only by clustering of the galaxies. A volume limited sample defined by an interval in

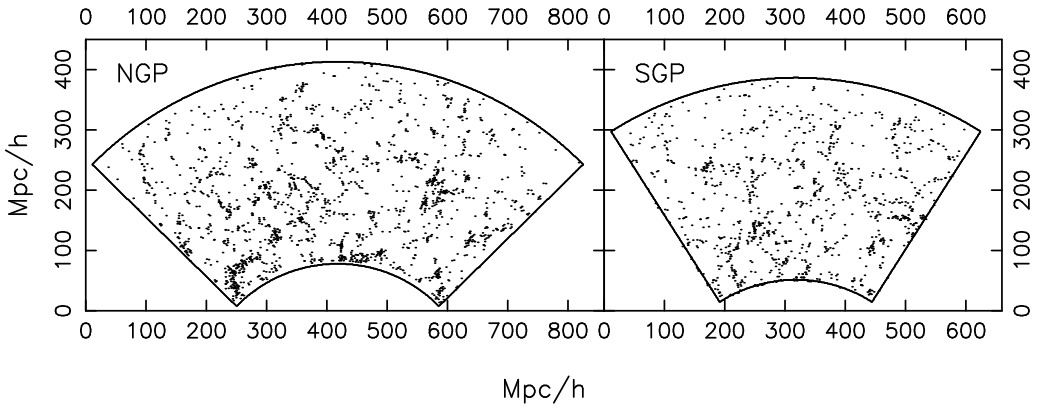


Figure 5.4: This shows the two dimensional galaxy distribution in the NGP and SGP subsamples of SDSS that have been analyzed here.

absolute magnitude translates into an interval in redshift. It has the nice property that in principle each galaxy could be displaced to any depth within the sample and would still remain within the apparent magnitude range of the survey. This resulted in 5315 galaxies distributed in two wedges, spanning 91° (NGP) and 65° (SGP) in *r. a.*, both with thickness 2° centered along the equatorial plane extending from $235h^{-1}$Mpc to $571h^{-1}$Mpc comoving in the radial direction.

The resulting subsamples are two thin wedges of varying thickness (from $8.2h^{-1}$Mpc to $20h^{-1}$Mpc) aligned with the equatorial plane. Our analysis is restricted to slices of uniform thickness $\pm 4.1\,h^{-1}$Mpc along the equatorial plane extracted out of the wedge shaped regions. These slices are nearly $2D$ with the radial extent and the extent along *r.a.* being much larger than the thickness. We have projected the galaxy distribution on the equatorial plane and analyzed the resulting 2D distribution (Figure 5.4). The SDSS-DR1 subsamples that we analyze here contains a total of 3032 galaxies.

5.2.3 N-Body Data

We have used a Particle-Mesh (PM) N-body code to simulate the dark matter distribution at the mean redshift $z = 0.14$ of our subsample. A comoving volume of $[645h^{-1}\text{Mpc}]^3$ is simulated using 256^3 particles on a 512^3 mesh with grid spacing $1.26h^{-1}$Mpc. The set of values $(\Omega_{m0}, \Omega_{\Lambda 0}, h) = (0.3, 0.7, 0.7)$ were used for the cosmological parameters,

and we used a ΛCDM power spectrum characterized by a spectral index $n_s = 1$ at large-scales and with a value $\Gamma = \Omega_m h = 0.2$ for the shape parameter of the power spectrum. The power spectrum was normalised to $\sigma_8 = 0.84$ (WMAP, Spergel et al., 2003) . Theoretical considerations and simulations suggest that galaxies may be biased tracer of the underlying dark matter distribution (e.g., Kaiser, 1984; Mo & White, 1996; Dekel & Lahav , 1999; Taruya & Suto , 2001; Yoshikawa et al., 2001). A "sharp cutoff" biasing scheme (Cole et al., 1998) was used to generate this kind of biased particle distributions. This is a local biasing scheme where the probability of a particle being selected as a galaxy is a function of local density only. In this scheme the final dark-matter distribution generated by the N-body simulation was first smoothed with a Gaussian of width $5h^{-1}$Mpc. Only the particles which lie in regions where the density contrast exceeds a critical value were selected as galaxies. The values of the critical density contrast were chosen so as to produce particle distributions with a low bias $b = 1.2$ and a high bias $b = 1.6$.

An observer is placed at a suitable location inside the N-body simulation cube and we use the peculiar velocities to determine the particle positions in redshift space. Exactly the same number of particles distributed over the same volume as the actual data was extracted from the simulations to produce simulated NGP and SGP slices. The simulated slices (Figure 5.5) were analyzed in exactly the same way as the actual data.

5.3 Method of Analysis

A fractal point distribution is usually characterized in terms of its fractal dimension. As discussed in chapter 2 there are different ways to calculate this dimension. The correlation dimension happens to be one of the methods which is of particular relevance to the analysis of galaxy distributions. The formal definition of the correlation dimension involves a limit which is meaningful only when the number of particles is infinite and hence this cannot be applied in the strict sense to galaxy surveys with a limited number of galaxies. To overcome this we adopt a "working definition" which can be applied to

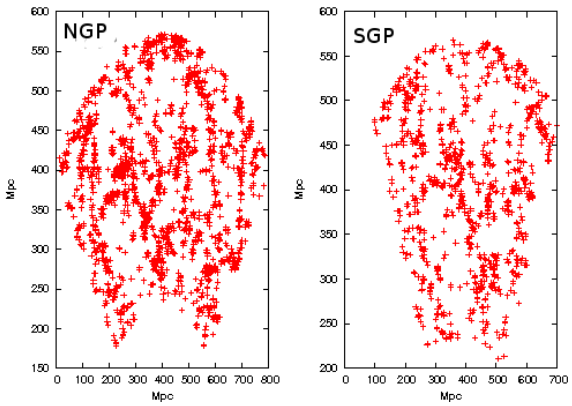


Figure 5.5: This shows the two dimensional galaxy distribution in the NGP and SGP subsamples of simulated slices of ΛCDM model that have been analyzed here.

a finite distribution of N galaxies. It should be noted that our galaxy distribution is effectively two dimensional, and we have largely restricted our discussion to this situation.

Labeling the galaxies from 1 to N, and using $\mathbf{x}_i$ to denote the comoving coordinates of the i^{th} galaxy, the number of galaxies within a circle of comoving radius r centred on the i th galaxy is given by

$$n_i(r) = \sum_{j=1\neq i}^{N} \Theta(r - \mid \mathbf{x}_i - \mathbf{x}_j \mid) \tag{5.8}$$

where $\Theta(x)$ is the Heaviside function. Averaging $n_i(r)$ by choosing M different galaxies as centers and dividing by the total number of galaxies gives us

$$C_2(r) = \frac{1}{MN} \sum_{i=1}^{M} n_i(r) \tag{5.9}$$

which may be interpreted as the probability of finding a galaxy within a circle of radius r centred on another galaxy. If $C_2(r)$ exhibits a power law scaling relation $C_2(r) \propto r^{D_2}$, the exponent D_2 is defined to be the correlation dimension. Typically, a power law scaling relation will hold only over a limited range of length-scales $r_1 \leq r \leq r_2$, and it may so happen that the galaxy distribution has different correlation dimensions over different

ranges of length-scales.

It is clear that $C_2(r)$ is closely related to the volume integral of the two point correlation function $\xi(r)$. In a situation where this has a power law behavior $\xi(r) = (\frac{r}{r_0})^{\gamma}$, the correlation dimension is $D_2 = D - \gamma$ on scales $r < r_0$. Here D is the dimension of the ambient space in which the galaxies are distributed, which in our analysis happens to be 2. Further, we expect $D_2 = D$ on large scales where the galaxy distribution is expected to be homogeneous and isotropic.

In the usual analysis the two point correlation does not fully characterize all the statistical properties of the galaxy distribution, and it is necessary to also consider the higher order correlations *e. g.* the three point and higher correlations. Similarly, the full statistical quantification of a fractal distribution also requires a hierarchy of scaling indices. The multifractal analysis used here does exactly this. It provides a spectrum of generalized dimension D_q, the Minkowski-Bouligand dimension, which is defined for a range of q.

Closely following the definition of the correlation dimension D_2, we can define the generalized dimension D_q using the $(q-1)^{th}$ moment of the number of neighbors $n_i(r)$. The quantity $C_2(r)$ is thus generalized to

$$C_q(r) = \frac{1}{MN} \sum_{i=1}^{M} [n_i(< r)]^{q-1} \tag{5.10}$$

We would once again like to stress that the $n_i(r)$ is the number of neighbors of the galaxy placed at position x_i. Equation 5.10 can now be used to define the generalized Minkowski-Bouligand dimension

$$D_q = \frac{1}{q-1} \frac{d \log C_q(r)}{d \log r} \tag{5.11}$$

Typically $C_q(r)$ will not exhibit the same scaling behavior over the entire range of length-scales, and it is possible that the spectrum of generalized dimension will be different in different ranges of length-scales. As is clear from equation 5.11 the correlation dimension

corresponds to the generalized dimension at $q = 2$. The other integer values of q are related to the scaling of higher order correlation functions. A mono-fractal is characterized by a single scaling exponent *i.e.* D_q is a constant independent of q, whereas the full spectrum of generalized dimensions is needed to characterize a multifractal. It is clear from equation 5.10 that for positive values of q the contribution to $C_q(r)$ will be dominated by the regions for which $n_i(r)$ is higher. This implies that positive value of q gives more weightage to the regions with high number density. On the other hand, when q is negative the dominant contribution to $C_q(r)$ will come from regions of the survey with lower $n_i(r)$. This is equivalent to saying that the negative values of q give more weightage to the underdense regions. Thus we may interpret D_q for $q > 0$ as characterizing the scaling behavior of the galaxy distribution in the high density regions like clusters whereas $q < 0$ characterizes the scaling inside voids. In the situation where the galaxy distribution, in 2-Dimensional slices that we have, is homogeneous and isotropic on large scales, we expect the generalized dimension D_q to take the value 2 independent of the value of q.

There are a variety of different algorithms which can be used to calculate the generalized dimension, the Nearest Neighbour Interaction (Badii & Politi, 1984) and the Minimal Spanning Tree (Sutherland & Efstathiou, 1991) being some of them. We have used the correlation integral method which we present below.

The two subsamples, NGP and SGP (see figure 5.4) contain 1936 and 1096 galaxies respectively and they were analyzed separately. For each galaxy in the subsample we considered a circle of radius r centred on the galaxy and counted the number of other galaxies within the circle to determine $n_i(r)$ (equation 5.8). The radius r was increased starting from $5\,h^{-1}\,\mathrm{Mpc}$ to the largest value where the circle lies entirely within the subsample boundaries. The values of $n_i(r)$ determined using different galaxies as centers were then averaged to determine $C_q(r)$ (equation 5.10). It should be noted that the number of centers fall with increasing r, and for the NGP there are ~ 800 centers for $r = 80h^{-1}\,\mathrm{Mpc}$ with the value falling to ~ 100 for a radius of $r = 150h^{-1}\,\mathrm{Mpc}$. The large scale behavior of $C_q(r)$ was carefully analyzed to determine the range of length-scales

where $C_q(r)$ exhibits a scaling behavior in order to calculate the scaling exponent D_q as a function of q.

In addition to the actual data, we have also constructed and analyzed random distributions of points. The random data contains exactly the same number points as there are galaxies in the actual data distributed over exactly the same region as the actual NGP and SGP slices. The random data are homogeneous and isotropic by construction, and the results of the multifractal analysis of this data gives definite predictions for the results expected if the galaxy distribution were homogeneous and isotropic. The random data and the simulated slices extracted from the N-body simulations were all analyzed in exactly the same way as the actual data. We have used 18 independent realizations of the random and simulated slices to estimate the mean and the $1-\sigma$ error-bars of the spectrum of generalized dimensions D_q. We have also checked that increasing the number of realizations to 36 does not significantly change the mean or the $1-\sigma$ error bars.

5.4 Results and Discussions

Figures 5.6 and 5.7 show $C_q(r)$ at $q = -4$ and 4, respectively, for the actual data, for one realization of the random slices and for one realization of the simulated slices for each value of the bias. The behavior of $C_q(r)$ at other values of q is similar to the ones shown here. Our analysis is restricted to $-4 \leq q \leq 4$. We find that $C_q(r)$ does not exhibit a scaling behavior at small scales ($5\,h^{-1}\,\mathrm{Mpc} \leq r \leq 40\,h^{-1}\,\mathrm{Mpc}$). Further, the small-scale behavior of $C_q(r)$ in the actual data is different from that of the random slices and is roughly consistent with the simulated slices for $b = 1.6$. We find that $C_q(r)$ shows a scaling behavior on length-scales of from somewhere around $60 - 70\,h^{-1}\,\mathrm{Mpc}$ to $150\,h^{-1}\,\mathrm{Mpc}$. Although the value of $C_q(r)$ for the actual data, the random and simulated slices appear to converge over this range of length-scales indicating that they are all roughly consistent with homogeneity, there are small differences in the slopes of each line. We have used a least-square fit to determine the scaling exponent or generalized

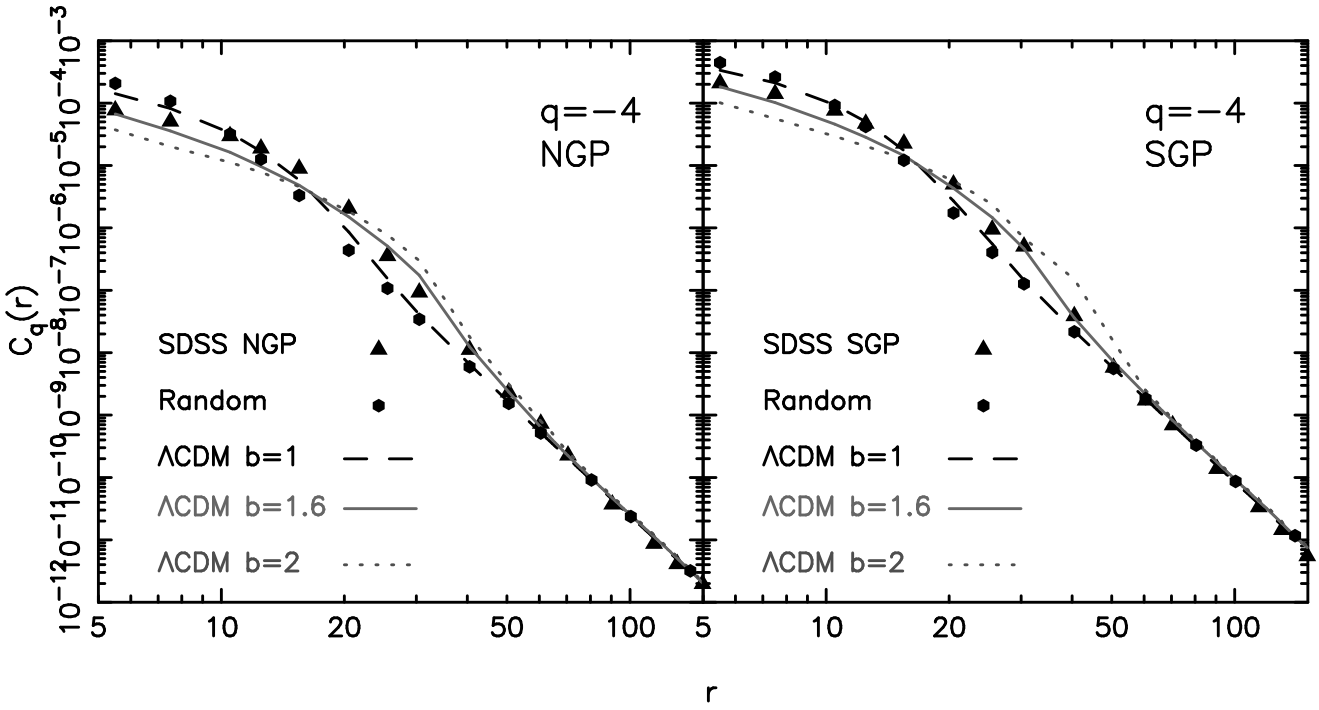


Figure 5.6: This shows $C_q(r)$ at $q = -4$ for the actual data, the random data and the simulated slices. The $1-\sigma$ error bars are not shown in the figure as they are too small to be seen in the logarithmic scale used here. For the random and unbiased $\Lambda\mathrm{CDM}$ model, the error bars are ~ 20 % on small scales ($\leq 30h^{-1}\mathrm{Mpc}$) and it decreases to ~ 2 and ~ 10 % on larger scales for the two models, respectively. For the two biased cases, the error bars are much larger ($\sim 80-100$ %) on small scales and it decreases to ~ 20 per cent at $\sim 70h^{-1}\mathrm{Mpc}$ and beyond.

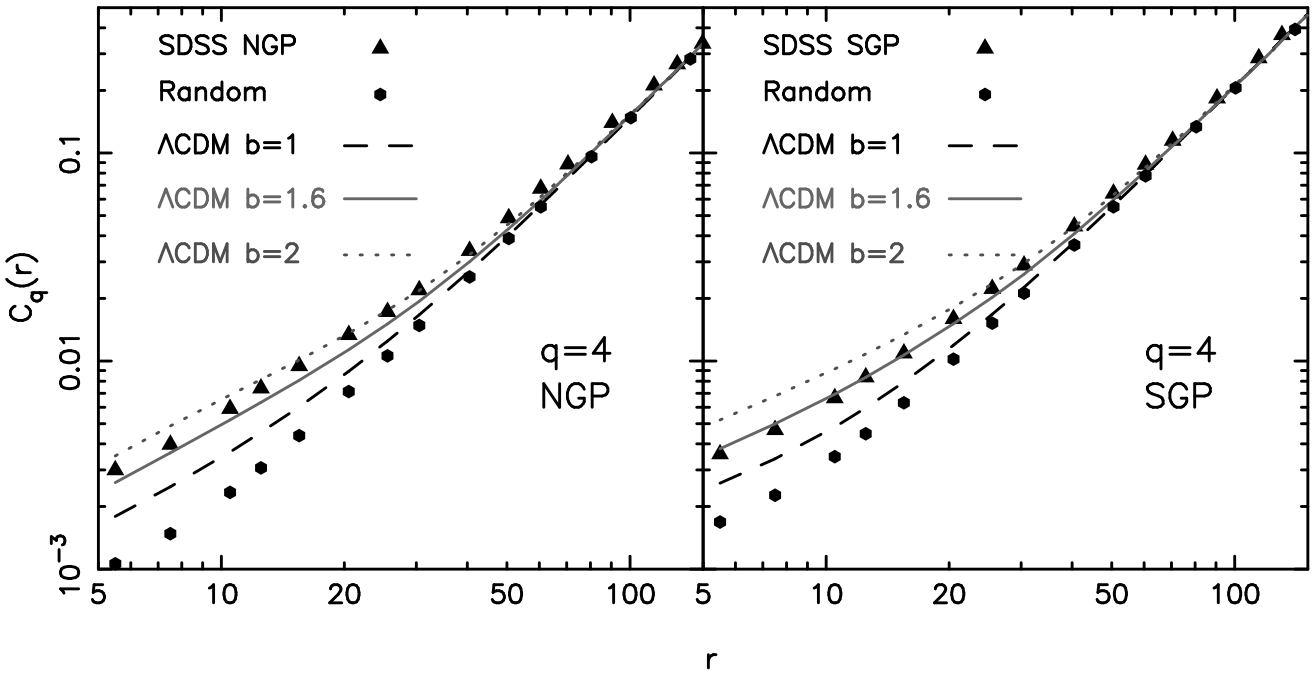


Figure 5.7: This shows $C_q(r)$ at $q = 4$ for the actual data, the random data and the simulated slices. The $1-\sigma$ error bars are not shown in the figure as they are too small to be seen in the logarithmic scale used here. The $1-\sigma$ error bars are $\sim 2-5$ % for the entire range of length-scales shown here. It may also be noted that the error bars decrease monotonically with increasing q.

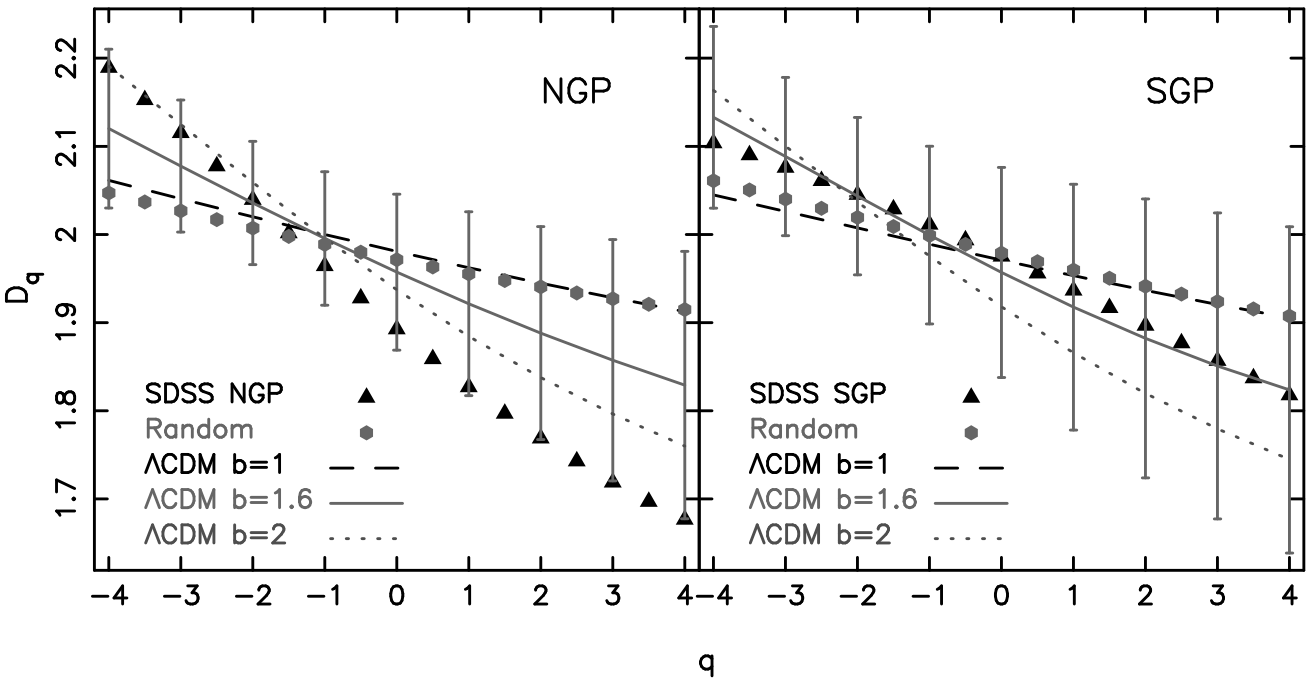


Figure 5.8: This shows the spectrum of generalized dimensions D_q as a function of q for the actual data, the random data and the simulated slices on length scales of from $60{-}70\,h^{-1}\,\mathrm{Mpc}$ to $150\,h^{-1}\,\mathrm{Mpc}$. The error bars shown are for $\Lambda\mathrm{CDM}$ model with bias=1.6.

dimension D_q shown in Figure 5.8.

Ideally we would expect $D_q = 2$ for a two dimensional homogeneous and isotropic distribution. We find that for the actual data D_q varies in the range 1.7 to 2.2 in the NGP and 1.8 to 2.1 in the SGP on large-scales in the range $80\,h^{-1}\,\mathrm{Mpc}$ to $130\,h^{-1}\,\mathrm{Mpc}$. In both the slices the value of D_q decreases with increasing q as expected. The value of D_q crosses $D_q = 2$ somewhere around $q = -1$. The variation of D_q with q shows a similar behavior in the random slices, but the range of variation is much smaller ($1.9 \leq D_q \leq 2.1$) in the same range of length scales as for the real data. Comparing the actual data with the random data we find that the actual data lies outside the $1-\sigma$ error-bars of the random data (not shown here) for most of the range of q except around $q = -1$ where $D_q = 2$ for both the actual and random data. Accepting this at face value, this would imply that the actual data is not homogeneous at large scales. In order to test if the

SDSS subsamples are *really* homogeneous and consistent with the ΛCDM model we have compared our results with different realizations of the ΛCDM model.

Considering the simulated data, we find that the variation in D_q depends on the value of the bias b. For the unbiased simulations D_q shows very small variations ($1.9 \leq D_q \leq 2.1$) and the results are very close to those of the random data. We find that increasing the bias causes the variations in D_q to increase. In all cases D_q decreases with increasing q and it crosses $D_q = 2$ around $q = -1$. Increasing the bias has another effect in that it results in larger $1 - \sigma$ error-bars.

Comparing the simulated data with the random data and the actual data we find that the unbiased simulations are consistent with the random data. This implies that the unbiased ΛCDM model has a transition to homogeneity at $60 - 70\,h^{-1}\,\mathrm{Mpc}$. The spectrum of generalized dimensions as determined from the unbiased simulations on length-scales $60-70\,h^{-1}\,\mathrm{Mpc}$ to $150\,h^{-1}\,\mathrm{Mpc}$ is different from that of the actual data. The actual data, in fact, lies outside the $1-\sigma$ error-bars of the unbiased ΛCDM model. This indicates that the unbiased ΛCDM model fails to reproduce the large scale properties of the galaxy distribution in our volume limited subsamples of the SDSS-DR1.

The simulations with bias $b = 1.6$ and $b = 2$ have larger $1 - \sigma$ error-bars and these are consistent with both the random and the actual data. Interpreting the actual data as being a realization of a biased ΛCDM universe, we conclude that it has a transition to homogeneity at $60-70\,h^{-1}\,\mathrm{Mpc}$ and the galaxy distribution is homogeneous on scales larger than this.

The galaxy subsample analyzed here contains the most luminous galaxies in the SDSS-DR1. Various investigations have shown the bias to increase with luminosity (Norberg et al., 2001; Zehavi et al., 2002) and the subsample analyzed here is expected to be biased with respect to the underlying dark matter distribution. Seljak et al. (2005) have used the halo model in conjunction with weak lensing to determine the bias for a number of subsamples with different absolute magnitude ranges. The brightest sample which they have analyzed has galaxies with absolute magnitudes in the range $-23 \leq M_r \leq -22$ for which they find a bias $b = 1.94 \pm 0.2$. Our results are consistent

with these findings.

A point to note is that the $1-\sigma$ error-bars of the spectrum of generalized dimension D_q increases with the bias. This can be understood in terms of the fact that $C_q(r)$ is related to volume integrals of the correlation functions which receives contribution from all length-scales. The fluctuations in $C_q(r)$ can also be related to volume integrals of the correlation functions. Increasing the bias increases the correlations on small scales ($\leq 40-50\,h^{-1}$Mpc) which contributes to the fluctuations in $C_q(r)$ at large scales and causes the fluctuations in D_q to increase.

The galaxies in nearly all redshift surveys appear to be distributed along filaments. These filaments appear to be interconnected and they form a complicated network often referred to as the "cosmic web". These filaments are possibly the largest coherent structures in galaxy redshift surveys. Recent analysis of volume limited subsamples of the LCRS by Bharadwaj, Bhavsar & Sheth (2004) and the same SDSS-DR1 subsamples analyzed here by Pandey & Bharadwaj (2004) shows the filaments to be statistically significant features of the galaxy distribution on length-scales $\leq 70-80\,h^{-1}$Mpc and not beyond. Larger filaments present in the galaxy distribution are not statistically significant and are the result of chance alignments. Our finding that the galaxy distribution is homogeneous on scales larger than $60-70\,h^{-1}$Mpc is consistent with the size of the largest statistically significant coherent structures namely the filaments.

Appendix B

B.1 Survey Coordinate System

The *SDSS* is mapped in a spherical coordinate system with poles at $\alpha = 95°, \delta = 0°$ and $\alpha = 275°, \delta = 0°$ ($J2000$). The survey equator is a great circle perpendicular to the $J2000$ celestial equator. The transformations between the equatorial system (α, δ) and the survey system (λ, η) are given by:

$$\begin{aligned} \cos(\alpha - 95)\cos(\delta) &= -\sin\lambda \\ \sin(\alpha - 95)\cos(\delta) &= \cos(\lambda)\cos(\eta + 32.5) \\ \sin(\delta) &= \cos(\lambda)\sin(\eta + 32.5) \end{aligned} \tag{B.1}$$

as explained in Stoughton et al. (2002).

B.2 SQL Query to get data from SDSS Data Server

SELECT

objID, ra, dec, z, petro, $r1.petroMag_r$

FROM Galaxy

WHERE

- - For Northern Galactic Region

ra between 145 and 236

- - For Southern Galactic Region

- - Right Ascention Range

and ra between 351 and 56

- - Declination Range

and dec between -1 and +1

- - Redshift Range

and z between 0.002 and 0.2

- - Extinction corrected Petrosin r band magnitude

and $((petroMag_r - extinction_r + 2.5 * LOG10(2 * 3.1415 * petroR50_r * petroR50_r)) < 17.7))$

- - Apparent magnitude Range

and $r1.petroMag_r$ BETWEEN 14.5 and 17.5

Chapter 6

Summary and future prospectus

The present chapter briefly summarizes the main findings of our thesis. In this thesis we have quantified the multifractal nature of the galaxy distribution focusing mainly on the SDSS. The main findings are as follows,

- The distribution of galaxies in the SDSS behaves as a multifractal on scales less than $60\,h^{-1}Mpc$. It has different scaling index in different range of scales.

- The distribution of galaxies in SDSS is homogeneous on scales larger than $60 - 70\,h^{-1}Mpc$.

- The unbiased ΛCDM model fails to reproduce the large scale properties of the galaxy distribution in our volume limited subsamples of the SDSS-DR1 whereas a biased ΛCDM model with bias $b = 1.6$ is consistent with the nature of galaxy distribution in SDSS.

- The Minkowski- Bouligand Dimension ($D_q(r)$) for a homogeneous distribution of points is given by

$$D_q(r) = D - \frac{(q-2)}{2}\frac{D}{\bar{N}} - \frac{D}{\bar{N}} \tag{6.1}$$

 implying that $D_q(r)$ does not coincide with the Euclidean dimension (D) even if the distribution of points is homogeneous. Thus the benchmark for a uniform sample of points is not (D) but $D_q(r)$ as obtained from equation 6.1. Thus if the

Minkowski-Bouligand dimension for a distribution of points coincides with $D_q(r)$ then it may be considered as a homogeneous distribution of points.

- The correction due to a finite size sample always leads to a smaller value for $D_q(r)$ than the D.

- The correction is small if $\bar{N} \gg 1$, as expected. The correction arises primarily due to discreteness. The major advantage of our approach is that we are able to derive an expression for the correction.

- For a slightly clustered the Minkowski- Bouligand Dimension ($D_q(r)$) is presented as

$$\begin{aligned} D_q(r) &= D - \frac{D\,(q-2)}{2\bar{N}} - \frac{Dq}{2}\left(\bar{\xi}(r) - \xi(r)\right) \\ &= D - (\Delta D_q)_{\bar{N}} - (\Delta D_q)_{clus} \end{aligned} \tag{6.2}$$

 implying that for hierarchical clustering, the value of D_q is always smaller than D for positive value of q.

- Unless the correlation function has a feature at some scale, smaller correlation corresponds to a smaller correction to the Minkowski-Bouligand dimension.

- If the correlation function has a feature then it is possible to have a small correction term $(\Delta D_q)_{clus}$ for a relatively large ξ. The relation between ξ and $(\Delta D_q)_{clus}$ is not longer one to one.

- For unbiased tracers of mass distribution (e.g. L_* type of galaxies) in the concordance model of cosmology $\Delta D_q = D_q - D$ is a very slowly varying function of scale above 100 h^{-1}Mpc. Hence this may be tentatively identified as the scale of homogeneity for this sort of population.

- For biased tracers of mass distribution (e.g. Large Redshift Galaxies (LRG)) our

model fails to predict homogeneity at 100 h^{-1}Mpc showing that the scale of homogeneity is much above 100 h^{-1}Mpc for this kind of population.

A more quantitative approach requires us to estimate not only the systematic offset ΔD_q but the dispersion in this quantity. The scale of homogeneity can then be identified as the scale where the offset is smaller than the expected dispersion. In future we plan to undertake estimation of dispersion in ΔD_q . We also plan to verify the results of our model using simulated distributions of points. In this thesis we have done a 2-D multifractal analysis of SDSS DR1 due ti its small data size. Now that large data sets is available in the form of SDSS DR6, we plan to do a 3-D multifractal analysis of the distribution.

Bibliography

Abazajian K. et al., 2003, A J, 126, 2081

Adelman-McCarthy, J. K., et al. 2008, ApJ Supplement Series, 175, 297

Amendola L., Palladino E., 1999, ApJ Letters, 514, L1

Badii R., Politi A., 1984, Physical Review Letters, 52, 1661

Bagla, J. S. 1998a, MNRAS, 297, 251

Bagla, J. S. 1998b, MNRAS, 299, 417

Bahcall, N. A. 1989, Highlights of Astronomy, 8, 435

Baleisis A., Lahav O., Loan A.J., Wall J.V., 1998, MNRAS, 297,545

Balian, R., & Schaeffer, R. 1989, A&A, 220, 1

Bardeen, J. M., Bond, J. R., Kaiser, N., & Szalay, A. S. 1986, ApJ, 304, 15

Baryshev Y. V., Bukhmastova Y. L., 2004, Astronomy Letters, 30, 444

Benoist, C., Maurogordato, S., da Costa, L. N., Cappi, A., & Schaeffer, R. 1996, ApJ, 472, 452

Bernardeau, F., Colombi, S., Gaztañaga, E., & Scoccimarro, R. 2002, Phys Reps, 367, 1

Bertschinger, E. 1987, ApJ Letters, 323, L103

Best J. S., 2000, ApJ, 541, 519

Bharadwaj S., Gupta A. K., Seshadri T. R., 1999, A&A, 351, 405

Bharadwaj S., Bhavsar S. P., Sheth J. V., 2004, ApJ, 606, 25

Blanton, M. R., Lin, H., Lupton, R. H., Maley, F. M., Young, N., Zehavi, I., & Loveday, J. 2003, A J, 125, 2276

Böhringer, H., et al. 2001, A&A, 369, 826

Bond, J. R., Cole, S., Efstathiou, G., & Kaiser, N. 1991, ApJ, 379, 440

Bond, J. R., Kofman, L., & Pogosyan, D. 1996, Nature, 380, 603

Bond, J. R., & Myers, S. T. 1996a, ApJ Supplement Series, 103, 1

Bond, J. R., & Myers, S. T. 1996b, ApJ Supplement Series, 103, 41

Bond, J. R., & Myers, S. T. 1996c, ApJ Supplement Series, 103, 63

Borgani S., Murante G., Provenzale A., Valdarnini R., 1993, PhRvE, 47, 3879

Borgani S., 1995, Phys Reps, 251, 1

Borgani S., Murante G., 1994, PhRvE, 49, 4907

Brainerd T. G., Villumsen J. V., 1994, ApJ, 431, 477

Calzetti, D., Giavalisco, M., Ruffini, R., Einasto, J., & Saar, E. 1987, Astrophysics and Space Science, 137, 101

Cappi A., Benoist C., da Costa L. N., Maurogordato S., 1998, A&A, 335, 779

Charlier, C. V. L. 1908, Ark. Mat. Astr. Fys., 4, 1

Charlier, C. V. L. 1922, Ark. Mat. Astr. Fys., 16, 1

Cole S., Hatton S., Weinberg D.H., Frenk C.S., 1998, MNRAS, 300, 945

Cole, S., et al. 2005, MNRAS, 362, 505

Cole, S., Sanchez, A. G., & Wilkins, S. 2006, To appear in Astronomical Society of The Pacific conference series: Cosmic Frontiers, ArXiv Astrophysics e-prints, arXiv:astro-ph/0611178

Coleman, P. H., Pietronero, L., & Sanders, R. H. 1988, A&A, 200, L32

Coleman P. H., Pietronero L., 1992, Phys Reps, 213, 311

Coles, P., & Lucchin, F. 2002, Cosmology: The Origin and Evolution of Cosmic Structure, Second Edition, by Peter Coles, Francesco Lucchin, pp. 512. ISBN 0-471-48909-3. Wiley-VCH , July 2002.,

Colless, M., et al. 2001, MNRAS, 328, 1039

Colless, M., et al. 2003, arXiv:astro-ph/0306581

Colombi, S., Pogosyan, D., & Souradeep, T. 2000a, Physical Review Letters, 85, 5515

Colombi S., Szapudi I., Jenkins A., Colberg J., 2000b, MNRAS, 313, 711

da Costa, L. N., Pellegrini, P. S., Davis, M., Meiksin, A., Sargent, W. L. W., & Tonry, J. L. 1991, ApJ Supplement Series, 75, 935

da Costa, L. N., et al. 1998, A J, 116, 1

Davis, M., & Peebles, P. J. E. 1983, ApJ, 267, 465

Davis, M., Meiksin, A., Strauss, M. A., da Costa, L. N., & Yahil, A. 1988, ApJ Letters, 333, L9

de Lapparent, V., Geller, M. J., & Huchra, J. P. 1986, ApJ Letters, 302, L1

de Lapparent, V., & Slezak, E. 2007, A&A, 472, 29

de Vaucouleurs, G. 1970, Science, 167, 1203

Dekel A., Lahav O., 1999, ApJ, 520, 24

Dressler, A. 1980, ApJ, 236, 351

Efstathiou G. et al., 2002, MNRAS, 330, L29

Ehlers J., Green P., Sachs R.K., 1968, J Math Phys, 9, 1344

Einstein, A. 1917, Sitzungsberichte der Königlich Preußischen Akademie der Wissenschaften (Berlin), Seite 142-152., 142

Einasto, J., Saar, E., & Klypin, A. A. 1986, MNRAS, 219, 457

Eisenstein, D. J., & Hu, W. 1998, ApJ, 496, 605

Eisenstein, D. J., & Loeb, A. 1995, ApJ, 439, 520

Eisenstein, D. J., et al. 2001, A J, 122, 2267

Falconer, K. J. 1990, Fractal Geometry: Mathematical Foundations and Applications, pp. 376 ISBN 0-470-84861-8, John Wiley & Sons Ltd, UK

Fournier d' Albe, E. E. 1907, *Two New Worlds* (Longmans, London)

Friedman, A. 1922, Zeitschrift fur Physik , 10, 377

Fry J. N., 1996, ApJ, 461, L65

Fukugita, M., Ichikawa, T., Gunn, J. E., Doi, M., Shimasaku, K., & Schneider, D. P. 1996, A J, 111, 1748

Gabrielli, A., Sylos Labini, F., Joyce, M., Pietronero, L. 2005, Statistical Physics for Cosmic Structures,pp. 424. ISBN 978-3-540-40745-4. Springer, 2005.,

Gunn, J. E., et al. 1998, A J, 116, 3040

Guzzo L., 1997, New Astronomy, 2, 517

Hamilton, A. J. S. 1993, ApJ, 417, 19

Harrison, E. R. 1970, PRD, 1, 2726

Hatton S., 1999, MNRAS, 310, 1128

Hawkins E. et al., 2003, MNRAS,346,78

Hoffman, Y., & Ribak, E. 1991, ApJ Letters, 380, L5

Hogg, D. W., Finkbeiner, D. P., Schlegel, D. J., & Gunn, J. E. 2001, A J, 122, 2129

Hogg D. W., Eistenstein D. J., Blanton M. R., Bahcall N. A., Brinkmann J., Gunn J. E., Schneider D. P., 2005, ApJ, 624, 54

Hoyle, F. 1950, Oxford, B. Blackwell [1950],

Hubble, E. P. 1925a, Popular Astronomy, 33, 252

Hubble, E. P. 1925b, ApJ, 62, 409

Huchra, J. P., & Geller, M. J. 1982, ApJ, 257, 423

Huchra, J., Davis, M., Latham, D., & Tonry, J. 1983, ApJ Supplement Series, 52, 89

Humason, M. L., Mayall, N. U., & Sandage, A. R. 1956, A J, 61, 97

Icke, V. 1973, A&A, 27, 1

Jones, B. J. T., Martinez, V. J., Saar, E., & Einasto, J. 1988, ApJ Letters, 332, L1

Jones B. J., Martínez V. J., Saar E., Trimble V., 2005, RvMP, 76, 1211

Kaiser N., 1984, ApJ Letters, 284, L9

Kaiser, N. 1987, MNRAS, 227, 1

Kapteyn, J. 1922, ApJ, 55, 65

Kim, R. S. J., et al. 2002, A J, 123, 20

Kirshner, R. P., Oemler, A., Jr., Schechter, P. L., & Shectman, S. A. 1981, ApJ Letters, 248, L57

Kirshner, R. P., Oemler, A. J., Schechter, P. L., & Shectman, S. A. 1987, ApJ, 314, 493

Komatsu, E., et al. 2008, arXiv:0803.0547

Kulkarni, G. V., Nichol, R. C., Sheth, R. K., Seo, H.-J., Eisenstein, D. J., & Gray, A. 2007, MNRAS, 378, 1196

Kurokawa T., Morikawa M., Mouri H., 2001, A&A, 370, 358

Lacey, C., & Cole, S. 1993, MNRAS, 262, 627

Lahav O., 2002, Classical and Quantum Gravity, 19, 3517

S. D. Landy and A. S. Szalay, Astrophys. J. **412**, 64 (1993).

Liddle, A. R., & Lyth, D. H. 2000, Cosmological Inflation and Large-Scale Structure, by Andrew R. Liddle and David H. Lyth, pp. 414. ISBN 052166022X. Cambridge, UK: Cambridge University Press, April 2000.,

Lin, C. C., Mestel, L., & Shu, F. H. 1965, ApJ, 142, 1431

Lin H., Kirshner R. P., Shectman S. A., Landy S. D., Oemler A., Tucker D. L., Schechter P. L., 1996, ApJ, 471, 617

Lupton, R. H., Ivezic, Z., Gunn, J. E., Knapp, G., Strauss, M. A., & Yasuda, N. 2002, Proceedings of Society of Photo-Optical Instrumentation Engineers (SPIE) Conference Series, 4836, 350

Lynden-Bell, D. 1964, ApJ, 139, 1195

Mandelbrot, B. B. 1982, The Fractal Geometry of Nature, San Francisco: Freeman, 1982,

Martinez V. J., 1999, Sci, 284, 445

Martinez, V. J., Jones, B. J. T., Dominguez-Tenreiro, R., & van de Weygaert, R. 1990, ApJ, 357, 50

Martinez, V. J., Pons-Borderia, M.-J., Moyeed, R. A., & Graham, M. J. 1998, MNRAS, 298, 1212

Martínez, V. J., & Saar, E. 2002, Statistics of the Galaxy Distribution, Published by Chapman & Hall/CRC, Boca Raton, ISBN: 1584880848,

Martínez V. J., López-Martí B., Pons-Bordería M., 2001, ApJ Letters, 554, L5

Mo H.J., White S.D.M., 1996, MNRAS, 282, 347

Narlikar, J. V. 2002, An introduction to cosmology. 3rd ed. / Jayant Vishnu Narlikar, Cambridge, UK: Cambridge University Press. ISBN 0-521-79376-9, 2002, XVII + 541 pp.,

Navarro, J. F., Frenk, C. S., & White, S. D. M. 1997, ApJ, 490, 493

Norberg P. et al., 2001, MNRAS, 328, 64

Nusser A., Lahav O., 2000, MNRAS, 313, L39

Oort, J. H. 1983, Annual review of astronomy and astrophysics, 21, 373

Padmanabhan, T. 1993, Structure Formation in the Universe, by T. Padmanabhan, pp. 499. ISBN 0521424860. Cambridge, UK: Cambridge University Press, June 1993.,

Padmanabhan, T. 2002, Theoretical Astrophysics, by T. Padmanabhan, Volume III: Galaxies and Cosmology, pp. 638. ISBN 0521562422. Cambridge, UK: Cambridge University Press, October 2002.,

Pan J., Coles P., 2000, MNRAS, 318, L51

Pandey B., Bharadwaj S., 2005, MNRAS, 357, 1068

Peacock, J. A. 1999, Cosmological Physics, by John A. Peacock, pp. 704. ISBN 052141072X. Cambridge, UK: Cambridge University Press, January 1999.,

Peebles, P. J. E. 1980, The large-scale structure of the universe, Princeton, N.J., Princeton University Press

Peebles, P. J. E. 1993, Principles of physical cosmology, Princeton, NJ: Princeton University Press

Peebles, P. J. E., & Yu, J. T. 1970, ApJ, 162, 815

Percival W. J. et al., 2001, MNRAS, 327, 1297

Percival W. J. et al., 2002, MNRAS, 337, 1068

Percival, W. J., et al. 2007b, ApJ, 657, 645

Pier, J. R., Munn, J. A., Hindsley, R. B., Hennessy, G. S., Kent, S. M., Lupton, R. H., & Ivezić, Ž. 2003, A J, 125, 1559

Pietronero, L. 1987, Physica A Statistical Mechanics and its Applications, 144, 257

Pietronero, L., Montuori, M., & Sylos Labini, F. 1997, Astrophysical Letters Communications, 36, 65

Press, W. H., & Schechter, P. 1974, ApJ, 187, 425

Ribeiro, M. B. 2001, General Relativity and Gravitation, 33, 1699

Richards, G. T., Hall, P. B., Vanden Berk, D. E., Schneider, D. P., Strauss, M. A., & Fan, X. 2002, Bulletin of the American Astronomical Society, 34, 1309

Roos, M. 2008, arXiv:0802.2005

Ross, N. P., et al. 2007, MNRAS, 381, 573

Sánchez, A. G., & Cole, S. 2008, MNRAS, 385, 830

Scharf C. A., Jahoda K., Treyer M., Lahav O., Boldt E., Piran T., 2000, ApJ, 544, 49

Scranton, R. 2002, MNRAS, 332, 697

Seljak, U., et al. 2005, PRD, 71, 043511

Shapley, H., Sweeney, J., & Kokaras, P. 1938, Annals of Harvard College Observatory, 106, 75

Shane, C. D., & Wirtanen, C. A. 1967, Publ. Lick Obs, 22, 1

Shectman, S. A., Landy, S. D., Oemler, A., Tucker, D. L., Lin, H., Kirshner, R. P., & Schechter, P. L. 1996, ApJ, 470, 172

Shen, J., Abel, T., Mo, H. J., & Sheth, R. K. 2006, ApJ, 645, 783

Sheth, R. K., Mo, H. J., & Tormen, G. 2001, MNRAS, 323, 1

Sheth, R. K., & Tormen, G. 2004, MNRAS, 350, 1385

Sheth, R. K., & van de Weygaert, R. 2004, MNRAS, 350, 517

Smith, J. A., et al. 2002, A J, 123, 2121

Smith, R. E., Scoccimarro, R., & Sheth, R. K. 2008, PRD, 77, 043525

Smoot, G. F., et al. 1992, ApJ Letters, 396, L1

Spergel D. N. et al., 2003, ApJ, 148, 175

Spergel, D. N., et al. 2007, ApJ Supplement Series, 170, 377

Springel, V. 2005, MNRAS, 364, 1105

Stoughton, C., et al. 2002, A J, 123, 485

Strauss, M. A., et al. 2002, A J, 124, 1810

Sugiyama, N. 1995, ApJ Supplement Series, 100, 281

Sutherland W., Efstathiou G., 1991, MNRAS, 248, 159

Sylos Labini, F., Montuori, M., Pietronero, L. 1998, Phys Reps, 293, 61

Szapudi I., Colombi S., Bernardeau F., 1999, MNRAS, 310, 428

T. R. Seshadri, 1988, Ph.D. Thesis, Bombay University

Taruya A., Suto Y., 2001,ApJ, 542, 559

Tegmark M. et al., 2004a, PRD, 69, 103501

Tegmark M. et al., 2004b, ApJ, 606, 702

Tucker D. L. et al., 1997, MNRAS, 285, 5

van de Weygaert, R. 2002, Modern Theoretical and Observational Cosmology, 276, 119

van de Weygaert, R. 2005, Appeared in proceedings workshop "Measuring the Diffuse Intergalactic Medium", eds. J-W. den Herder and N. Yamasaki, Hayama, Japan, October 2005, arXiv:astro-ph/0607539

van de Weygaert, R., & Bertschinger, E. 1996, MNRAS, 281, 84

van de Weygaert, R., & Schaap, W. 2007, lecture notes summerschool "Data Analysis in Cosmology" (Valencia), eds. V. Martinez, E. Saar, E. Martinez-Gonzalez, M. Pons-Borderia, Springer-Verlag, ArXiv e-prints, 708, arXiv:0708.1441

Verde, L., et al. 2002, MNRAS, 335, 432

Weinberg, S., 2008, Cosmology, Oxford University Press, USA, April 2008

White, S. D. M., & Silk, J. 1979, ApJ, 231, 1

Wu K., Lahav O., Rees M., 1999, Nature, 397, 225

York, D. G., et al. 2000, A J, 120, 1579

Yoshikawa K., Taruya A., Jing Y.P., Suto Y., 2001, ApJ, 558, 520

Zehavi I. et al., 2002, ApJ,571,172

Zel'Dovich, Y. B. 1970, A&A, 5, 84